Precise Tracking of Things via Hybrid 3-D Fingerprint Database and Kernel Method Particle Filter

A thesis submitted to the faculty

of

WORCESTER POLYTECHNIC INSTITUTE

in partial fulfillment of the requirements of the

Degree of Doctor of Philosophy

in

Electrical and Computer Engineering

Nader BARGSHADY

August 22, 2017

Approved by:

Thesis Advisor:
Prof. Kaveh PAHLAVAN

Head of Department:
Prof. John MCNEILL

Acknowledgements

To properly acknowledge the individuals who positively impacted my life at WPI, I will resort to using two quotes by David Joseph Schwartz and John Quincy Adams:

*. . . **David Joseph Schwartz**: "Here is the basic rule for winning success. Let's mark it in the mind and remember it. The rule is: Success depends on the support of other people. The only hurdle between you and what you want to be is the support of other people."*

I would like to extend my utmost gratitude to Vice Provost of Research, Prof. Bogdan M. Vernescu who was instrumental in opening a new beginning for my Ph.D. endeavor at WPI. In few occasions that I have had the pleasure of meeting with Prof. Varnescu, he inspired me by his respectful mannerism, his willingness to support, and his sound advice.

And more close to home, ECE department, Department Head, Prof. Yehia Massoud resolved my administration issue very quickly and efficiently. I greatly appreciate his whole humble demeanor despite his high scholarly achievements. We have a proverb in IRAN that states: "The more fruitful the tree, the more bent it is" and, on the contrary, a fruitless tree with its light weight stands upright!

*. . . **John Quincy Adams**: "If your actions inspire others to dream more, learn more, do more and become more, you are a leader."*

My advisor, Prof. Kaveh Pahlavan can easily be described by the above quote. With his accomplishment and tenure track for many years, he does not swing his weight against the student and on the contrary, there is no iota of ill-intention towards any student. Under Prof. Pahlavan's leadership, I have greatly benefitted from his selflessness, keenness and visionary ideas. We have shared many laughs and has made this endeavor highly educational and fun.

I would also like to extend my deepest regards and thanks to my committee members, Prof. Yousef A. Mahmoud and Dr. Bardia Alavi for overseeing my progress and their insightful inputs throughout my Ph.D. program. And, I conclude this acknowledgment by a poem (Rubaiyat) from a Persian mathematician, astronomer, philosopher, and poet:

*. . . **Omar Khayyám, Rubaiyat:** "As far as you can avoid it, do not give grief to anyone. Never inflict your rage on another. If you hope for eternal rest, feel the pain yourself; but don't hurt others."*

Dedicated to
two dearest ladies of my life,
my Mother,
&
my Wife

... **Omar Khayyám, Rubaiyat:**
"To wisely live your life, you don't need to know much
Just remember two main rules for the beginning:
You better starve, than eat whatever
And better be alone, than with whoever."

...

Contents

List of Figures

List of Tables

List of Abbreviations

PToT	Precise Tracking of Things
RF	Radio Frequency
WiFi	IEEE 802.11 standard for *Wireless Local Area Networking*
UWB	Ultra Wide Band
LAN	Local Area Network
WLAN	Wireless Local Area Network
RSS	Received Signal Strength
TOA	Time Of Arrival
DOA	Direction Of Arrival
UDP	Undetected Direct Path
LOS	Line Of Sight
NLOS	Non Line Of Sight
COOP	Cooperative
NCOOP	Non Cooperative
PF	Particle Filter
KMPF	Kernel Method Particle Filter
HRSD	High Resolution Signature Database
LIDAR	Light Detection And Ranging
IMU	Inertial Measurement Unit
PMF	Probability Mass Function
CDF	Cumulative Distribution Function
CRLB	Cramér Rao Lower Bound
STD	Standard Deviation
RMSE	Root Mean Square Error
AKL	Atwater Kent Laboratory
BS	Base Station
AP	WiFi Access Point
RP	Reference Point
MO	Moving Object
FA	Fixed Anchor
BW	BandWidth

Abstract

Precise Tracking of Things (PToT) using RF signals has posed a serious challenge in an indoor environment. The precision localization information is an enabler for better coordinated-tasks and is essential for a successful launch of many emerging applications. PToT relies on two principal components, a novel navigation (tracking) algorithm, and a hybrid 3D fingerprint database. In this dissertation, we begin by using the two widely known ranging techniques, Time Of Arrival (TOA) associated with Ultra-wideband (UWB) and Received Signal Strength (RSS) with WiFi signals. *First,* we use the theoretical models derived from empirical measurement of TOA and RSS to analyze the performance of hybrid (WiFi & UWB) cooperative localization accuracy in a multi-robot operation in a typical office environment. To measure the performance of this hybrid localization, we derive a mathematical formulation for the *Cramér-Rao-Lower-Bound* (CRLB). The hybrid method shows more accuracy over WiFi-only approach. In achieving more precision, we extend our work. *Second,* we introduce a novel approach, a Kernel Method Particle Filter (KMPF) for tracking and predicting the position by accessing the information created by hybrid 3D fingerprint database. We derive the mathematical and statistical framework for the Particle Filter based on the statistical assumptions about the behavior of channel models. We also describe the formation of one of the necessary PToT component, a 3D fingerprint database. We compare the performance of the KMPF against the CRLB using WiFi signal channel models.

1 Introduction

The indoor mapping is gaining momentum and applications for more precise indoor localization range from inventory tracking, detecting the location of the Hazardous material, location based services [1, 2] and first responders rescue mission and the list is getting longer every day. In robotic applications, for finding the coordinate information [3, 4], vision modality is used. Vision requires a Line-Of-Sight (LOS) condition. In most indoor environments there are walls, partitions, and furniture that block the view and create a Non- Line-Of-Sight (NLOS [1]) situation. A loss of visual data results in severe degradations in localization precision. One of the well-known methods for robotics localization is the optical method [5, 6] in the context of simultaneous localization and mapping (SLAM) [7–9]. Additionally, since most of these applications take place inside buildings where GPS reception is either non-existent or inferior, other RF methods are used as alternatives. Using the radio propagation signals and models we can potentially overcome this problem and achieve better localization in the absence of visual data. The GPS signals are used for traditional RF localization however it does not work properly in an indoor environment. As a result, recently non-GPS localization using other opportunistic signals have attracted considerable attention [10–12]. Time Of Arrival (TOA) [13–19] of the UWB signals and Received Signal Strength (RSS) of WiFi signals [20–27] are two

---

[1]Ultra Wide Band (UWB) is adversely affected by NLOS. In particular, in between floors where the blocking is fairly severe, and that is why we stay on one floor for our simulation.

most popular RF localization techniques used by an indoor geolocation system.

WiFi localization is the most popular technique used in smart devices today [28–30]. However, this technique has its serious shortcoming due to RF signal distortion [31,32] resulting from multipath, Non-line of sight and lack of reliable GPS signal. The TOA-based UWB signals provide for more precise localization but the coverage is limited, and the design needs new hardware infrastructure. The RSS-based WiFi localization can be implemented in software and on the existing wide spread WiFi infrastructure with a significantly more coverage than UWB systems. As a result, UWB localization has found its way in wireless sensor networks [33–36] and the WiFi localization is used for both indoor and outdoor applications. The results of quantitatively comparative performance evaluation of UWB and WiFi localization in [37–39] reveals that RSS WiFi localization provides a statistically smooth but less reliable localization while the UWB's localization in most occasions provides more precise localization than the RSS localization. Some shortcomings in accuracy when using RF localization techniques, cooperative localization offers itself as a solution for applications in wireless sensor networks [20,33,37]. For WiFi ranging error we use the IEEE 802.11 channel model for calculation of the RSS and the CRLB for RSS links presented in [40–42].

For performance evaluation, we examine the relative performance of various approaches by calculating the Cramér-Rao-Lower-Bound (CRLB) for localization presented in [44–48]. The TOA-based UWB signaling results in more precise localization than RSS-based WiFi. However, the WiFi infrastructure is more readily available and widespread over UWB infrastructure making it more commercially viable. WiFi by itself is not conducive for applications demanding

high precision hence, much less localization error. However, using WiFi in conjunction with other RF signals and sensor's data will enable us to overcome this shortcoming, sub meter accuracy. The performance of our approach is measured against CRLB. The CRLB results for the Time Of Arrival (TOA) of UWB and the Received Signal Strength (RSS) of WiFi was investigated and analyzed in [40,49] respectively. In dynamic tracking applications, adaptive filters are used to improve the localization accuracy by reducing the estimation error hence, RMSE. Particle filters have shown to be more efficient for online and nonlinear/non-Gaussian Bayesian tracking [50–53]. Many applications, such as Autonomous Positioning and Navigation use PF-based algorithms to reduce the inertial navigation system (INS) [54, 55], Real-time Prognosis for the estimation of Li-ion battery discharge time [56] and Reliable Localization and Tracking of Wireless Sensor Networks [57–60]. We simulate many different scenarios to analyze the effect of various parameters on Particle Filter (PF) performance for localization.

The parameters in consideration for better performance, include the number of fixed anchors, hybrid RF signaling using Ultra Wide Band (UWB) and WiFi, the merit of moving objects collaboration (Cooperative, COOP) on their location information and compare it to when in non-collaborating mode (Non-Cooperative, NCOOP). As for effect on Particle Filter performance, we examined the number of Particles, the variation of Observation and State variances. In [61], we showed that Cooperative localization was very efficient in lowering Root Mean Square Error (RMSE) when using RSS or UWB or a combination of both (Hybrid) signaling. The CRLB was calculated [61] for the Hybrid and Cooperative localization using a combination of WiFi and UWB signaling [62]. The TOA-based

UWB signaling renders more precise localization than RSS-based WiFi. However, the WiFi infrastructure [63] is more readily available and more cost effective than UWB which makes it ubiquitous. We then use the above findings and show the need for a signature database. There are discussions of the signature database and the comparison in [64–69]. We introduce a Grid based RF signature database, a Hybrid 3D database with dense Grid points. The information stored per grid point includes the fusion of Light Detection and Ranging (LIDAR) 3D coordinates, Inertial Measurement Unit (IMU) attributes using *Kalman* filtering in conjunction with Bluetooth and WiFi RF signaling. The formation of this database includes the Probability Mass Function (PMF), to be used for PF *Importance Sampling.* We then introduce a novel approach to PF, Kernel Method Particle Filtering (KMPF). KMPF will enable us to achieve more precise indoor localization and navigation.

In the world of Internet of Things (IOT), a Precise Tracking of Things (PToT) can play a significant role in many emerging applications. To pave the way to more precision, we introduce a High-Resolution Signature Database (HRSD) and a novel method, KMPF. We assess the merits of our approach in WiFi environment and compare it to CRLB.

The area of indoor localization is laden with many scholarly publications. In our survey of existing literature, we came across some interesting efforts as per citation in the following section 1.1.

1.1   Related Research

Visible Light based localization is an active and engaging area of the research. Light operates at higher frequency range than Radio signals hence, higher band-

width. Visible Light Communication (VLC) with high bandwidth can lend itself to more precise localization. Some different research activities are ranging from system implementation, use of Wearables, use of Smartphones (and Sensors), Spinning light and Fingerprinting maps. In this section, we address some citation based on the categories as mentioned above. ***Implementation;*** Implementing a light-weight visible light positioning with intended polarization to avoid flickering [71]. Implementing Epsilon, a visible light based localization system that exploits Light Emitting Diode (LED) lamps and has no dependency on network access [72]. Performing Pharos, a visible light based localization using LED lights to accurately estimate the distance between a receiver and LED bulbs [73]. ***Wearables;*** To track changing light condition as a source for user displacement, the wearable solar cells are used hence, user tracking [74]. ***Smartphones;*** Using an unmodified smartphone and slightly modified LED lighting to higher positioning accuracy [75]. There is quite few localization research around Light emitters and sensors to achieve one-centimeter precision [76]. A system that leverages a previously under-utilised source of information luminaries in indoor spaces, for localization. It does not require modification to existing light infrastructure or end user devices [77]. ***Spinning;*** Using rotating source of light (SpinLight) so the receiver can identify the spatial beam hence more accuracy than pure stationary light [78]. ***Fingerprinting;*** Using light illumination value under static lighting condition to create fingerprint [79]. SurrondSense using sound, light, color, RF to map out fingerprint based on logical location as opposed to the usual physical coordinate [80]. Using solid-state luminaries to send data through rolling shutter cameras on mobile devices as a landmark for localization [81].

VLC research is fascinating but lacks the wide spread infrastructure deployment like

WiFi, and it depends heavily on Line of Sight so it can not address situations where there is no line of sight or the intended support, illumination source.

1.2   Motivation

Shortly after joining Center for Wireless Information Network Studies (CWINS) group, I was motivated by the work of former CWINS Ph.D. student, Dr. Nayef Alsindi and published my first paper [70]. The paper was a follow-up work to Dr. Alsindi's paper [44] where the use of WiFi Received Signal Strength (RSS)-signaling was a new addition to the existing UWB Time of arrival (TOA)-based work. The paper was a great warm-up to my next years of research at CWINS. Research idea span from, analysis of multi-sensor localization, Hybrid of RSS and UWB, choice of algorithm for localization and methods to improve the precision with the help of signature indoor mapping.

We began with the detailed analysis in understanding the issues, limitations and the feasibility of using the current wireless infrastructure as a conduit for an indoor localization. The efforts evolved around surveying the current literature in the field and analyzing different approaches and their effect on localization. We assessed the merits of our development versus the calculation of Cramér-Rao-Lower-Bound (CRLB). The methods included multi-sensor network; Wifi Received Signal Strength(RSS)-, Ultra Wide Band(UWB) Time of arrival (TOA)-based RF signaling and, Hybrid of WiFi plus UWB. We further investigated Kalman and Particle filters for our study, and due to nature of the nonlinear and non-gaussian behavior of our sensors, we opted for Particle Filter and expanded our effort to two step solutions for more precise localization. The steps involved

in creating[2] a 3D, High-Resolution Database(HRSD) and Kernel Method Particle Filtering (KMPF). *Our research analysis and simulations were all conducted in the Matlab environment.*

1.3 Contributions

In this section, we summarize the result of our efforts and highlight two main contributions. We started with exploring the use of WiFi RSS theoretical model along with UWB TOA empirical model, added multi-sensor to operate in cooperative mode. Later one due to nature of our sensor model, we opted for Particle Filter for estimation and tracking. We compared the results versus the calculated CRLB. All these efforts culminated in **two main contributions**:

1. **The performance analysis of hybrid (WiFi & UWB) cooperative indoor localization for a multi-robot operation in an office environment and the derivation of mathematical formulation of CRLB to compare against.**
   This work resulted in two conference papers [61,70] and, a book chapter [82]. The details of this contribution are covered in chapters 3 and 4.

2. **Introducing a novel approach, a Kernel Method Particle Filter (KMPF) and a Hybrid 3D Database to achieve high precision localization in an indoor environment and the mathematical and statistical derivation of Particle Filter based on statistical assumptions on the behavior of channel models.**
   This work resulted in an article in the IEEE Sensor Journal [83], a Conference paper [84] and a book chapter [82]. The details of this contribution are available in chapter 5 and 6.

---

[2]in collaboration of Startup company, Reckon Point, San Antonio, in Texas 78249.

1.4 Outline

The rest of the dissertation is organized as follows: In chapter 2, We describe some of the approaches for modeling and analyzing the performance of various sensors for localization. In chapter 3, We analyze the merits of RF cooperative localization using TOA- based UWB and RSS-based WiFi. In chapter 4, We examine the performance bounds on hybrid (WiFi/UWB) cooperative localization in robotic applications. In chapter 5, We propose a novel Hybrid WiFi-UWB cooperative localization using Particle Filter (PF). In chapter 6, We discuss our solution for overcoming the WiFi's submeter error (accuracy) by introducing a novel Kernel Method Particle Filter (KMPF) and describe the formation of an accompanying Hybrid 3D Database for more precise localization. In chapter 7, We summarize our result and discuss future venues for reseach area. Appendix A, a brief CRLB formulation is outlined. Appendix B, the detailed derivation of Bayesian Recursion for Particle Filter.

2 Fundamentals of RF Localization

In this chapter, we describe some of the approaches for modeling and analyzing the performance of various sensors for localization[1]. In particular, we discuss the performance bounds on the ranging technique used for localization. Figure 2.1 illustrates the functional block diagram of a wireless Geolocation system, depicting the functionality for positioning.
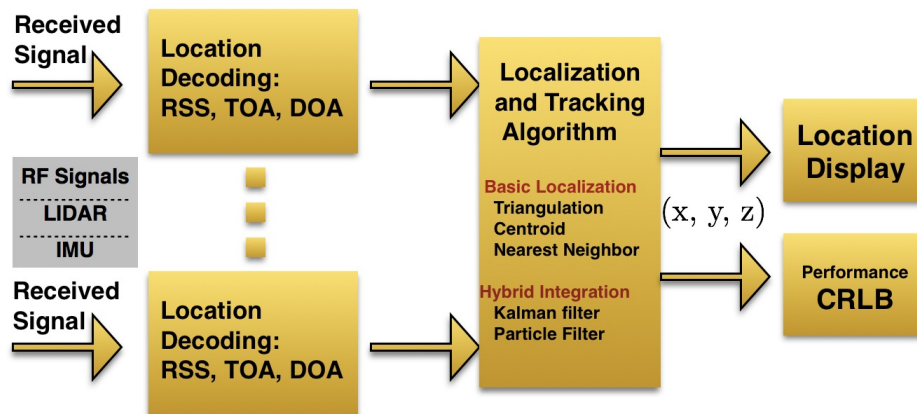
FIGURE 2.1: *Functional block diagram of a wireless geolocation system.*

Whereby,

LIDAR	Light Detection And Ranging, providing 3D coordinates
IMU	Inertial Measurement Unit, measuring dynamic orientation via its sensors
CRLB	Cramér-Rao-Lower-Bound, a measure of lower bound on the variance of an estimator

The main elements of the system are comprised of; location-sensing devices that provide metrics related to the relative position of a mobile station on a known

---

[1]For more detailed discussions of the topics are covered in [82]

landmark called reference point (RP), positioning algorithm that processes metrics reported by location sensing elements to estimate the coordinates of moving object (MO) and, a display system that illustrates the location of the MO on a map. The metrics may indicate the approximated received signal strength (RSS) or its received RF signal time of arrival (TOA). The positioning algorithm processes the received metrics to determine the coordinates of the MO. *To compensate for less reliable measurements, the complexity of the algorithm increases.* The display system shows the estimated location coordinates to a map of an area. This display system could be a service or an application residing on a server or a mobile device, or a universally accessible service on the web such as Google Maps. With the ever increasing the need fo accessibility of the information, there grows the complexity of the display system. In navigation applications, when we have some information regarding the movement of the MO, we combine the RF position estimates with the information on the pattern of movements to refine the location estimates.

There are two basic approaches that have been used to design an RF localization system. The first approach is to develop a signaling system and a network infrastructure of location sensors focused primarily for Geolocation applications. The second approach is to use an existing wireless network infrastructure to locate a MO. The advantage of the first approach is that the physical specification, and consequently the quality of the location sensing results, is under the control of the system designer. The MO can be equipped with a very small wearable tag or a sticker and the density of sensors in the infrastructure can be adjusted to meet the required accuracy of localization. The advantage of the second approach is that it avoids expensive and time-consuming deployment of a special infrastructure.

These systems, however, need to use more intelligent algorithms to compensate for the lack of granularity of the measured metrics. As we transform a localization application from one environment to another, the behavior of the metrics changes and we need to study RF propagation in the area to understand this behavior. As a result, RF propagation analysis remains essential for comparative performance evaluation of different approaches to localization.

In principle, the behavior of the RSS and TOA are adequate for understanding of RF based technologies. Both these approaches try to estimate the distance between a mobile device whose location is unknown and a set of reference points (RPs) whose locations are known. The behavior of the RSS for communication and localization is the same and therefore models developed for the RSS are also useful for performance analysis of RSS-based localization. While in TOA-based localization we are interested in the power and arrival time of the first path and other multipath components arriving in its vicinity.

2.1   Modeling of the Behavior of RF Sensors

As the number of applications for RF location sensing increases, and in response to that some of different technologies for localization are developed, we need a framework for comparative performance evaluation of these technologies. Most performance evaluation techniques require statistical models for the behavior of the sensors that describes the deviation of the measured metrics from the expected value, while operating under ideal conditions. These models help us in relating the performance of the system to the density and deployment strategy of the sensors. The behaviors of different sensors using TOA, RSS, or location

signature of the delay-power profile are quite different; hence, we need to develop appropriate models under different metrics.

2.1.1 Behavior of RSS Sensors

Models to characterize the extensive multipath in indoor and urban areas represent the overall channel impulse response for a given location of the transmitter and receiver by:

$$h(\theta, \tau, t, d) = \sum_{i=1}^{L} \beta_i^d(t) \cdot \exp^{j\phi_i^d(t)} \cdot \delta^2[t - \tau_i^d, \theta - \theta_i(t)]$$

$$\delta^2[t - \tau_i^d, \theta - \theta_i(t)] = \delta(t - \tau_i^d) \cdot \delta(\theta - \theta_i(t))$$

(2.1)

where β, ϕ, θ, and τ represent the amplitude, phase, angle and delay of arrival of each one of the L paths traveling between the transmitter and the receiver and d is the distance between them. $\delta^2[\cdot]$ represents two dimentional Dirac delta function. The received signal strength based RF sensors process the received signal to determine the average RSS and use it to estimate, $\hat{d}$, the distance between the moving object and the location sensor. The average RSS, P_d, in dB at distance d is given by:

$$P_d = 10 \log[RSS_d] = 10 \log \left[\sum_{i=1}^{L} \overline{|\beta_i^d(t)|^2} \right]$$

(2.2)

where β_i is the amplitude of the arriving paths defined in Eq. (2.1) and, the bar over, $\overline{|\beta_i^d(t)|^2}$ denotes the time average of $|\beta_i^d(t)|^2$. The measurement of the average RSS is independent of the bandwidth of the measurement device and therefore, the measured distance using RSS is independent of the bandwidth. In

the case of wideband measurements, the effects of multipath fading is averaged over the spectrum of the signal and this average is computed by measuring the strength of each arriving path and using it in Eq. (2.2). For narrowband systems, where we have only one arriving pulse with fluctuating amplitude according to the multipath fading characteristics, we need to average the signal over a longer period of time to make sure that the multipath fading is averaged out.

To calculate the distance between the transmitter and the receiver, we use the measured average RSS and a distance-power relationship to determine the distance between the target object and the location sensor. If we define the distance measurement error as the difference between the measured and actual value of distance, $\epsilon_d = \hat{d} - d$, this error in RSS systems is also independent of the bandwidth of the system. The measurement of the RSS is relatively simple and accurate, but the relation between the measured RSS and the distance is complex and diversified. *Therefore, the accuracy of RSS-based techniques depends on the accuracy of the model used for the estimation of the distance using the RSS.* A number of statistical models for relating RSS to the distance between the transmitter and the receiver in indoor areas, developed for wireless communication applications, are presented in [85, 86], Chapter 2. In [85], Chapter 2, it was shown that the Raytracing algorithms provide a much more reliable estimation of the received power by using the layout of the building. Therefore, it can be used to improve the performance of sensors using RSS. Raytracing algorithms are however computationally intensive and an alternative approach, much less computation, is geometrical statistical models. The advantage of geometrical statistical modeling and its ability to model site specificity while eliminating the complexity of ray tracing computations is described in [87]. One of the pioneering applications of raytracing for indoor positioning and intruder detection is reported

in [88].

2.1.2   Behavior of TOA Sensors

In TOA systems, the measurement of the TOA requires more complex receivers
and the accuracy of the measurements depends on the bandwidth of the sys-
tem and multipath conditions. A TOA sensor estimates the distance between
the transmitter and receiver from the relation $\hat{d}_w = c\,\hat{\tau}_{1,w}$ where c is the speed of
light and, given in Eq. (2.1), $\hat{\tau}_{1,w}$ is the estimate of the TOA of the direct straight-
line path between the transmitter and the receiver. The estimate of the TOA
is obtained by detecting the first peak of the received signal and this value is
a function of the signal bandwidth and the environment multipath conditions.
For example, in the case of a free-space channel that can be used for GPS appli-
cations when the receiver is in an open area, the multipath effects are negligible.
We can thus measure the distances from the satellites that are tens of thousands
of kilometers away to an accuracy that is within a value smaller than a few me-
ters using a signal with a bandwidth of one MHz. However, in multipath rich
environments, such as indoor areas, attaining similar accuracies even by using
the TOA with RPs around the building and UWB devices with several GHz of
bandwidth faces serious challenges.

Figure 2.2 [89] illustrates the effects of multipath on the estimation of the TOA.
The multipath components in the channel model described by Eq. (2.1) are rep-
resented by impulses. The lower parts of Figure 2.2 show these impulses ob-
tained by raytracing in a typical indoor area. In a practical implementation of
a localization system, we have a finite bandwidth and each impulse is replaced
by a waveform. To measure the TOA, we detect the timing of the peak of the
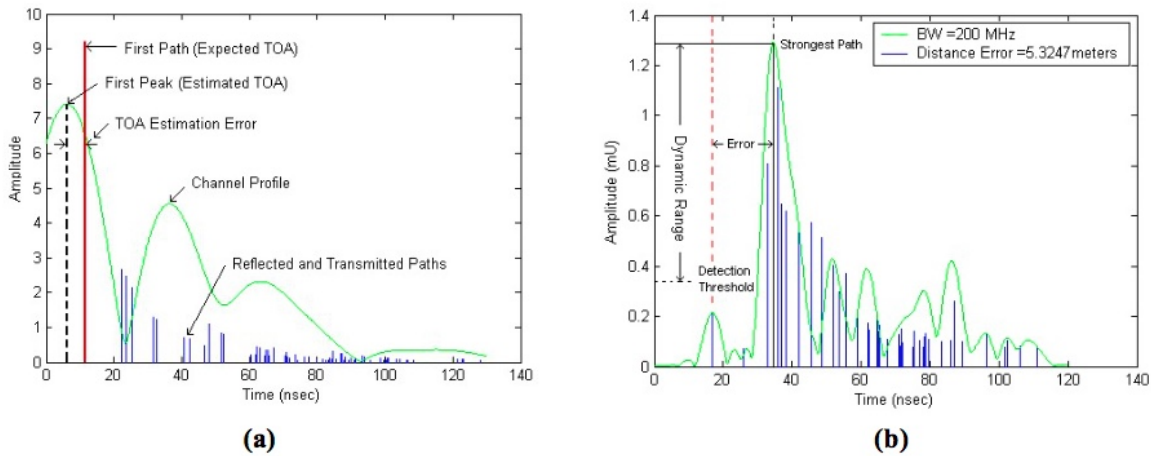
FIGURE 2.2: *Effects of multipath when the Bandwidth(BW) is 200MHz.*
(a) Multipath components close to the arrival of the direct path
(b) Undetectable Direct Path (UDP) hence, higher error

first arriving path and use it as the TOA of the direct path between the transmitter and the receiver. In line-of-sight conditions, the first path in the profile is the strongest path and also the representative of the direct path between the transmitter and the receiver and the timing of the peak of this path is measured to determine the TOA. As shown in Figure 2.2(a) in multipath conditions, the peak of this pulse will shift from its expected value because of the effects of other multipath components that are close to the first path. The shift in the peak causes an error in estimating the TOA and consequently the estimated distance between the transmitter and the receiver. This error is a function of the width of the pulse and consequently the bandwidth (BW) of the system that is inversely proportional to the width of the pulse.

In obstructed line-of-sight conditions, sometimes the direct path is blocked by objects (e.g., metallic doors) and if the strength of this path falls below the detection threshold of the receiver, as shown in Figure 2.2(b) we have an undetected direct path (UDP) condition that causes a large error in the measurement of the TOA. In principle this error will occur no matter how large the bandwidth of

the system is. To understand the behavior of the TOA systems in multipath rich areas we need to model the relation between the TOA estimation error and the multipath conditions in an environment. Since this relationship is very complex, in a manner similar to other statistical models for RF propagation, we need to resort to statistical and empirical modeling. We proceed with the description of one of these models relating the distance measurement error to the bandwidth and the distance described in [90].

We define the distance measurement error for a system with a bandwidth of w as:

$$\epsilon_{d,w} = \hat{d}_w - d \tag{2.3}$$

where d is the actual distance between the RP and the mobile device and $\hat{d}_w$ is the estimate of the distance obtained from measurement of the timing of the first peak of the received channel profile for a given bandwidth. In [89] the distance measurement error is divided into two components, one caused by multipath arrivals close to the first detected peak, $\epsilon_{m,w}$, and the other, the UDP error, $\epsilon_{U,w}$. The UDP error is added to multipath error when an object significantly blocks the direct path. $\xi(d)$, is a binary random variable, denoting the probability of occurrence of a UDP condition as a function of distance d which determines the presence of UDP error hence, is added to multipath error:

$$\epsilon_{d,w} = \epsilon_{m,w} + \xi(d) \cdot \epsilon_{U,w} = \gamma_w \cdot \log(1 + d) + \xi(d) \cdot \epsilon_{U,w} \tag{2.4}$$

The multipath error has two components, a $log(1 + d)$ scaling factor that adjusts the amount of error with distance using a logarithmic scale starting with a minimum of zero and logarithmic growth after that, and a Gaussian random variable

γ_w with the mean and variance of m_w and σ_w^2 with the probability density function:

$$f_{\gamma_w} = \frac{1}{\sigma_w \sqrt{2}} \exp -\frac{(x - m_w)^2}{2\sigma_w^2} \tag{2.5}$$

The statistics of this random variable adjusts the error to the bandwidth of the system. This approach isolates the effects of distance and bandwidth on the distance measurement error. The UDP error is multiplied by a binary random variable that reflects the probability of occurrence of a UDP condition as a function of distance d and another Gaussian random variable $\epsilon_{U,w}$ with the mean and variance of $m_{U,w}$ and $\sigma_{U,w}^2$ and a probability density function:

$$f_{\epsilon_{U_w a}} = \frac{1}{\sigma_{U,w} \sqrt{2}} \exp -\frac{(x - m_{U,w})^2}{2\sigma_{U,w}^2} \tag{2.6}$$

As the distance increases, the probability of occurrence of the UDP condition increases. The variance of the error decreases with the increase in bandwidth of the system.

2.1.3 Models of TOA based on empirical result

As evident in previous section, the closed form solution is a formidable task. At CWINS For UWB signals we use empirical ranging error for TOA-based channel model reported in [44, 91].

The ranging techniques are susceptible to noise variation of the channel models hence, the Distance Measurement Error (DME), ϵ_{ij} is defined as:

$$\epsilon_{ij} = \hat{d}_{ij} - d_{ij} \tag{2.7}$$

where $\hat{d}_{ij}$ is the estimate of the distance between pairs. ϵ_{ij} will vary between the pairs according to selected link error discussed The variance, $\sigma^2_{\epsilon_{UWB}}$ of Distance Measurement Error in (2.7) with tabulated range in Table 2.1 [2].

TABLE 2.1: TOA-Based Empirical data

	Power (dBm)		$\sigma^2_{\epsilon_{UWB}}$
	$RSS(d_{ij})$	> -80	$(0.13)^2$
-100 <	$RSS(d_{ij})$	≤ -80	$(0.3)^2$
	$RSS(d_{ij})$	≤ -100	$(1.4)^2$

There is more general discussion of Distance Measurement Error in [91].

2.2 Performance Bounds using CRLB

In the design of an RF localization system, we need to compare the performance of different alternatives for localization. In the same way that we were using the Shannon-Hartleys bound to compare modulation schemes for achieving a maximum data rate given a signal-to-noise ratio, in localization, it is common to use the Cramer-Rao Lower Bound (CRLB) on the variance, which is a measure of the spread of the error associated with a location estimate, for comparing the precision of location estimations by alternative approaches for localization. The

---

[2]The thresholds and variances defined in table 2.1 are based on Empirical data [44]

smaller the variance, the smaller is the chance that the error in location estimate is large. In the same way that different information transmission applications have different error rate requirements, different localization applications have different precision requirements. For a conceptual system design, a positioning engineer may compare the CRLB for different metrics used for localization to select the appropriate technology or decide on the density for installation of the infrastructure to meet certain precision.

2.2.1 Performance Bounds for Ranging

To explain the application of the CRLB for localization, we start with a simple example, shown in Figure 2.3. Let's assume we have a parameter that we want to measure, for example, the distance between a mobile device and a reference point. Let us suppose that we measure that parameter as $\mathbf{O}$, from a metric such as the TOA of the received signal. The measured observation is not the same as the parameter and if we measure the metric multiple times, each time we may observe a different value. If the probability distribution function of the observation, given the actual value of the measurement, is given by $f(\mathbf{O}/\alpha)$, the smallest variance of the estimate of the parameter can be determined by the CRLB. This is given by what is called the inverse of the Fisher information matrix [92]:
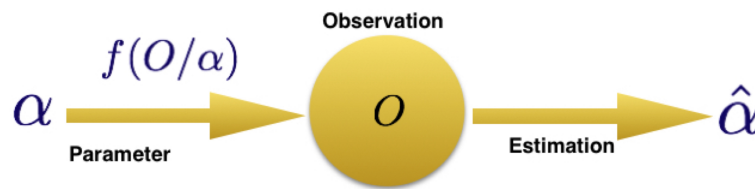
FIGURE 2.3: *Basics of the estimation process and the CRLB for a single parameter.*

$$F = \mathbf{E}\left[\frac{\partial \ln f(\mathbf{O}/\alpha)}{\partial \alpha}\right]^2 = -\mathbf{E}\left[\frac{\partial^2 \ln f(\mathbf{O}/\alpha)}{\partial \alpha^2}\right] \qquad (2.8)$$

In other words, the CRLB is given by:

$$CRLB = Var[\hat{\alpha}(\mathbf{O}) - \alpha] \geq \mathbf{F}^{-1} \qquad (2.9)$$

2.2.1.1 RSS-Based Localization

In an RSS based localization system, we use the measured (observed) received power to determine the distance between a mobile device and a reference point. In [85], it was shown that RSS approximately drops linearly with the logarithm of the distance.

$$L_p = L_0 + 10 \cdot \alpha \cdot \log(d) \qquad (2.10)$$

This presents the total path-loss [3] as the path-loss in the first meter, L_0 plus the loss relative to the given distance, d and it is a function of the distance power gradient α. In terms of received power, the observed power at the receiver is:

$$\mathbf{O} \rightsquigarrow P_r = P_0 - 10 \cdot \alpha \cdot \log d + \chi \qquad (2.11)$$

where χ is the shadow-fading random component that is modeled as a Gaussian distributed random variable with standard deviation of σ.

Since we want to use this observation to estimate the distance d, the probability distribution function of the observation is:

---

[3]There is more detailed disccussion in [93]

$$f(\mathbf{O}/d) = \frac{1}{\sqrt{2\pi}\sigma} \exp -\frac{(\mathbf{O} - P(d))^2}{2\sigma^2} = \frac{1}{\sqrt{2\pi}\sigma} \exp -\frac{(P_r - P_0 - 10\log d)^2}{2\sigma^2} \quad (2.12)$$

Then,

$$\mathbf{F} = -\mathbf{E}\left[\frac{\partial^2 \ln f(\mathbf{O}/d)}{\partial d^2}\right] = \mathbf{E}\left[\frac{\partial \ln f(\mathbf{O}/d)}{\partial d}\right]^2 = \frac{(10)^2 \alpha^2}{(\ln 10)^2 \sigma^2 d^2} \quad (2.13)$$

and the CRLB wil be:

$$CRLB = \mathbf{F}^{-1} = \frac{(\ln 10)^2}{100} \cdot \frac{\sigma^2}{\alpha^2} \cdot d^2 \quad (2.14)$$

Since the CRLB is the variance of the estimate the standard deviation of error is the square root of this value.

$$\sigma_p \geq \frac{\ln 10}{10} \cdot \frac{\sigma}{\alpha} \cdot d \quad (2.15)$$

That means the spread of the error around its mean value is on the order of the distance.

2.2.1.2 TOA-Based Localization

The TOA based systems measure the distance based on an estimate of signal propagation delay. The system is designed so that the received signal waveform in free space has a sharp peak and the variations of the TOA of the peak is measured to determine the distance between a transmitter and a receiver. For a

TOA-based localization system operating in free space, if the transmitted pulse is $s(t)$ the observed signal at the receiver is given by:

$$O(t) = s(t - \tau) + \eta(t) \tag{2.16}$$

where τ is the time of flight of the signal between the transmitter and the receiver and $\eta(t)$ is the additive white Gaussian noise component, with a spectral height of $N_0/2$ observed at the receiver. To form the probability density function of the observation given the value of the parameter τ we should note that we are observing the entire pulse in a Gaussian noise with variance of σ^2, as if we were observing K points on the signal when K grows to infinity. In other words, the probability density function of the observation would be:

$$f(O/\tau) = \frac{1}{(\sqrt{2\pi})^K} \exp\left\{ -\frac{1}{2\sigma^2} \sum_{k=1}^{K} [O_K - S_K(\tau)]^2 \right\}_{\lim_{K \to \infty}} \propto$$
$$\exp\{\frac{1}{N_0} \int_{T_0} [O(t) - s(t - \tau)]^2 \partial t\} \tag{2.17}$$

The Fisher matrix is now calculated from the second derivative of natural log of this function:

$$ln[f(O/\tau)] = \frac{1}{N_0} \int_{T_0} [O(t) - s(t - \tau)]^2 \partial t =$$
$$\frac{1}{N_0} \int_{T_0} [O^2(t) - 2O(t) \cdot s(t - \tau] + s^2(t - \tau)] \partial t \tag{2.18}$$

Since

$$\frac{\partial^2}{\partial \tau^2} \int_{T_0} \mathbf{E}[O^2(t)] \partial t = \frac{\partial^2}{\partial \tau^2} \int_{T_0} \mathbf{E}[s^2(t - \tau)] \partial t = 0 \tag{2.19}$$

the Fisher matrix for the TOA estimation is given by:

$$
\begin{aligned}
F_\tau &= \mathbf{E}\left[\frac{\partial^2}{\partial \tau^2}\{\ln[f(O/\tau)]\}\right] = \\
&\frac{2}{N_0}\int_{T0}\frac{\partial^2}{\partial \tau^2}\mathbf{E}[O(t)\cdot s(t-\tau)]\partial t = \\
&\frac{2}{N_0}\int_{T0}\frac{\partial^2}{\partial \tau^2}s^2(t-\tau)\partial t = \\
&-\frac{1}{\pi N_0}\int_{-\infty}^{+\infty}w^2|S(w)|^2\partial w
\end{aligned}
\tag{2.20}
$$

Therefore the CRLB representing the variance of the estimate is given by:

$$
CRLB = F^{-1} = \frac{\pi N_0}{\int_{-\infty}^{+\infty}w^2|S(w)|^2\partial w}
\tag{2.21}
$$

Since the energy per symbol is defined as:

$$
E_s = \int_{-\infty}^{+\infty}S^2(t)\partial t = \frac{1}{2\pi}\int_{-\infty}^{+\infty}|S(w)|^2\partial w
\tag{2.22}
$$

and the signal to noise ratio as:

$$
\rho^2 = \frac{2E_s}{N_0}
\tag{2.23}
$$

If we define the normalized bandwidth of the pulse as:

$$
\beta^2 = \frac{\int_{-\infty}^{+\infty}w^2|S(w)|^2\partial w}{\int_{-\infty}^{+\infty}|S(w)|^2\partial w}
\tag{2.24}
$$

The CRLB will for TOA-based ranging will be:

$$CRLB = \frac{1}{\rho^2 \cdot \beta^2} \tag{2.25}$$

Which is a function of the inverse of the signal-to-noise ratio and the normalized bandwidth of the transmitted waveform used for TOA measurements.

2.2.2   Performance Bounds for Hybrid Localization

Performance of sensors depend on the environment and certain sensors fit better to specific conditions. For example, TOA-based localization suites better to the line-of-sight (LOS) condition and in certain obstructed LOS condition have very poor performance. However, RSS-based localization, provide a more uniform performance. Hybrid localization is used to integrate the results of different sensors to improve the localization accuracy in changing environments. Calculation of CRLB for hybrid localization will change and has many different possibilities. In this section we provide an example calculation of CRLB for a hybrid RSS and TOA based localization for a moving object with mixed LOS and NLOS environmental experiences. This way we demonstrate how hybrid localization improves the performance in an example scenario of operation.

In our previous work [84], we used *Hybrid* of WiFi and Ultra Wide Band RF signals for localization. Our simulation environment included eight WiFi-enabled fixed Anchors and three Moving Objects. The moving objects were simulated in two different scenarios, WiFi or UWB enabled RF signaling. In addition to *Hybrid* RF signaling, we also took advantage of *cooperative information* whereby, moving objects share their location information. In our review of the results, we use the 50th percentile and assess the performance accordingly. Also, in each of the figures to be discussed, there is a mix of cooperative and non-cooperative

both for Particle Filter and CRLB. The cooperative and non-cooperative graphs for CRLB are represented by solid lines, Blue and Red respectively. In general, one can observe an improving trend stemming from both *Hybrid and cooperative mode.* The resuts in Figures 2.4(a) [4], 2.4(b) [5] are analyzed as follow:
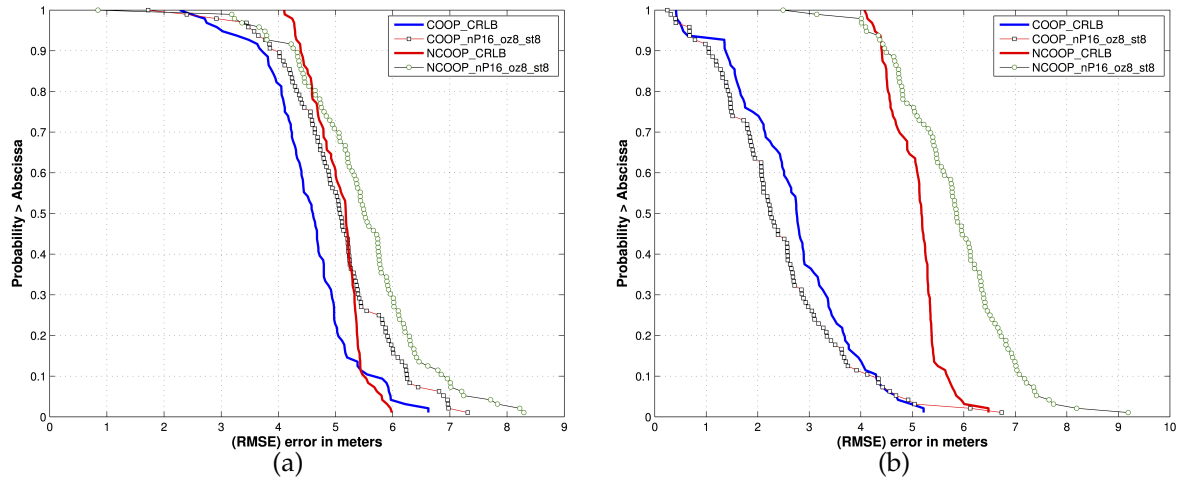
WiFi only (*WiFi*$_{fixed\ anchors}$, *WiFi*$_{moving\ objects}$)   Hybrid (*WiFi*$_{fixed\ anchors}$, *UWB*$_{moving\ objects}$)

FIGURE 2.4: *Particle filter error versus CRLB when operating in cooperative and non-cooperative mode in two different RF signaling scenarios,* **WiFi** *only and* **Hybrid** *signaling.*

Figure 2.4(a), where fixed anchors and moving objects are both WiFi-enabled ($WiFi_{\text{fixed anchors}}$, $WiFi_{\text{moving objects}}$), resulting in high root-mean-square error. The Particle Filter closely tracks the CRLB both in cooperative and non-cooperative mode. It is off by 0.5 meter both in cooperative and non-cooperative mode with respect to the CRLB.

Figure 2.4(b), Hybrid mode, where fixed anchors remain as WiFi-enabled and the moving objects are UWB-enabled ($WiFi_{\text{fixed anchors}}$, $UWB_{\text{moving objects}}$). In here, we have high WiFi root-mean-square error aided by low UWB root-mean-square error of moving objectives hence, improving the overall root-mean-square error.

---

[4]Duplicate of figure 5.5 for ease of referencing.
[5]Duplicate of figure 5.6 for ease of referencing.

In non-cooperative mode, there are not much differences relative to non-Hybrid mode as in Figure 2.4(a). The Particle Filter performs better by 0.5 meter in cooperative and is off by 0.7 meter in non-cooperative mode relative to the CRLB.

An improved root-mean-square error is achieved both by the aide of UWB RF signals in Hybrid mode and sharing location information (Cooperative) mode.

2.3   Wireless Positioning Algorithms

In the last section, we analyzed localization approaches and bounds on their precision when we use the RSS, TOA, or DOA [94] as a metric to determine the distance between a landmark and a mobile terminal. To find the position of a mobile terminal, as shown in Figure 2.1, we need a positioning algorithm to combine the metrics read from different reference points (landmarks) to locate the mobile terminal. Algorithms with well-defined properties are available for satellite based GPS systems. There are least-squares algorithms and maximum-likelihood algorithms; there are algorithms based on a single snapshot of the measurements, and those using measurement and movement history. There are various kinds of sequential filters, which adaptively estimate some unknown parameters of the noise processes [95–97].

GPS, in particular, has focused a great deal of attention on positioning algorithms based on TOA with considerable success. GPS can provide positioning accuracy ranging from tens of meters to centimeters in close to real time depending upon the user's resources [95, 98]. In essence, these techniques are readily applicable to indoor location sensing systems. However, indoor location sensing involves quasi-stationary applications and a number of unreliable reference

points for which existing GPS algorithms, designed for mobile systems with a few reliable reference points, does not provide the best solution. The unreliability of localization in indoor and urban areas is caused due to the fact that more precise TOA and DOA techniques, as we explained in section 2.1, become unreliable in multipath environments. As a result, today, RSS based localization that has less accuracy but performs more consistently in multipath conditions is the most popular approach used in popular commercial applications such as localization in smart devices [99–101]. The RSS-based localization techniques use the existing WLAN infrastructure in buildings for localization in commercial applications. In public safety and military first responder applications, however, hybrid localization techniques using variety of RF and mechanical location sensors have been under investigation for the past decade or more [102]. As we discussed previously, TOA and RSS metrics are the most popular in wireless positioning systems for urban and indoor areas. TOA metrics provide a more accurate measure of distance but may need additional infrastructure. The RSS is an easier metric to measure and integrates well with the existing communications infrastructure, but it is less reliable (widely varying) and often needs more complex algorithms and additional calibration procedures. Some of the simpler algorithm approaches was first implemented using the Nearest Neighbor for localization in indoor areas [103]. Moving forward, Our discussion of the algorithms will emphasize on TOA-, RSS- based and a hybrid of both.

Beside TOA and RSS, there is a Direction of Arrival (DOA) models in [104–106] that uses TOA. However, further research is needed to examine the accuracy of these models in the event of obstructed path and multipath while measuring TOA.

3 Cooperative Localization

In this chapter, we analyze the merits of RF cooperative localization using TOA-based UWB and RSS-based WiFi technologies for cooperative robotic applications in our *modeling and simulation* environment. In our simulation environment we take advantage of empirical results obtained from third floor of AKL for portion of our modeling (TOA) to be described in Section 3.1. We define a movement scenario for multi-robot operation based on the layout of the third floor of AKL in Fig. 3.1, with respect to four *static* reference points. With the use of our mix-mode (empirical and theoretical) modeling we derive *Cramér-Rao-Lower-Bound* (CRLB) for calculation of the localization error for individual robot and when they operate in a cooperative manner both for UWB and WiFi systems. We assume the robots to be equipped with UWB or WiFi in our simulation environment.

Localization error consists of ranging error and positioning error. For UWB systems we use empirical ranging error models for TOA-based systems reported in [44, 91]. For WiFi ranging error we use the IEEE 802.11 channel model for calculation of the RSS and the CRLB for RSS links presented in [40]. For performance evaluation, we examine the relative performance of the two approaches by applying the CRLB for cooperative localization presented in [44, 45].

Section 3.1 describes our models for ranging error in each link. Section 3.2 presents the CRLB for localization used in this chapter. Section 3.3 describes

the multi-robot operation scenario. In Section 3.4 we provide the comparative performance evaluation results and in Section 3.5 we conclude this chapter.
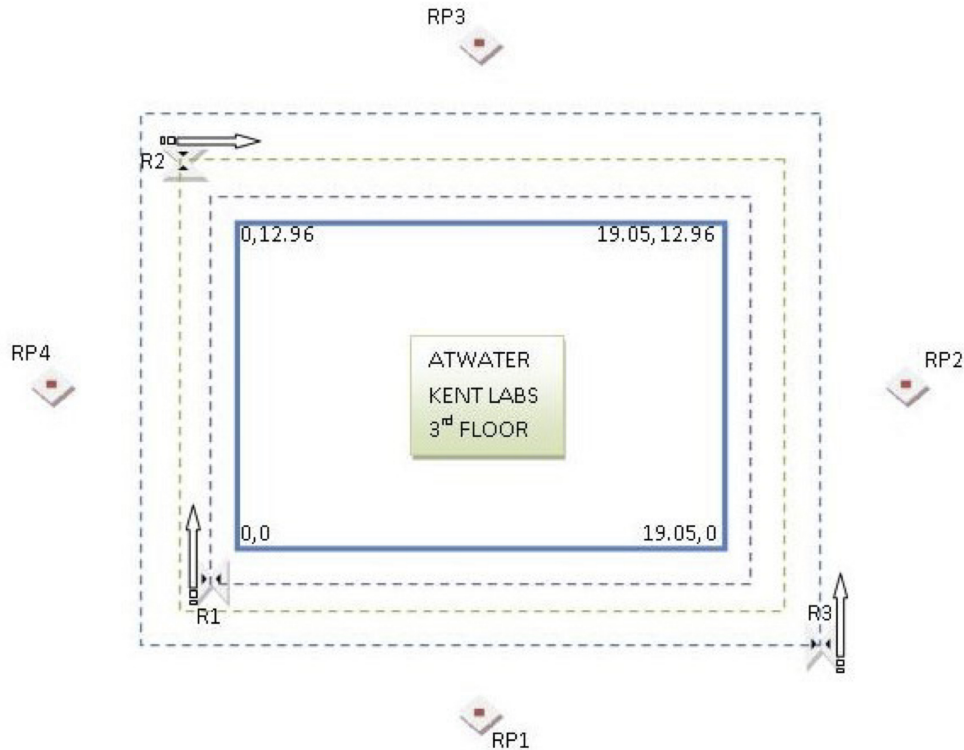
FIGURE 3.1: Tracks for movement of robots: Four **reference points** (RP1, RP2, RP3, RP4) and *three robots* (R1, R2, R3). Each move about its respective (*dotted rectangles*) with 0.4 meter separation among them. The *three arrows* point in the direction of each robot's movement.

3.1   Models for Link Errors for TOA and RSS

In this section we describe the two TOA- and RSS-based models that provide us with variance of the link's ranging error as a function of distance between two RF radiating sources.

Remark 1. A source is defined as a reference point (UWB or WiFi) or a robot (equipped with UWB or WiFi). In our simulation, we use four static reference points to localize the robots. We further simulate the result of cooperation among robots by calculating the distance between the robots to achieve more accuracy in localization.

The variance of TOA- or RSS-based model is used to calculate *Cramér-Rao-Lower-Bound* (CRLB) for our localization performance bound in Section 3.2.

For calculation of variance of the ranging error for RSS-based WiFi localization we use the result of derivation of CRLB for the ranging error in RSS systems from [40]:

$$\sigma_R^2 = var(\widehat{d}) \geq \left(\frac{\ln 10}{10}\right)^2 \cdot \frac{\eta^2}{\alpha^2} \cdot d^2 \qquad . \tag{3.1}$$

Where d is the distance between two sources, η^2 is the variance of the log-normal $\mathcal{N}(0, \eta^2)$ shadow fading of the environment, and α is the so-called distance-power gradient of the environment. Using IEEE 802.11 path-loss model [85] for our simulations, $\eta = 8$ and α takes on a value of 2 for LOS situations and 3.5 for NLOS conditions. The distance d between two sources $Si(x_i, y_i)$ and $Sj(x_j, y_j)$ is:

$$d = \sqrt{(x_j - x_i)^2 + (y_j - y_i)^2} \qquad . \tag{3.2}$$

For TOA based systems in the absence of multi-path the CRLB is given by [49]:

$$\sigma_D^2 \geq \frac{1}{8\pi^2} \cdot \frac{1}{SNR} \cdot \frac{1}{T \cdot W} \cdot \frac{1}{f_0^2} \cdot \frac{1}{1 + \frac{W^2}{12f_0^2}} \qquad . \tag{3.3}$$

Where T is the observation time, SNR is the Signal-To-Noise-Ratio, f_0 is the center frequency of operation and W is the bandwidth of the system. This bound is valid for GPS applications in the open areas and provides very small errors

regardless of the distance. However, in multi-Path rich indoor environments, where direct paths between the sources are blocked, this bound is loose and researchers resort to empirical modeling of the ranging error [85]. Hence, we also resort to empirical models presented in [44,91]. In our simulations we have used the specific model for ranging error in UWB systems presented in [44]. In this empirical model the ranging error is assumed to be a Gaussian random variable whose mean and variance are functions of two power thresholds:

$$\sigma_T^2 = \begin{cases} \mathcal{N}(\mu_1, \sigma_1^2) & RSS(d) > Th_1 \\ \mathcal{N}(\mu_2, \sigma_2^2) & Th_2 < RSS(d) \leq Th_1 \\ \mathcal{N}(\mu_3, \sigma_3^2) & RSS(d) \leq Th_2 \end{cases} . \tag{3.4}$$

Where RSS(d) is the received power at a robot in a distance d from a reference point, $Th_{1,2}$ are the power thresholds, and μ_i and σ_i^2 are mean and variance of the ranging error which are also a function of existence of the direct paths. The thresholds used in the model are Th_1 = -80dBm and Th_2 = -100dBm and the corresponding σ_i^2 are:

$$\sigma_i^2 = \begin{cases} (0.13)^2 & RSS(d) > -80 \\ (0.3)^2 & -100 < RSS(d) \leq -80 \\ (1.4)^2 & RSS(d) \leq -100 \end{cases} . \tag{3.5}$$

The mean and variance for calculation of the error for different channel conditions are given in [44]. The model used for calculation of the RSS is given by:

$$RSS(d) = RSS(1) - 10 \cdot \alpha \cdot \log d - \chi \tag{3.6}$$

in which $RSS(1)$ is the received signal strength at 1 meter distance from a reference point, d is a distance, and χ is the lognormal shadow fading.

In our simulation [44], $RSS(1)$ = -42 (dBm) and (χ, α) take on the set values of ($\chi = 6.8dB$, $\alpha = 2.0$) when in Line-Of-Sight (LOS) and ($\chi = 8.5dB$, $\alpha = 5.6$) when in Non-Line-Of-Site (NLOS).

3.2   CRLB for Cooperative Localization

In this section we do not discuss higher level protocols or implementation issues. We merely derive the performance bound based on Cramér-Rao-Lower-Bound (CRLB). The CRLB provides a lower bound on the variance achievable by any unbiased location estimator. The bound is useful as a guideline: knowing the best an estimator (TOA- or RSS-based) can possibly do that can help us judge our approach in this section.

The derived values for *distance d and variance (σ_R^2 or σ_T^2)* in *Section 3.1* are used in this section to calculate CRLB that allow us to assess the performance of our estimate. We describe our derivation for CRLB from papers [44, 45].

Remark 1.   For further simplification we assume the LOS and NLOS variances can coexist as part of the same diagonal matrix Λ_λ:

$$\Lambda_\lambda = \begin{pmatrix} \lambda_1 & \dots & 0 \\ \vdots & \ddots & \vdots \\ 0 & \dots & \lambda_M \end{pmatrix} \quad . \tag{3.7}$$

Where M refers to number of "reference points" (UWB or WiFi), for minimum of 3 where in our case we use 4 reference points. The element $\lambda_{1:M}$ is the inverse of σ_R^2 or σ_T^2 for the corresponding $d_{1:M}$ for every robot location. The corresponding distance d from Eq. 3.2 is used to assemble our geometry vector with respect to our reference points:

$$\Delta_{vec} = \begin{pmatrix} \Delta_{x_1} & \dots & \Delta_{x_M} \\ \Delta_{y_1} & \dots & \Delta_{y_M} \end{pmatrix} \quad . \tag{3.8}$$

Where Δ_x and Δ_y are partial derivatives of calculated distance, d with reference to x and y coordinates respectively:

$$\Delta_x = \frac{(x_i - x_j)}{d_{ij}} \qquad \Delta_y = \frac{(y_i - y_j)}{d_{ij}} \quad . \tag{3.9}$$

The Fisher Information Matrix, FIM is calculated as:

$$FIM = \Delta_{vec} \cdot \Lambda_\lambda \cdot \Delta_{vec}^T \quad . \tag{3.10}$$

Remark 1. FIM matrix is always *full rank* and its inverse always exists in the cases we investigated.

The Cramér-Rao-Lower-Bound(CRLB) for each *individual* link d_{ij} is derived by the inverse of FIM matrix:

$$CRLB = \left[\Delta_{vec} \cdot \Lambda_\lambda \cdot \Delta_{vec}^T \right]^{-1} \qquad . \tag{3.11}$$

Finally, evaluating the Root-Mean-Square-Error, RMSE for each *individual* link, d_{ij}:

$$RMSE^1 = \sqrt{trace\left(\left[\Delta_{vec} \cdot \Lambda_\lambda \cdot \Delta_{vec}^T \right]^{-1} \right)} \qquad . \tag{3.12}$$

In Section 3.3, we analyze the CRLB results for our simulation scenario.

3.3 Performance Evaluation Scenario

For our performance evaluation, we define a scenario in the third floor of the AKL in Worcester Polytechnic Institute, shown in Fig. 3.2. In this scenario we assume the three robots are moving in the connected corridors in the central part of the third floor. This route is shown by solid blue line in the center of the building layout. Fig. 3.1 shows a closeup route for the robots, location of the reference points and the track for each robot. There are four *reference points (RP1, RP2, RP3, RP4)* and *three robots (R1, R2, R3)*. The dotted lines in Fig. 3.1 shows the route taken by individual robot that are 0.4 meters apart to avoid collision. The arrows in Fig. 3.1 show the direction and the starting point of each robot's movement. The first two robots move clockwise and the third, counterclockwise. We assume all robots start at the same time and move at the same speed. The reference points are located in the center of each side of the Route 2.6

---

[1]"trace" stands for the trace of matrix.

meters away from the central track of the robot number one (R1). In our performance evaluation scenarios we assume the reference points to be either an UWB transmitter or a WiFi access point.

For each sample of time we use the location of each robot to determine its distance from other reference points and robots when in cooperating mode. The distances are used in the equations provided in Section 3.1 to determine the variance of the localization error, σ_R^2 or σ_T^2, associated with UWB or WiFi links, respectfully. The variances of ranging errors obtained for appropriate links are then used for calculation of the CRLB for positioning, described in Section 3.2.

CAD FORMAT: AUTOCAD 2002

WORCESTER POLYTECHNIC INSTITUTE

ATWATER KENT LABS
3RD FLOOR

DRAWN BY: RNG
DATE: 01/08/03
REV.: B
SCALE: 1"=25'
SHEET: 4 OF 5
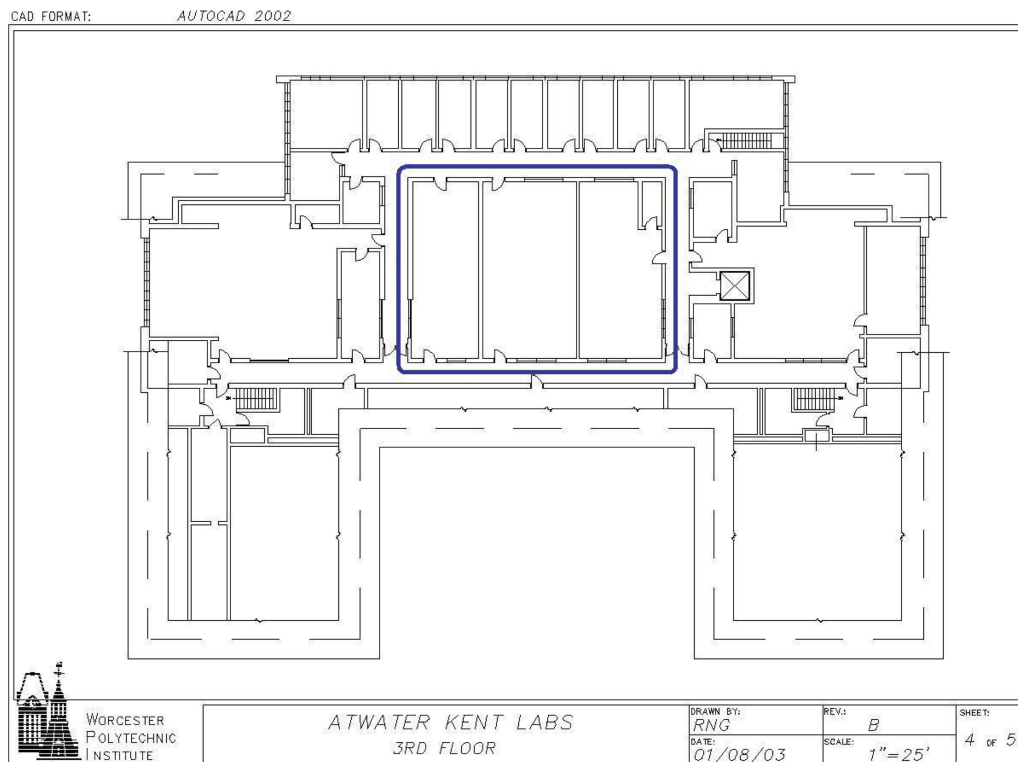
FIGURE 3.2: ATWATER KENT LABS 3rd Floor, Worcester Polytechnic Institute the corridor chosen for the movement of robots is identified by dark solid blue rectangle. More details are shown in Fig. 3.1.

3.4   Results and Discussion

In this section we discuss the results of our simulation runs presented in *figures 3.3*, *3.4*, *3.5 and 3.6*. We compare the performance of cooperative and non-cooperative operations for UWB and WiFi localization. Fig. 3.3 shows the performance of cooperative versus non-cooperative operation in sixty four equally distanced locations across the route when sources are using UWB signals. The lower curve shows the RMSE for variance of positioning error of all robots when they cooperate for localization. The three top plots show the RMSE of localization for each individual robot when they obtain their location from reference points only (no cooperation). As expected, in the vicinity of reference points we notice better performance, the few undershoots as shown in Fig. 3.3. On average, cooperation among the robots show improvement in the RMSE of localization by a factor of 5. Fig. 3.4 shows the cumulative distribution function of the RMSE across the route. As shown on the left of Fig. 3.4, the RMSE is nicely confined in a narrow range $\simeq 0.03$ whereas in the individual cases we notice RMSE as high as 0.16.

In Fig. 3.5, shows the performance of cooperative versus non-cooperative operation in sixty four equally distanced locations across the route when sources are using WiFi signals. The lower curve shows the RMSE for variance of positioning error of all robots when they cooperate for localization. The three top plots show the RMSE of localization for each individual robot when they obtain their location from reference points in lieu of cooperation. On average cooperation among the robots show improvement in the RMSE of localization by a factor of 15. Fig. 3.6 shows the cumulative distribution function of the RMSE across the route. As shown in Fig. 3.6, the RMSE for cooperative localization is confined
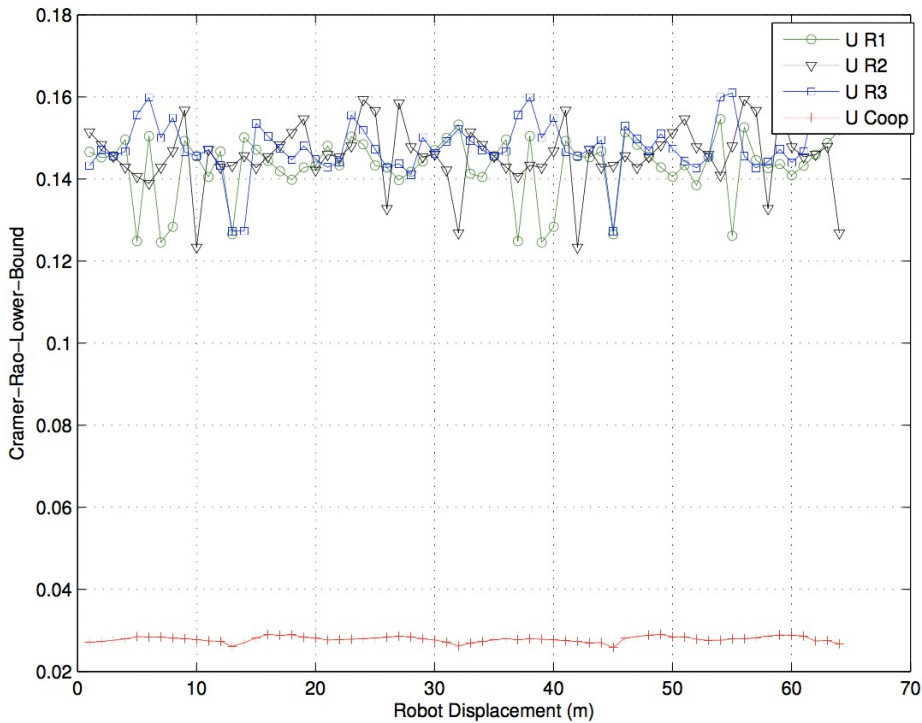
FIGURE 3.3: UWB : *RMSE versus robot displacement*

in a narrow range of approximately $\simeq 0.5$ whereas in the individual cases, we notice an error as high as 8.5.

The factors of improvement are significantly higher in WiFi, 15 times on average as compared with UWB, 5 times. The range of error in WiFi localization, shown in Fig. 3.5, is between 6.5 to 8.5 while in UWB, as shown in Fig. 3.3, this range is restricted between 0.125 to 0.16. Fig. 3.7, shows the overall performance of UWB and WiFi in cooperative and non-Cooperative for our scenario side-by-side.

As shown in far left, UWB with cooperation is the best performer with the rate of error of 0.03 meters and on the far right, WiFi without cooperation is the worst performer with the rate of error of 6.5 to 8.5 meters.
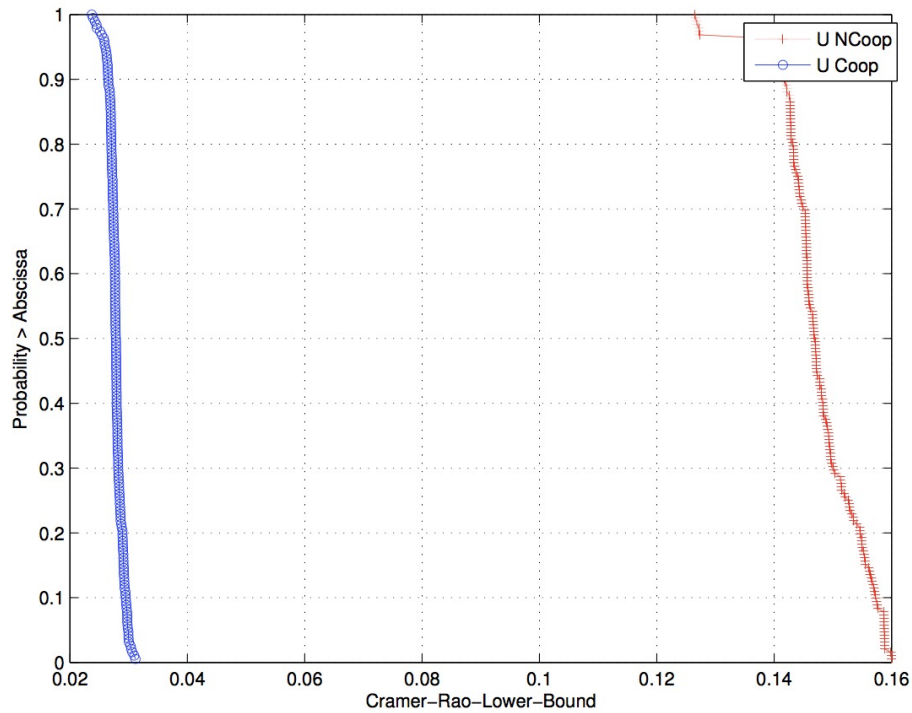
FIGURE 3.4: UWB : *Probability versus RMSE*

3.5 Summary

With recent proliferation of wireless devices in robotic applications, support for localization services using radio signals has attracted tremendous attention in research community. In this chapter we simulated our models and analyzed the quantitative performance of two widely used localization techniques based on TOA and RSS using UWB and WiFi transmission medium, respectively. Our results of modeling and simulation for our scenario at the third floor of the AKL showed that UWB-based localization provides error in the range of 0.125 to 0.16 meters for non-cooperative and 0.025 to 0.029 meters for cooperative localization. The WiFi localization range for non-cooperative localization was 6.5 to 8.5 meters and for cooperative 0.47 and 0.64 meters. These quantitative results provides an insight to the common believe that UWB is more accurate than WiFi
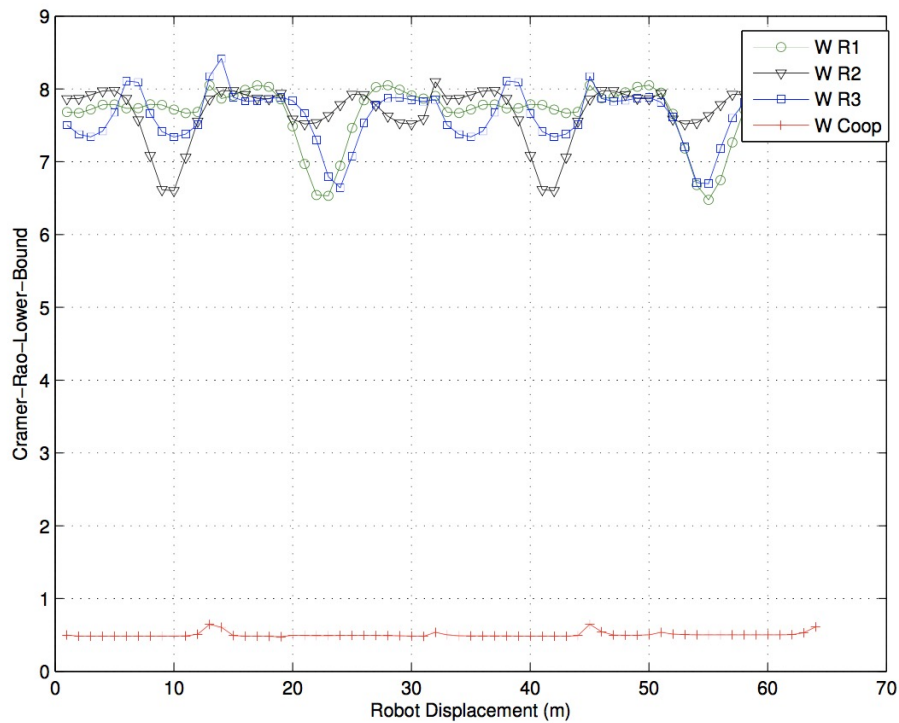
FIGURE 3.5: WIFI : *RMSE versus robot displacement*

both in cooperative and non-Cooperative mode. In both cases of UWB and WiFi gained significant improvement by cooperative localization using robots. However, WiFi localization benefits much higher rate of improvement through cooperation (15 times) as compared with UWB localization (5 times).
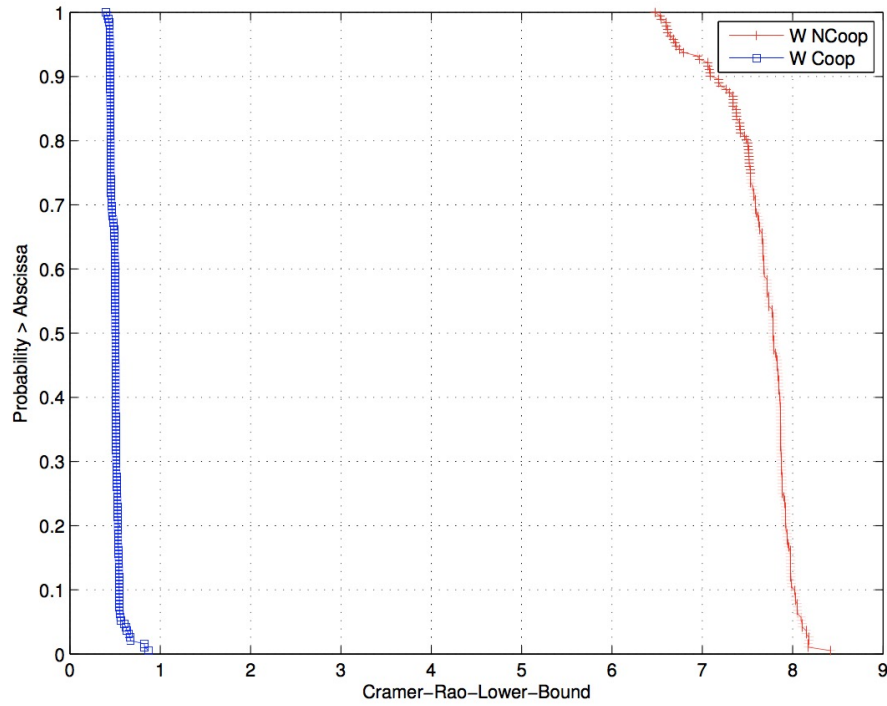
FIGURE 3.6: WIFI : *Probability versus RMSE*
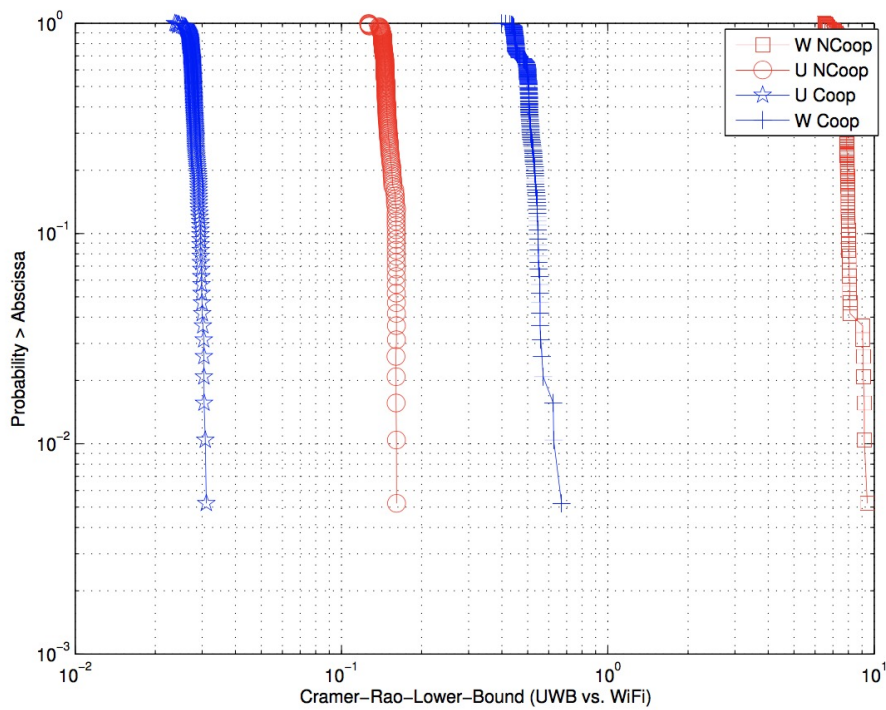
FIGURE 3.7: *Comparing UWB versus WIFI : Probability versus RMSE*

4 Hybrid (RSS & TOA) Localization

Due to the complex nature of radio propagation, employing a single method is not always adequate and hence it needs to be accompanied by supplementary methods to achieve the precise localization goal. Combination of various methods by exploiting their individual advantages such as the robustness of WiFi under harsh environments and accuracy of UWB under LOS conditions provides us with better overall localization results in GPS denied environments. Hence hybrid methods prove much better in terms of yield and accuracy and is thus important for localization in cooperative robotic applications. In chapter 3, we showed that cooperative UWB is superior to cooperative WiFi methods. However, in most practical situations there is no UWB infrastructure in buildings.

In this chapter, we examine the performance bounds on hybrid (WiFi/UWB) cooperative localization in robotic applications. In hybrid localization we refer to a technique where by ranging between fixed anchors and mobile robots use hybrid ranging techniques. Ranging between fixed anchors and mobile robots is achieved through WiFi RSS-based techniques, while robot-robot is achieved through UWB TOA-based techniques. This approach is interesting from a practical point of view where deployed robots in an indoor environment can quickly and effectively take advantage of the available WiFi infrastructure to achieve cooperatively a global location information. This approach to our understanding is unique and proves a novel contribution to cooperative localization in indoor

robotic applications. In order to validate the effectiveness of our a approach we analyze the results of extensive simulation in a typical indoor office environment.

In our simulation environment we take advantage of empirical results obtained from third floor of AKL for portion of our modeling (TOA) to be described in Section II. We define a movement scenario for multi-robot operation based on the layout of the third floor of AKL (Fig. 4.1) with respect to four and eight *static* reference points as well as two and three robots at play. With the use of our empirical and theoretical modeling we derive *Cramér-Rao-Lower-Bound* (CRLB) for calculation of the localization error for non-cooperative (individual) and cooperative scenarios for UWB-Only, WiFi-Only and hybrid WiFi-UWB systems where reference points are WiFi and robots are equipped with UWB. Localization error consists of ranging error and positioning error. For UWB signals we use empirical ranging error for TOA-based channel model reported in [44, 91]. For WiFi ranging error we use the IEEE 802.11 channel model for calculation of the RSS and the CRLB for RSS links presented in [40]. For performance evaluation, we examine the relative performance of various approaches by determining the CRLB for localization presented in [44, 45].

The rest of this chapter is organized as follows: In section II, we define the analytical formulation for performance analysis. Section III describes the multi-robot operation scenario. Section IV we provide the comparative performance evaluation results. Section V we conclude this chapter.

4.1 Analytical formulation for performance analysis

In this section we will derive the CRLB for hybrid system localization based on empirical ranging error models for TOA and RSS. We will first formulate our problem and derive the general CRLB and then give the ranging error models we used for calculating the CRLB.

4.1.1 CRLB for hybrid system localization

When there are N robots cooperatively working together and M reference points available, the reference points (such as WiFi access points) act as anchors and the robots act as blind nodes. The wireless networks between the blind nodes allow them to transfer ranging information between them. In a typical robotic application,$N >> M$. In a 2-dimensional plane, the coordinates of all the nodes (including robots and anchors) are given by:

$$\theta = [x, y]^T, \tag{4.1}$$

where $x = [x_1, ..., x_N]^T$ and $y = [y_1, ..., y_N]^T$ are the $x-$ and $y-$ coordinates of the N robots. Similarly, the coordinates of the M anchor nodes are given by:

$$\varphi = [x_{N+1}, ...x_{N+M}, y_{N+1}, ..., y_{N+M}]^T, \tag{4.2}$$

For node pairs, i and j, which are within communication range, a range measurement d_{ij} can be obtained using one of the ranging techniques, UWB TOA ranging between robots and WiFi RSS ranging between anchors and robots. For instance, in TOA ranging the range estimate between the ith and j^{th} node is

given by

$$\hat{d}_{ij} = \hat{\tau}_{ij} \times v, \tag{4.3}$$

where $\hat{d}_{ij}$ is the estimated distance between the nodes, τ_{ij} is the TOA measurement and v is the speed of signal propagation. Regardless of the ranging techniques, the distance estimate will be corrupted by noise

$$\hat{d}_{ij} = d_{ij} + \epsilon_{ij}, \tag{4.4}$$

where $d_{ij} = \sqrt{(x_i - x_j)^2 + (y_i - y_j)^2}$ is the actual distance between the pair of nodes and ϵ_{ij} is a random variable representing the statistics of the ranging error which is specific to the ranging techniques and will be discussed in more detail in the following section. Note that the statistics between different node pairs need not be the same. For example, the UWB based TOA ranging links between robots generally provides smaller ranging error compared to the WiFi based RSS ranging links between anchors and robots in LOS scenario.

For a given robot operating configuration, ranging technique, and coverage characteristics, the robots can collaborate in a cooperative fashion to reach a final estimate given by

$$\hat{\theta} = [x_1, ...x_N, y_1, ...y_N]^T, \tag{4.5}$$

For known anchor locations $\varphi = [x_{N+1}, ...x_{N+M}, y_{N+1}, ..., y_{N+M}]^T$, we wish to estimate the unknown locations of robots, $\theta = [x_1, ...x_N, y_1, ..., y_N]^T$. The CRLB provides a lower bound on the error covariance matrix for an unbiased estimate of θ [92]. For a given estimate of the sensor locations $\hat{\theta}$ and Gaussian range measurement X, the Fisher Information Matrix (FIM) can be represented by [92]

$$J(\theta) = E[\bigtriangledown_\theta ln f_X(x;\theta)][\bigtriangledown_\theta ln f_X(x;\theta)]^T \tag{4.6}$$

where $f_X(x; \theta)$ is the joint Gaussian PDF given by

$$f_X(x; \theta) = \frac{1}{(2\pi)^K |\sum|^{\frac{1}{2}}} exp\left\{-\frac{1}{2}[x - \mu(\theta)]^T \sum\nolimits^{-1} [x - \mu(\theta)]\right\} \tag{4.7}$$

where $\mu(\theta)$ is the vector of the actual distances between the nodes corresponding to available K measurements. FIM for the specific PDF in equation (4.7) can be written as

$$J(\theta) = [G(\theta)]^T \sum\nolimits^{-1} [G(\theta)] \tag{4.8}$$

where

$$G(\theta)^T = \begin{pmatrix} cos\phi_1 & cos\phi_2 & ... & cos\phi_k \\ sin\phi_1 & sin\phi_1 & ... & sin\phi_k \end{pmatrix} \tag{4.9}$$

$$\sum = diag(\lambda_1 \quad \lambda_2 \quad ... \quad \lambda_k) \tag{4.10}$$

ϕ_i representing the angle between the nodes from ith measurement. And λ_i is the variance of range estimate from the ith measurement. The CRLB is then given by:

$$CRLB = [J(\theta)]^{-1} \tag{4.11}$$

4.1.2 Models for link errors using TOA and RSS

To calculate the CRLB, we need the variance of distance measurement error(DME) for all the links among the robots and the reference points. The link between two robots use UWB TOA ranging and the link between each robot and a reference point uses WiFi RSS ranging.

In our simulation, we use four or eight anchor reference points to localize the

robots. We further simulate the results of cooperation among robots by calculating the distance between the robots to achieve more precision in our localization.

For calculation of variance of ranging error of RSS-based WiFi localization, we followed the CRLB derivation in [40, 107]. The time averaged power loss is formulated as:

$$Lp = 10\alpha \cdot logd + \chi \tag{4.12}$$

where

$$d = \sqrt{(x_i - x_j)^2 + (y_i - y_j)^2} \tag{4.13}$$

is the distance between two sources S_i and S_j and "noise" χ is independent Gaussian variables $N(0, \sigma_\chi)$. Hence the p.d.f of Lp conditioned on d is

$$f_d(Lp) \propto exp(-\frac{1}{2\sigma_\chi^2}(Lp - 10 \cdot \alpha \cdot logd)^2) \tag{4.14}$$

Therefore, the CRLB is given by:

$$J_p^{-1} = (G(\theta)^T \cdot \sum^{-1} \cdot G(\theta))^{-1} \tag{4.15}$$

where J_p is the Fisher matrix and

$$G(\theta)^T = \frac{10\alpha}{ln10} \cdot \begin{pmatrix} cos\phi \\ sin\phi \end{pmatrix} \cdot d^{-1} \tag{4.16}$$

$$\sum = \sigma_\chi^2 \tag{4.17}$$

where ϕ is the angle between the two sources and account for the effect of geometric relation on ranging accuracy. Substitute equations (4.16), (4.17) into equation (4.15), we get the variance of ranging error:

$$trace(J_p^{-1}) = var(\hat{d}) \geq (\frac{ln10}{10})^2 \cdot \frac{\sigma_\chi^2}{\alpha^2} \cdot d^2 \qquad (4.18)$$

For RSS based WiFi links, we used the IEEE 802.11 path loss model [85] and the parameters are listed in table 4.1

TABLE 4.1: Parameters used in WiFi Simulation

	α	σ_χ (dB)
LOS	2.0	8.0
NLOS	3.5	8.0

For TOA based systems, the link error model without considering multipath combination and NLOS influence was given by [49]:

$$\sigma_D^2 \geq \frac{1}{8\pi^2} \frac{1}{SNR} \frac{1}{T \cdot W} \frac{1}{f_0^2} \frac{1}{1 + \frac{W^2}{12f_0^2}} \qquad (4.19)$$

where T is the observation time, SNR is the signal to noise ratio, f_0 is the center frequency of operation and W is the normalized bandwidth of the system. This model is too optimal for indoor environment because of the rich multipath components and frequent occurrence of NLOS scenario. Therefore, we resort to empirical models presented in [108] which were developed for indoor geolocation applications and more close to reality.

In our simulation, we have used a specific model for ranging error in UWB systems similar in [108]. In this empirical model, the ranging error ϵ is assumed to be a Gaussian random variable whose mean and variance are correlated with

the total received signal strength:

$$f_\epsilon(\epsilon) = \frac{1}{2\pi\sigma_\epsilon^2} exp[-\frac{(\epsilon - \mu_\epsilon)^2}{2\sigma_\epsilon^2}]$$ (4.20)

where

$$(\mu_\epsilon, \sigma_\epsilon^2) = \begin{cases} (\mu_1, \sigma_1^2) & RSS(d) \leq Th_1 \\ (\mu_2, \sigma_2^2) & Th_1 < RSS(d) \leq Th_2 \\ (\mu_3, \sigma_3^2) & Th_2 < RSS(d) \end{cases}$$ (4.21)

where $RSS(d)$ is the received signal strength of a robot at a distance d from a reference point. $Th_{1,2}$ are the power thresholds, μ_i and σ_i^2 are the mean and variance of ranging error with and without the availability of direct path. The values used in the model are $Th_1 = -100dBm$ and $Th_2 = -80dBm$ and the corresponding σ_ϵ^2 based on table 4.2 [1] :

TABLE 4.2: TOA-Based Empirical data

	Power (dBm)		$\sigma_{\epsilon_{UWB}}^2$
	$RSS(d_{ij})$	> -80	$(0.13)^2$
-100 <	$RSS(d_{ij})$	≤ -80	$(0.3)^2$
	$RSS(d_{ij})$	≤ -100	$(1.4)^2$

The mean and variance for calculation of the error for different channel conditions are given in [108]. The model we used for calculation of the RSS of UWB link is given by:

$$RSS(d) = RSS(L_0) - 10\alpha \cdot logd + \chi$$ (4.22)

where $RSS(L_0)$ is the received signal strength at a reference distance (1m here). d is the distance, α is the path loss gradient and χ is the lognormal shadow

[1] Table 2.1 is duplicated here for the ease of referencing.

fading with zero mean and variance σ_χ^2. The values of α, σ_χ are listed in table 4.3

TABLE 4.3: Parameters used for UWB Simulation

	$RSS(L0)$ (dBm)	α	σ_χ (dB)
LOS	-42	2.0	6.8
NLOS	-42	5.6	8.5

4.2 Performance Evaluation Scenario

For our performance evaluation, we define a scenario in the third floor of the AKL in Worcester Polytechnic Institute. In this scenario we assume the three robots are moving in the connected corridors in the central part of the third floor. This route is shown by solid blue line in the center of the building layout. Fig. 4.1 shows a close-up route for the robots, location of the reference points and the track for each robot. There are four or eight *reference points* configurations, *(RP1, RP2, RP3, RP4), (RP1L, RP1, RP1R, RP2, RP3R, RP3, RP3L, RP4)* and there are *three robots (R1, R2, R3)*. The dotted lines in Fig. 4.1 shows the route taken by individual robot that are 0.4 meters apart to avoid collision. The arrows in Fig. 4.1 show the direction and the starting point of each robot's movement. The first two robots move clockwise and the third, counterclockwise. We assume all robots start at the same time and move at the same speed. The reference points are located in the center of each side of the Route 2.6 meters away from the central track of the robot number one (R1). In our performance evaluation scenarios we assume the reference points to be either an UWB transmitter or a WiFi access point.

For each sample of time we use the location of each robot to determine its distance from other reference points and, robots when in cooperating mode. The distances are used in the equations provided in Section II to determine the variance of the localization error, σ_R^2 or σ_T^2, associated with UWB or WiFi links, respectively. In hybrid WiFi-UWB mode the links between cooperative robots are assumed UWB and the anchors to robots as WiFi links.
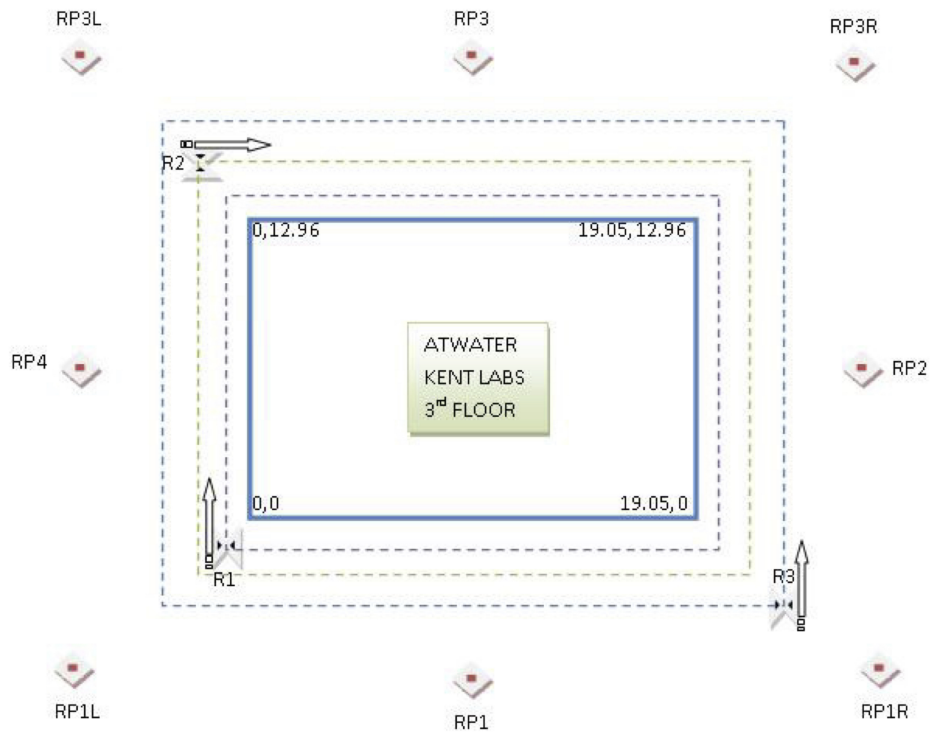
FIGURE 4.1: Tracks for movement of robots: eight **reference points** (RP1L, RP1, RP1R, RP2, RP3R, RP3, RP3L, RP4) and *three robots* (R1, R2, R3). Each move about its respective (*dotted rectangles*) with 0.4 meter separation among them. The *three arrows* point in the direction of each robot's movement.

4.3   Results and Discussion

In this section we discuss the results of our simulations for WiFi-Only in (Figs. 4.2 & 4.3), UWB-Only in (Figs.4.4 & 4.5), Hybrid WiFi-UWB in (Figs. 4.6 & 4.7)

and finally overall performance for all in (Figs. 4.8 & 4.9).

In all our simulation runs, we have used thirty two equally distanced locations across the route for all robots. For all scenarios, there are two anchor configurations, four or eight and for each one both two and three robots are used.

In general, one can observe a trend of improvement stemming from more anchors as well as more robots the degree of which depends on the RF signaling and methodology for example, hybrid of WiFi and UWB renders the best results. In the following paragraphs the various methods are discussed.

In our review of the results we use the 50th percentile and assess the performance accordingly.

WiFi-Only (Figs. 4.2&4.3): In this scenario, robots and anchors are assumed to be WiFi-equipped. By doubling the number of anchors there is 1.5 meter improvement in errors across all three curves. While using 3 robots versus 2 robots in cooperative mode we only get 0.5 meter improvement in errors. Overall by using 3 cooperative robots plus doubling the number of anchors versus 3 non-cooperative robots in 4 anchor configuration, we get 3.75 meters improvement that is 42 percent improvement in error.

UWB-Only (Figs. 4.4&4.5): In this scenario, robots and anchors are assumed to be UWB-equipped. In here, we start off with very low error in comparison to WiFi-Only scenario and doubling the anchors has resulted in narrowing the gap between non-coop, coop and 2 versus 3 robots scenario. We observe that by doubling the number of anchors and cooperative robots we can achieve 0.9 meters improvement, that is 75 percent improvement.
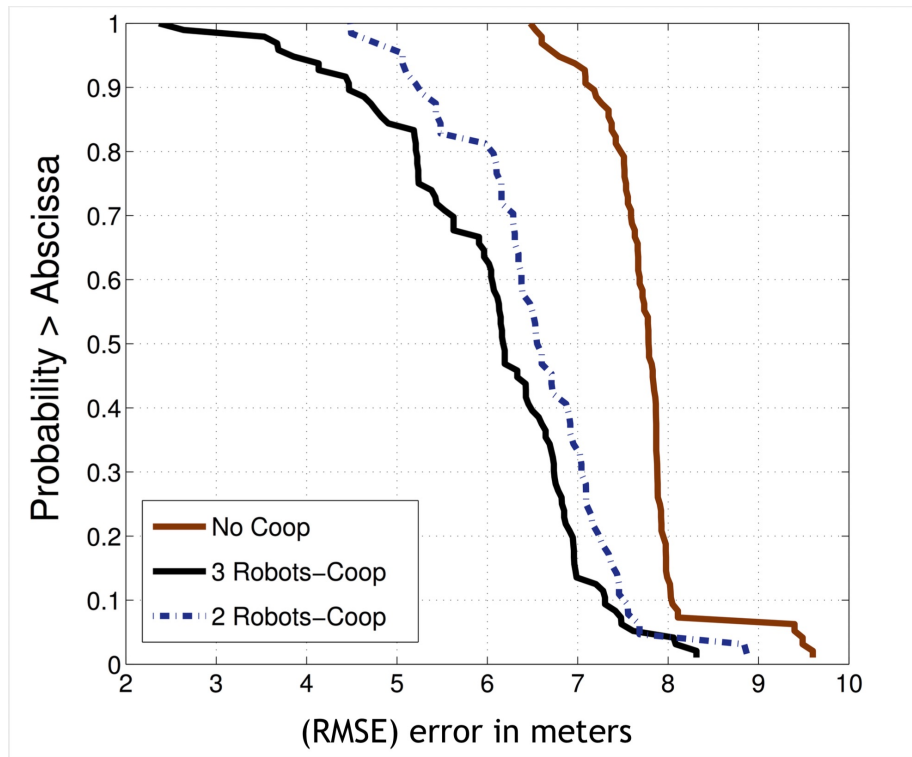
FIGURE 4.2: *RMSE(m) for 2 and 3 Robots using **4 Anchors** configuration and **WiFi mode.***

Hybrid, WiFi-UWB (Figs. 4.6&4.7): In this scenario, robots are assumed to be equipped with UWB in cooperative mode and anchors WiFi-equipped. By doubling the number of anchors we get 2.75, 1 and 0.25 meters improvement in 3 robots non-coop (WiFi), 2 robots coop (hybrid) and 3 robots coop (hybrid) respectively. While using 3 robots versus 2 robots in cooperative mode there is 1.5 to 2 meter improvement. Overall by using 3 cooperative robots (hybrid) plus doubling the number of anchors versus 3 non-cooperative robots (WiFi) in 4 anchor configuration, we get 5 meters improvement that is 63 percent improvement in error.

Comparison of results (Figs. 4.8&4.9): Here we compare the hybrid 3 cooperative robot vs WiFi-Only 3 cooperative, WiFi-Only 2 cooperative and WiFi-Only 3 non-cooperative robots. Hybrid with 3 cooperative robots gives us the best
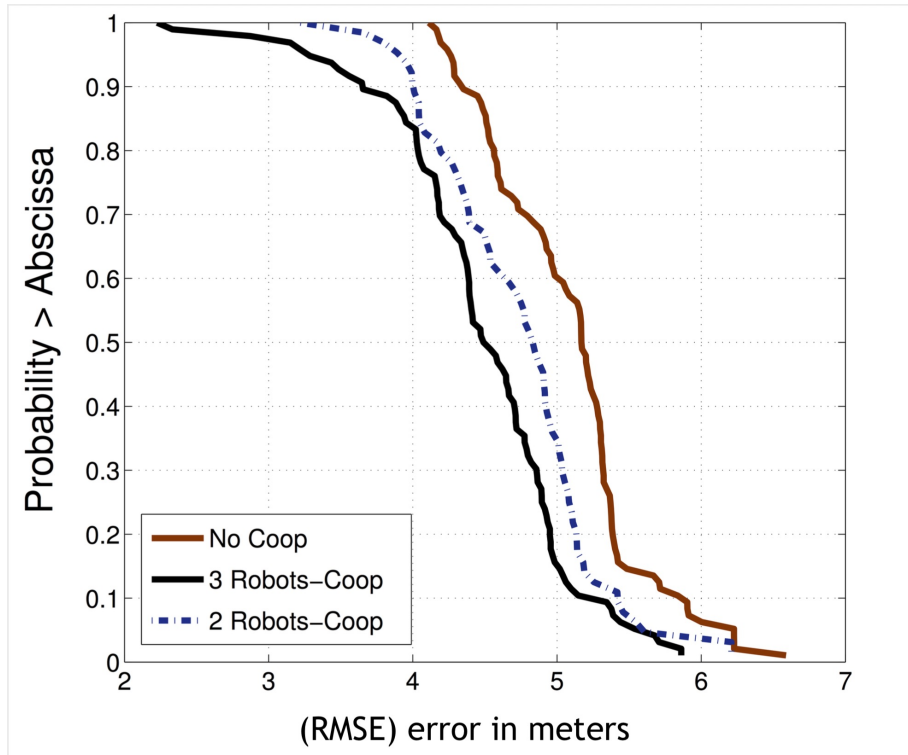
FIGURE 4.3: *RMSE(m) for 2 and 3 Robots using **8 Anchors** configura-
tion and **WiFi mode**.*

results followed by WiFi-Only 3 and 2 cooperative robots. WiFi-Only 3 non-
cooperative robot case is the worst performer in our comparison.

Section 4.4 gives the detailed tabulated results.

4.4   Summary

In this chapter, we simulated and analyzed the quantitative performance of two
widely used localization ranging techniques based on TOA and RSS for UWB
and WiFi transmission medium, respectively. We further examined the merits of
hybrid WiFi-UWB for our main scenario which tends to be more applicable due
to ubiquity of WiFi reference points and the advantage of UWB precision. The
results are tabulated in tables 4.4, 4.5 & 4.6. As an example we refer to table4.4.
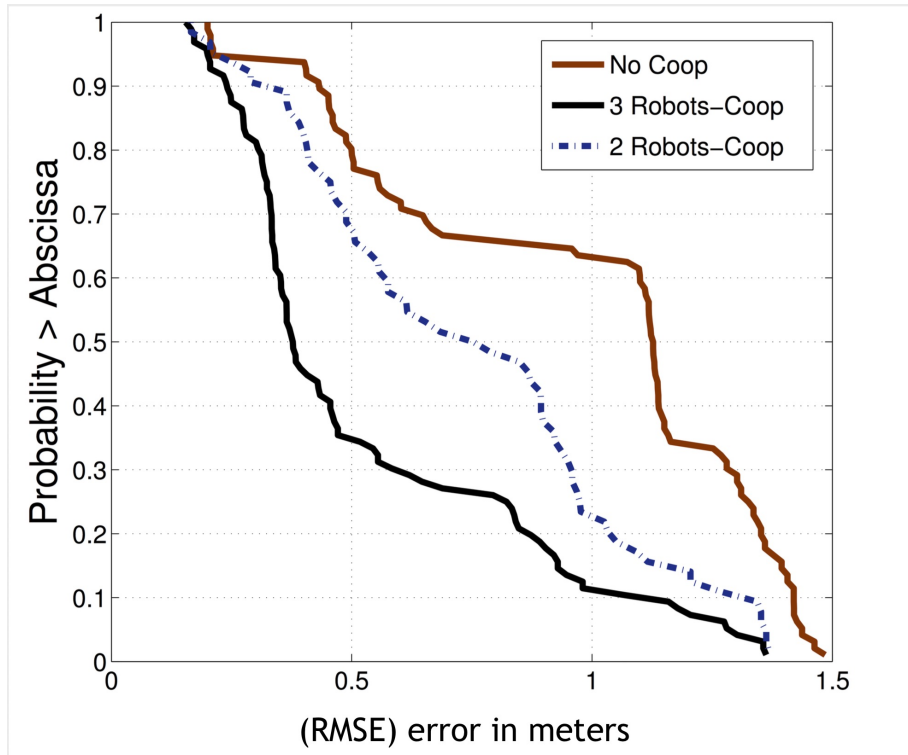
FIGURE 4.4: *RMSE(m) for 2 and 3 Robots using **4 Anchors** configuration and **UWB mode.***

Hybrid Coop with 3.22 meters in error versus ***3 No Coop*** with 7.76 meters in error renders an improvement of 59 percent.

For the effect of anchors, we see that (table 4.6) by doubling the number of anchors we get anywhere from 20 to 34 percent improvement in each likewise scenarios, for example Hybrid versus Hybrid or 2 Coop (WiFi) versus 2 Coop (WiFi) and so forth.

In conclusion, hybrid WiFi-UWB which by default is assumed to be in cooperative mode can render 49 percent improvement over ***3 No Coop*** in 8 anchors configuration. The combination of hybrid WiFi-UWB localization and 8 anchors yields the least error among other scenarios considered in this study.
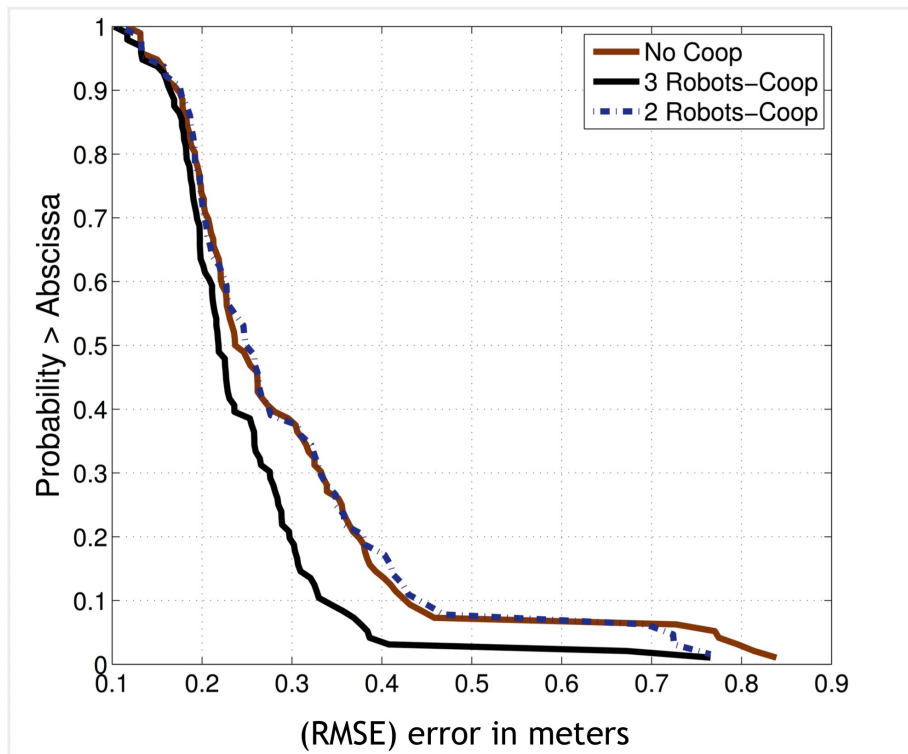
FIGURE 4.5: *RMSE(m) for 2 and 3 Robots using **8 Anchors** configuration and **UWB mode.***

Hybrid localization, with almost 50 percent improvement and widespread availability of WiFi, appears to be a viable alternative for precise indoor localization.
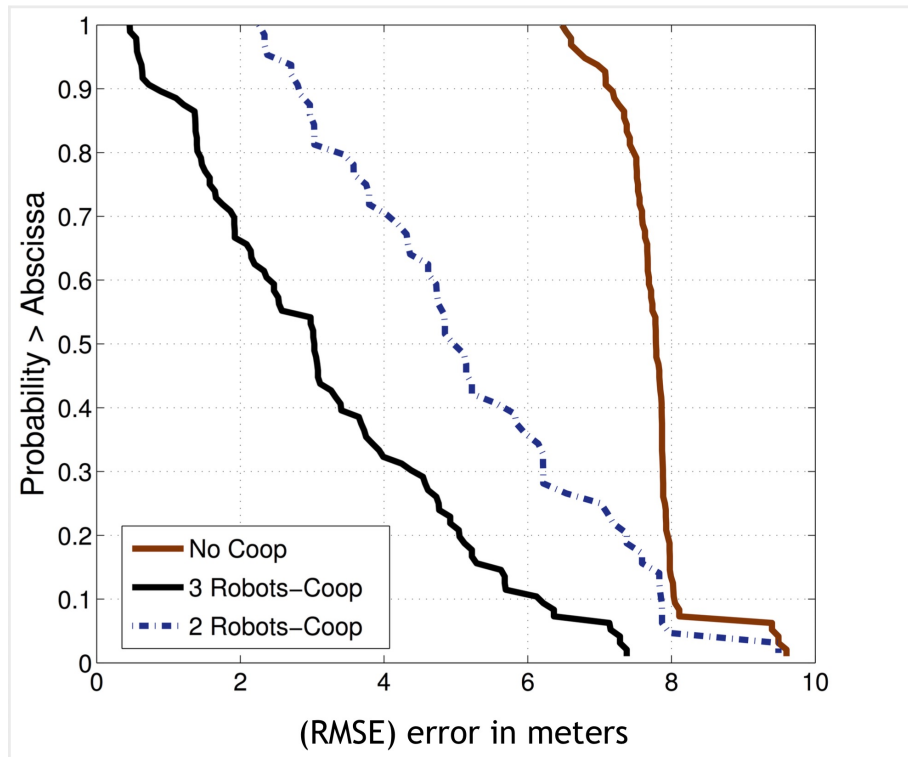
FIGURE 4.6: *RMSE(m) for 2 and 3 Robots using **4 Anchors** configuration and **Hybrid mode.***

TABLE 4.4: Error improvement **4 anchors** configuration, in percentage

	Hybrid Coop	3 Coop	2 Coop	3 No Coop
Mean error (m)	3.22	6.04	6.53	7.76
Hybrid Coop	n/a	47	51	59
3 Coop	–	n/a	8	22
2 Coop	–	–	n/a	16
3 No Coop	–	–	–	n/a

TABLE 4.5: Error improvement **8 anchors** configuration, in percentage

	Hybrid 3 Coop	3 Coop	2 Coop	3 No Coop
Mean error (m)	2.57	4.47	4.73	5.09
Hybrid Coop	n/a	43	46	49
3 Coop	–	n/a	6	12
2 Coop	–	–	n/a	7
3 No Coop	–	–	–	n/a
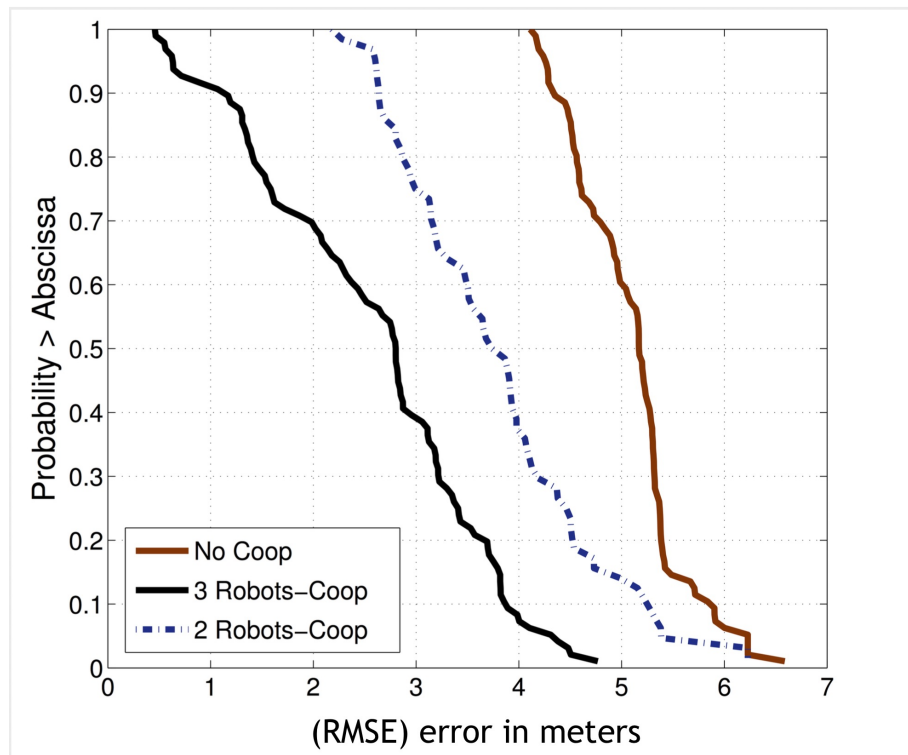
FIGURE 4.7: *RMSE(m) for 2 and 3 Robots using **8 Anchors** configuration and **Hybrid mode.***

TABLE 4.6: Taking the average of all RMSE(m) points, below table shows on average improvement for **8 Anchors versus 4**, in percentage

	Hybrid Coop	3 Coop	2 Coop	3 No Coop
8 Anchors	2.57	4.47	4.73	5.09
4 Anchors	3.22	6.04	6.53	7.76
8 versus 4	20	26	28	34
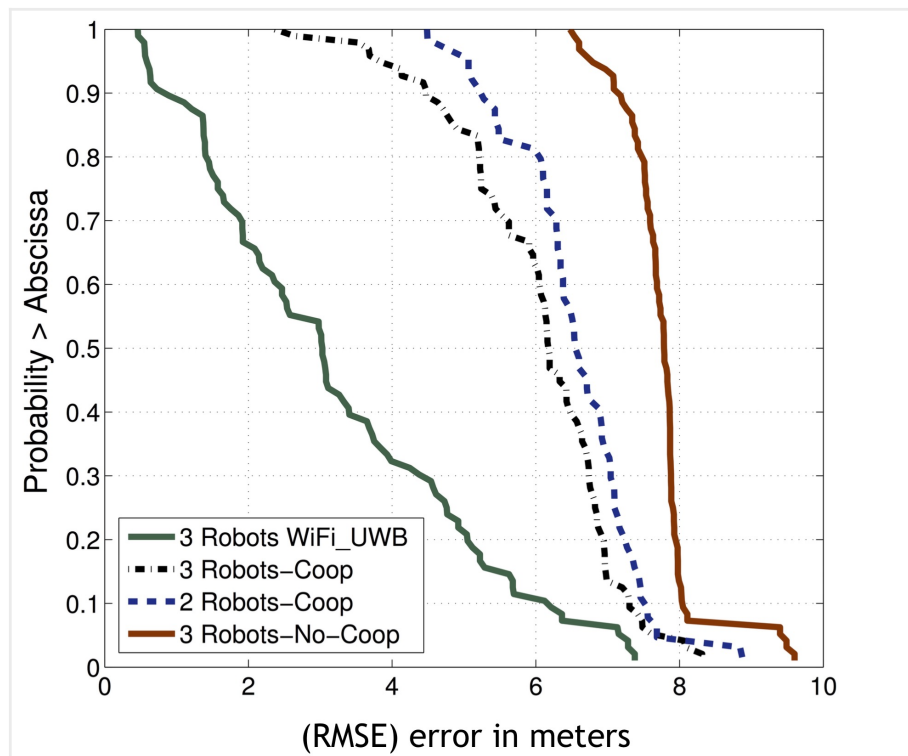
FIGURE 4.8: Comparing *RMSE(m) for WiFi, UWB and hybrid modes in **4 Anchors** configuration.*
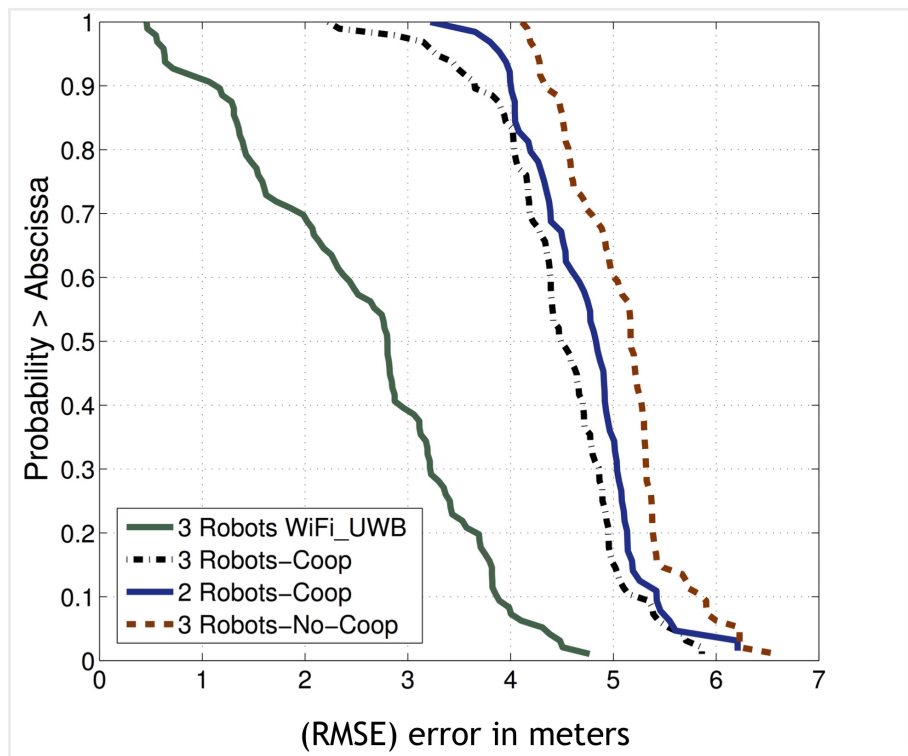
FIGURE 4.9: Comparing *RMSE(m) for WiFi, UWB and hybrid modes in **8 Anchors** configuration*.

5 Particle Filter for Localization

In this chapter, we propose a novel Hybrid WiFi-UWB cooperative localization using Particle Filter. There are different issues in implementing particle filters, one important implementation issue is the Resampling. Our implementation of the PF is similar to Systematic Resampling approach discussed in [109–111]. Due to the complex nature of radio propagation, employing Hybrid and Cooperative localization methods has become increasingly attractive. Accuracy of methods such as TOA and RSS are highly susceptible to non-linear, non-Gaussian channel models in indoor environments. The Particle Filter is chosen for this work to deal with such an environment. We analyze the performance of the Particle Filter versus CRLB by using the theoretical, IEEE 802.11 channel model for RSS and the empirical one for UWB ranging error as presented in [44]. For our performance platform, we leverage off the previous findings in [61], where we used eight fixed anchors (FAs) along with three moving objects (MOs). The performance of the PF results are evaluated in a typical indoor scenario and are compared with CRLB result for the Hybrid (UWB & WiFi), in Cooperative (COOP) and non-Cooperative (NCOOP) modes.

The rest of the chapter is organized as follows: In section 5.1, we define distance measurement error, describe power calculation based on 802.11 RSS model, use the power for TOA-based link error variance selection according to empirical model from [44] and calculate RSS-based link error variance from [40]. Section

5.2, a brief CRLB formulation is outlined. Section 5.3, we formulate the Particle Filter steps based on Bayesian method. Section 5.4, we describe the simulation environment, the definition for Hybrid, Cooperative, non-Cooperative and various configurations. Section 5.5, the results of our research are analyzed in detail. Section 5.6, we show the conclusion of our research and findings.

5.1 Channel models and Ranging error variances

In this section, we define ranging error, power calculation and channel models for ranging error variances of UWB TOA-based and WiFi RSS-based ranging techniques. First, we describe the distance definition and its error, Distance Measurement Error (DME). We then describe the IEEE 802.11 channel model for power (RSS) calculation. The calculated power is used to select link error variance for UWB TOA-based ranging technique according to empirical data [44]. Lastly, we describe the theoretical ranging error variance of RSS-based ranging technique [40].

5.1.1 Ranging Error

Let us assume there are M moving objects (MOs) and A fixed anchor points (FAs), the 2-dimensional coordinates for M MOs, L_M and A FAs, L_A are given by:

$$
\begin{aligned}
L_M &= [(x_1, y_1), ..., (x_M, y_M)]^T \\
L_A &= [(x_{f1}, y_{f1}), ..., (x_{fA}, y_{fA})]^T
\end{aligned}
$$

(5.1)

where (x_i, y_i); $i = 1, ... , M$ denotes the x-y coordinate of M moving objects. and (x_{fj}, y_{fj}); $j = 1, ... , A$ denotes the x-y coordinate of A fixed anchors.

For pairs of MO-to-MO or MO-to-FA within the communication range, a measurement of Euclidean distance $d_{ij} = \sqrt{(x_i - x_j)^2 + (y_i - y_j)^2}$ can be obtained using TOA-UWB or RSS-WiFi ranging techniques. The ranging techniques are susceptible to noise variation of the channel models hence, the Distance Measurement Error (DME), ϵ_{ij} is defined as:

$$\epsilon_{ij} = \hat{d}_{ij} - d_{ij} \tag{5.2}$$

where $\hat{d}_{ij}$ is the estimate of the distance between pairs. ϵ_{ij} will vary between the pairs according to selected link error discussed in subsections 5.1.3 and 5.1.4. The intent is to find the location of moving object with respect to fixed Anchor (FA) locations and compare it with actual location.

We are only analyzing the ranging error variance resulting from distance estimate, $\hat{d}_{ij}$ using the non-linear, non-Gaussian channel model and Particle Filter estimator. We make no assumptions of the speed and the trajectory complexity of the MOs in our analysis.

5.1.2   Power calculation to select ranging error variance for TOA-based technique

The Received Signal Strength (RSS) for a link between a pair is calculated based on the distance, d_{ij} by:

$$RSS(d_{ij}) = RSS_{1m} - 10\alpha \cdot log(d_{ij}) + \chi \tag{5.3}$$

Where RSS_{1m} is the received signal strength at a reference distance of $1m$, α is the path loss gradient and χ is the lognormal shadow fading with zero mean and variance σ_χ^2. The values of $\alpha,\ \ \sigma_\chi$ for LOS and NLOS conditions are listed in different rows in table 5.1.

TABLE 5.1: Path loss gradient & Shadow fading STD

	RSS_{1m}	**UWB**		**WiFi**	
	(dBm)	α	σ_χ	α	σ_χ
LOS	-42	2.0	6.8	2.0	8.0
NLOS	-42	5.6	8.5	3.5	8.0

5.1.3   TOA-based ranging error variance

The variance, $\sigma_{\epsilon_{UWB}}^2$ of Distance Measurement Error in (5.2) for UWB-based link is determined by comparing the value of calculated power in (5.3) with tabulated range in Table 5.2 [1] .

TABLE 5.2: TOA-Based Empirical data

	Power (dBm)		$\sigma_{\epsilon_{UWB}}^2$
	$RSS(d_{ij})$	$>$ -80	$(0.13)^2$
-100 $<$	$RSS(d_{ij})$	$\leq$ -80	$(0.3)^2$
	$RSS(d_{ij})$	$\leq$ -100	$(1.4)^2$

The thresholds and variances defined in table 5.2 are based on Empirical data [44]. There is more general discussion of Distance Measurement Error in [91].

---

[1] Table 2.1 is duplicated here for the ease of referencing.

5.1.4 RSS-based ranging error variance

The variance of Distance Measurement Error in (5.2) for WiFi-based link is determined theoretically based on derivation outlined in [40]. The values of $\alpha, \ \sigma_\chi$ for LOS and NLOS conditions are listed in different rows of table 5.1.

$$\sigma^2_{\epsilon_{WiFi}} \geq (\frac{ln10}{10})^2 \cdot \frac{\sigma_\chi^2}{\alpha^2} \cdot d_{ij}^2 \tag{5.4}$$

5.2 Calculation of CRLB for Performance

To calculate the CRLB, we need to calculate the variance(s) of Distance Measurement Error(s) (DME) for all the links among the MOs and the MOs-to-FAs points. The CRLB provides a lower bound on the error covariance matrix for an unbiased estimate of L_M. For a given estimate of the MOs, $\hat{L_M}$ and Gaussian range measurement R, the Fisher Information Matrix (FIM) can be represented by [92]:

$$J(L_M) = E[\triangledown_{L_M} ln f_R(r; L_M)][\triangledown_{L_M} ln f_R(r; L_M)]^T \tag{5.5}$$

where $f_R(r; L_M)$ is the joint Gaussian PDF given by:

$$f_R(r; L_M) = \frac{1}{(2\pi)^K |\sum|^{\frac{1}{2}}} \times E \tag{5.6}$$

where

$$E = exp\left\{-\frac{1}{2}[r - \mu(L_M)]^T \sum^{-1}[r - \mu(L_M)]\right\} \tag{5.7}$$

and $\mu(L_M)$ is the vector of the actual distances between the nodes corresponding to available K measurements. FIM for the specific PDF in (5.6) can be written

as:

$$J(L_M) = [G(L_M)]^T \sum{}^{-1} [G(L_M)] \tag{5.8}$$

where

$$G(L_M)^T = \begin{pmatrix} cos\phi_1 & cos\phi_2 & ... & cos\phi_k \\ sin\phi_1 & sin\phi_1 & ... & sin\phi_k \end{pmatrix} \tag{5.9}$$

$$\sum = diag(\lambda_1 \quad \lambda_2 \quad ... \quad \lambda_k) \tag{5.10}$$

ϕ_i representing the angle between the nodes from ith measurement. and λ_i is the variance of range estimate from the ith measurement. The variance calculation are discussed in subsections 5.1.3 and 5.1.4 that are used to replace λ_i based on a given configuration shown in Table 5.3.

TABLE 5.3: Configuration & selected Ranging Technique

Mode	FA	MO	MO to FA	MO to MO (COOP mode)
	WiFi	WiFi	RSS-based	RSS-based
Hybrid	WiFi	UWB	RSS-based	TOA-based
	UWB	UWB	TOA-based	TOA-based
Hybrid	UWB	WiFi	TOA-based	WiFi-based

The CRLB is given by:

$$CRLB = [J(L_M)]^{-1} \tag{5.11}$$

And, the Root-Mean-Square-Error, RMSE is given by:

$$RMSE = \sqrt{trace(CRLB)} \tag{5.12}$$

5.3   Particle Filter Formulation

The Particle Filter is chosen for this work due to nature of non-closed form, non-linear and non-Gaussian channel models for RF localization algorithm. The PF

state is defined by uniformly Random X or Y movement of moving object (MO). The PF observation is modeled based on empirical data for UWB-TOA and theoretical approach for WiFi-RSS ranging. The distance of the moving object is obtained with respect to fixed anchors (FA) and other moving objects in cooperative mode. In the following subsections we describe the assumptions for PF setup, derive PF recursion step, outline the PF implementation and discuss the simulation environment.

5.3.1   PF setup

The notations moving forward and the assumptions for Bayesian recursion are defined here. First, the notations used are, $\mathbb{P}$ denoting probability, p denoting the index of a particle, nP denoting number of particles and $nSMP$ denoting number of samples (movement). Second, the PF State (or movement) and Observation (or measurement) are defined as d_p and RSS_p respectively. Lastly, given the random nature of MO movements and independent Observations we assume that the current location of MO depends only on the previous location hence, a Markov Process for the MOs movement (PF State),

$$\mathbb{P}(d_p/d_{0:p-1}) = \mathbb{P}(d_p/d_{p-1}) \tag{5.13}$$

and, the current PF observation, RSS_p depends only on the current PF state d_p, therefore:

$$\mathbb{P}(RSS_p/d_{0:p}, RSS_{0:p-1}) = \mathbb{P}(RSS_p/d_p) \tag{5.14}$$

5.3.2 PF Recursion Step

Leveraging off of the assumptions highlighted in subsection 5.3.1, we start with Bayesian rule and skip detail derivation for future chapter, we arrive at the recursion for $Posterior$ of State given our measurements, $\mathbb{P}(d_{0:p}/RSS_{0:p})$, applying Bayes rule:

$$\mathbb{P}(d_{0:p}/RSS_{0:p}) = \frac{\mathbb{P}(RSS_{0:p}/d_{0:p}) * \mathbb{P}(d_{0:p})}{\mathbb{P}(RSS_{0:p})} \tag{5.15}$$

Starting with Bayes rule and applying our assumptions we arrive at PF Recursion step:

$$\mathbb{P}(d_p/RSS_{0:p}) = \frac{\mathbb{P}(RSS_p/d_p)}{\mathbb{P}(RSS_p/RSS_{0:p-1})} * \mathbb{P}(d_p/RSS_{0:p-1}) \tag{5.16}$$

where $p = 1, 2, ..., nP$. Basically, we want to pick the most suitable next state d_p given the set of observations RSS_p. Obviously, we like to pick the most likely or highest marginal $Posterior$.

5.3.3 PF implementation

Our model for state are sample points shown on Fig. 5.1. The Observation model is defined in (5.3). However, this is just a Power measurement and there are other transformations due to LOS, NLOS, UWB, WiFi conditioning in order to evaluate our Distance Measurement Error hence, link error variance.

By observing (5.16), it appears that the $Prior$ for the past $p - 1$ observations are scaled to form the marginal $Posterior$ on the left hand side. The Scale factor can be considered as $Weight$ factor where we can recursively update by performing
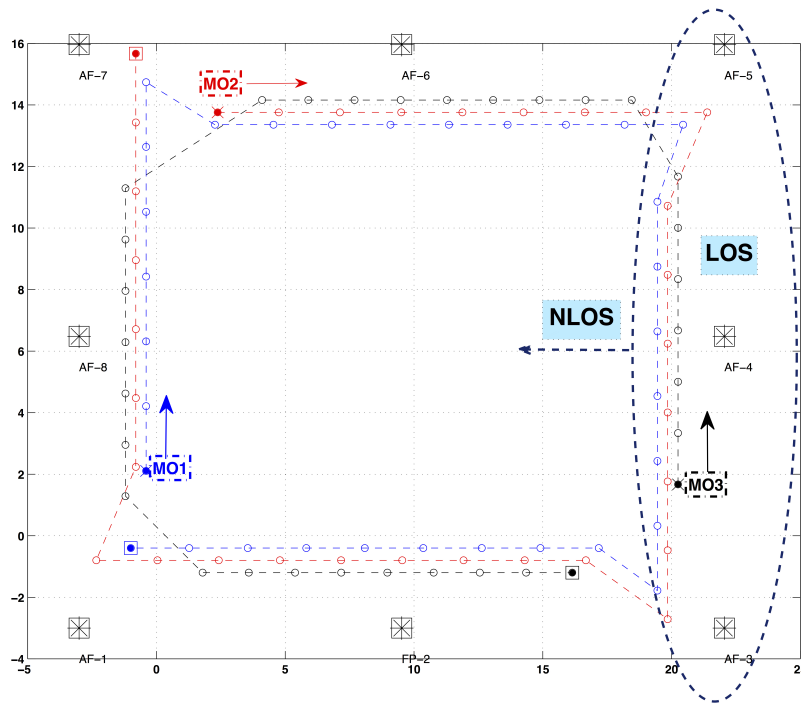
FIGURE 5.1: **Eight Fixed Anchors** {AF1, AF2,.....,AF8} and **three moving objects** {MO1, MO2, MO3}. The objects move along the dotted lines and in the direction of arrows.

nP scaled version of $Prior$ to form a new $Posterior$ distribution.

$$Weight_p = \frac{\mathbb{P}(RSS_p/d_p)}{\mathbb{P}(RSS_p/RSS_{0:p-1})} \tag{5.17}$$

Given d_p, the numerator can be measured and the denominator does not depend on the state, d_p. For the purpose of our simulation we will use a Gaussian $Prior$ with variance σ_{RSS}^2 and the mean is adjusted by the power calculated for d_p, RSS_p.

$$f_W(w_p) = \frac{1}{2\pi\sigma_{RSS}^2} exp \left\{ -\frac{(RSS_{ref} - RSS_p)^2}{2\sigma_{RSS}^2} \right\} \tag{5.18}$$

RSS_{ref} is the power at the actual location. The state samples are also distributed in random using Gaussian with a different variance $\sigma_{d_p}^2$ prior to Observation (measurement). All the configurations outlined in Table 5.3 are simulated using

the pseudo steps in Algorithm 1. Now that we got some idea of the work in-
volved, let us evaluate some initial result for performance of PF in subsection
5.4.1 and set the stage for the intended evaluation in section 5.5.

Algorithm 1 PF Algorithm flow

 1: **if** (NCoop) **then**   ▷ MOs in NCoop mode
 2:      RefPoints = 8;   ▷ 8 Fixed Anchors
 3: **else**   ▷ 3 Coop MOs
 4:      RefPoints = 11;
 5: **end if**
 6: **for** $S = 1 \rightarrow nSMP$ **do**   ▷ *Objects movement*
 7:      **for** $R = 1 \rightarrow RefPoints$ **do**
 8:          **for** $p = 1 \rightarrow nP$ **do**   ▷ *Particle iterations*
 9:              *a) Measurement*
10:              *b) Weight update*
11:          **end for**
12:          *1) Normalize the Weight*
13:          *2) Randomly Sample the above CDF*
14:          *3) Pick maximum likelihood sample*
15:          *4) Selection of new State, hence lowest DME*
16:      **end for**
17: **end for**

5.4   Performance Analysis scenarios

In this section, we describe the simulation environment and setup in detail. The
Hybrid, Cooperative, non-Cooperative are defined and various configurations
are presented in tabular form.

5.4.1 Simulation environment

In Fig. 5.1, there are eight FAs and three MOs, two moving clockwise and the third counter-clockwise. The X or Y movements are advanced according to uniformly random distribution. In this section we are evaluating the effect of number of particles nP, different variance values for State and Observation to set the stage for the intended evaluation. In Fig. 5.2, we are evaluating the effect of 8 and 16 particles ($nP = 8, 16$) for FA and MO in WiFi-enabled mode. In COOP mode, the results are very close however, in NCOOP mode the result for higher number of particle ($nP = 16$) is slightly better, from here on the evaluation is focused on $nP = 16$.
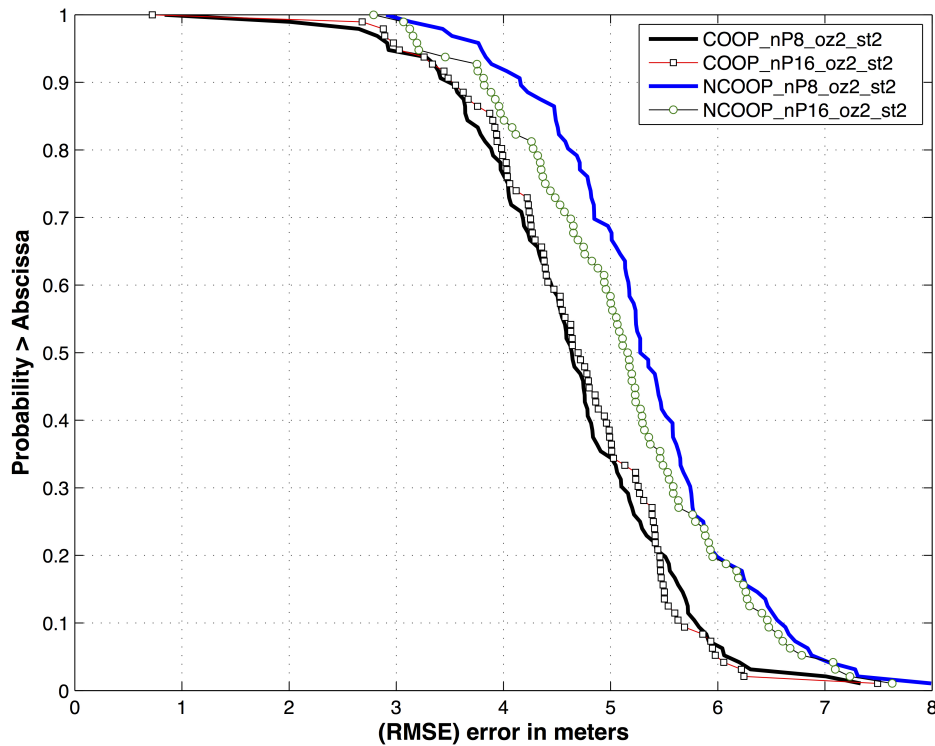
FIGURE 5.2: **32** Samples, **8** Fixed Anchors and **3** Moving Objects. Comparison of 8 vs. 16 particles for **Coop.** and **Non-Coop.** mode.

In Fig. 5.3 and 5.4 the variances for State (st) and Observation (oz) are varied for COOP and NCOOP respectively. The FAs and MOs are UWB-enabled. As

expected, at low variances for state and observation, both at 2 we get the best performance and conversely we get the worst when both are set to 8. The result for UWB-enabled mode is presented graphically in Figs. 5.3 and 5.4. For other scenarios (WiFi, Hybrid) are reviewed (is not included in this chapter) and the results corroborates with the results shown in this chapter. After this initial PF evaluation, we use the following parameters for the reset of this chapter: $nP = 16$, $\sigma_{d_p}^2 = 8$, & $\sigma_{RSS}^2 = 8$.
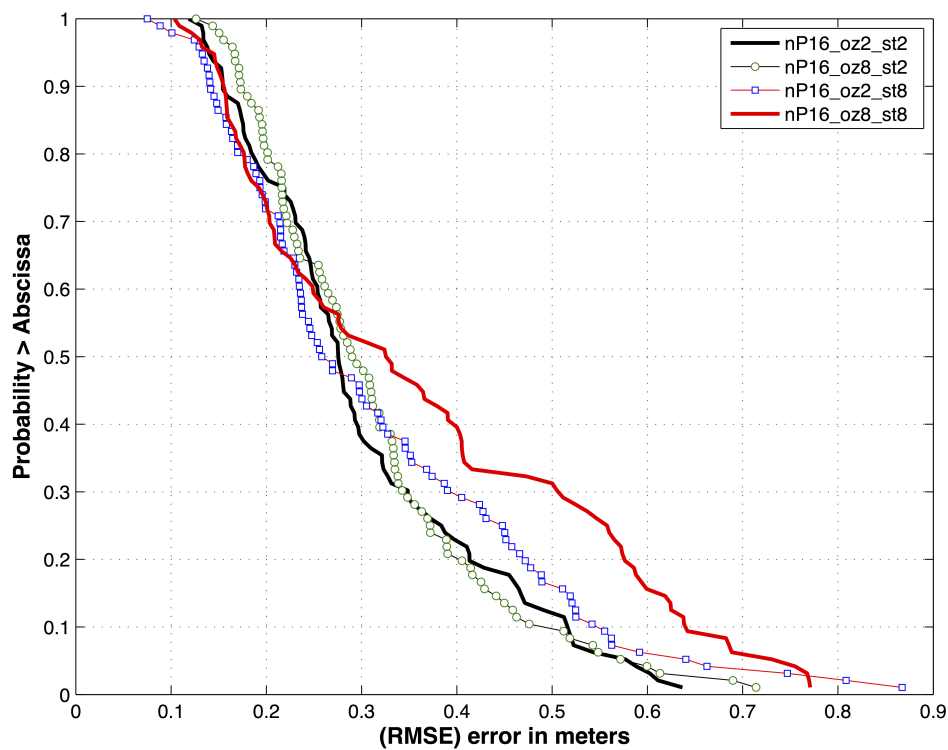
FIGURE 5.3: Using **16** particles and assessing the *Effect of different State and Observation variances on error in cooperative (COOP) mode.*

5.4.2 Hybrid and Cooperative Configuration

Hybrid is when a pair (MO-to-MO or MO-to-FA) can communicate over WiFi and UWB RF signaling hence RSS-based and TOA-based ranging is applied respectively. Cooperative, refers to MOs communicating among each other in
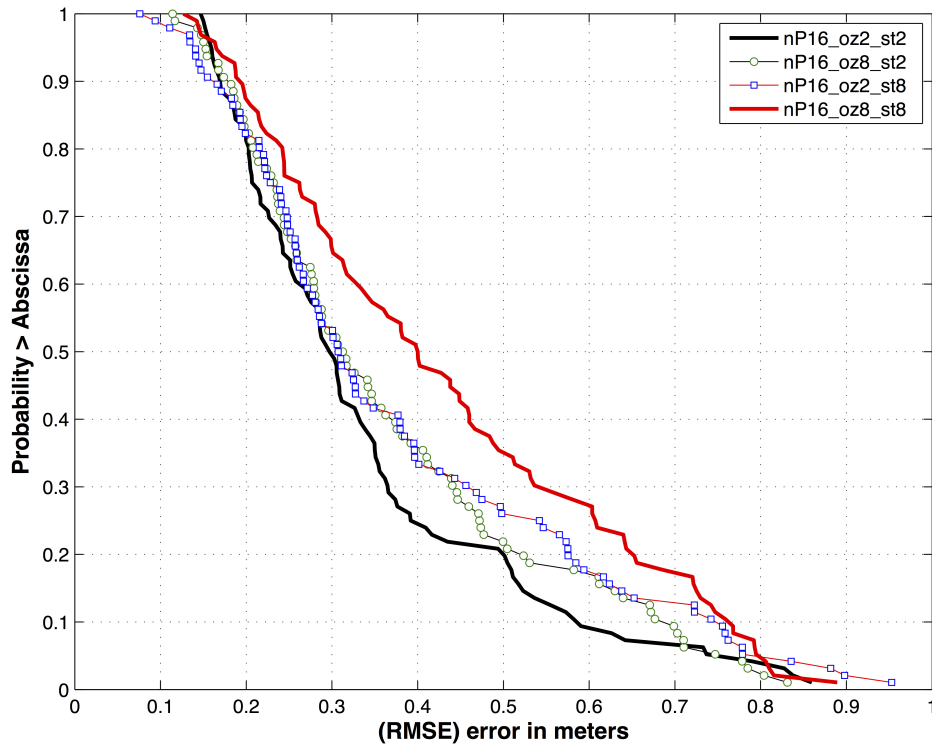
FIGURE 5.4: Using **16** particles and assessing the *Effect of different State and Observation variances on error in Non-cooperative (NCOOP) mode.*

pairwise configuration. The choice of ranging technique is determined based on a given configuration shown in Table 5.3.

5.5   Results and Discussion

The simulation environment for all our simulation runs moving forward is based on parameters outlined in Table 5.4. In this section, the Figs. 5.5, 5.6, 5.7, 5.8 and tabulated results in tables 5.5 and 5.6 are analyzed and the performance of PF is compared to CRLB. In our review of the results we use the 50th percentile and assess the performance accordingly. Also, in each of the figures to be discussed, there is a mix of COOP and NCOOP both for PF and CRLB. The COOP and

TABLE 5.4: Simulation environment

Sim Parameters			PF Parameters		
$nSMP$	FAs	MOs	nP	$\sigma_{d_p}^2$	σ_{RSS}^2
32	8	3	16	8	8

NCOOP graphs for CRLB are represented by solid Blue and Red lines respectively. In general, one can observe an improving trend stemming from Hybrid COOP mode. However, it is evident that PF does not perform as well in low error condition, for example UWB. The highlights are as follow:

$WiFi_{Anc.}, WiFi_{Obj.},$ Fig. 5.5, where FAs and MOs are WiFi-enabled hence high RMSE values, the PF tracks the CRLB both in COOP and NCOOP mode. The PF is off by 0.5 meter both in COOP and NCOOP mode with respect to the CRLB.
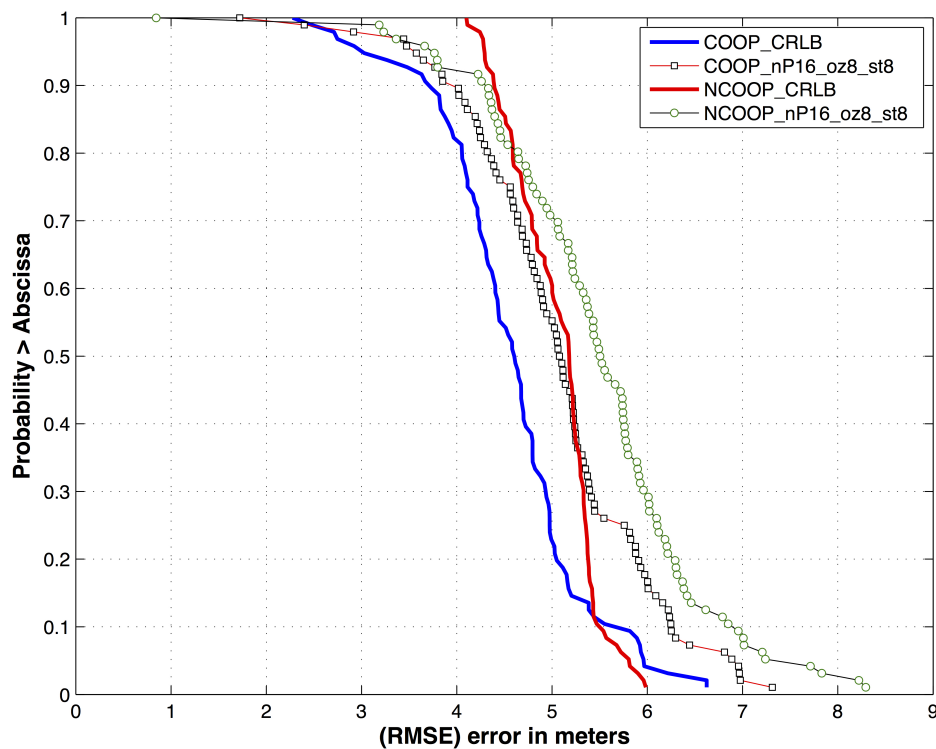
FIGURE 5.5: *Particle filter error versus CRLB operating in COOP and NCOOP mode using **WiFi** signaling where FAs and MOs are both WiFi-enabled.*

$Hybrid$ ($WiFi_{Anc.}, UWB_{Obj.}$), Fig. 5.6, in Hybrid mode, the MOs are UWB-enabled and FAs remain WiFi-enabled. In here, we have high RMSE values aided by low RMSE values MOs improving the overall RMSE. As a result, the PF outperforms the CRLB when in COOP mode. In NCOOP mode, there are not much differences relative to non-Hybrid mode per Fig. 5.5. The PF performs better by 0.5 meter in COOP and is off by 0.7 meter in NCOOP mode relative to the CRLB.
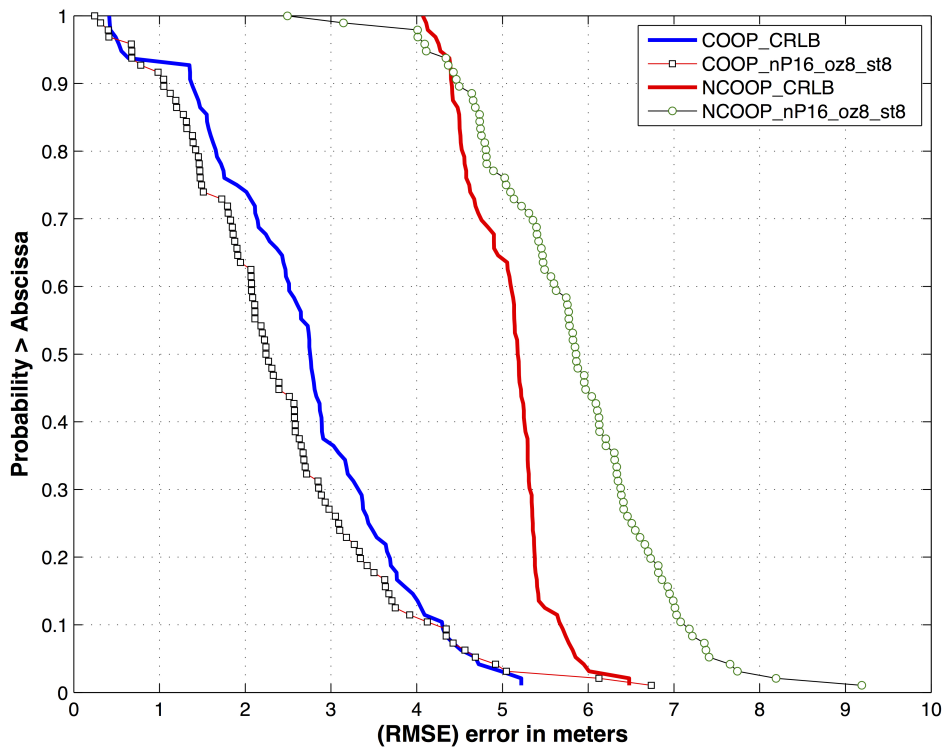
FIGURE 5.6: *Particle filter error versus CRLB operating in COOP and NCOOP mode using **Hybrid** signaling where FAs are WiFi-enabled and MOs are UWB-enabled.*

$UWB_{Anc.}, UWB_{Obj.}$, Fig. 5.7, where FAs and MOs are UWB-enabled hence low RMSE values, the PF does not perform well relative to the CRLB in neither cases, COOP or NCOOP mode. The PF performs worse by 0.12 meter in COOP and 0.17 meter in NCOOP mode compared to the CRLB.
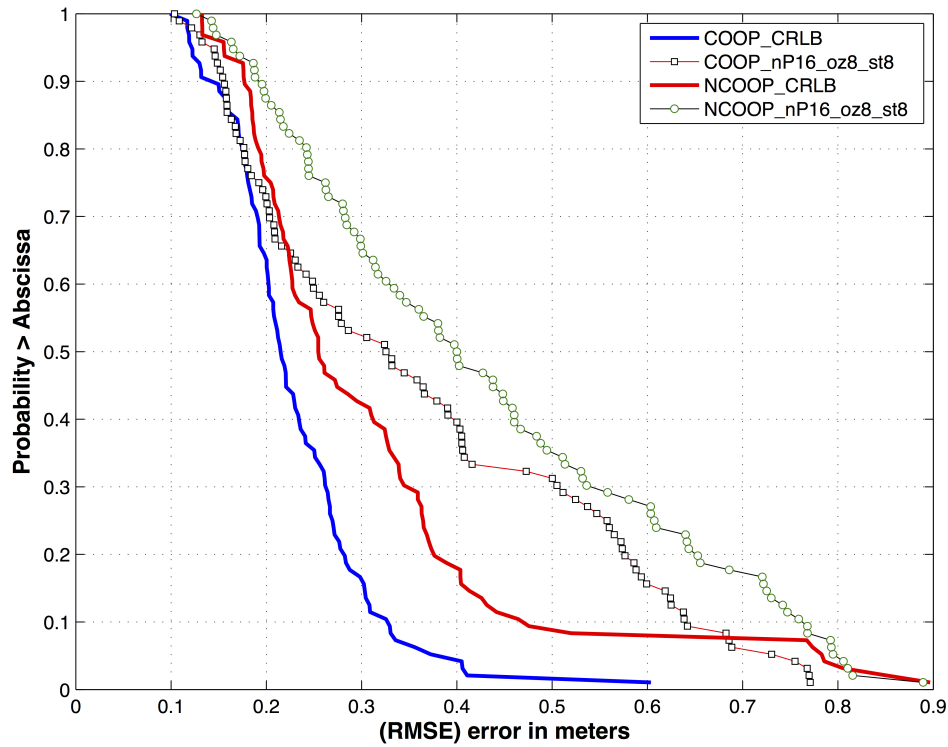
FIGURE 5.7: *Particle filter error versus CRLB operating in COOP and NCOOP mode using **UWB** signaling where FAs and MOs are both UWB-enabled.*

$Hybrid\,(UWB_{Anc.}, WiFi_{Obj.})$, Fig. 5.8, in Hybrid mode, the MOs are WiFi-enabled and FAs remain UWB-enabled. In here, we have low RMSE values mixed in with high RMSE values MOs which are not helping the overall RMSE as compare to 5.6. The PF performs better in COOP than NCOOP mode. In NCOOP mode, the performance is similar to non-Hybrid mode result per Fig. 5.7. The PF performs worse only by 0.025 meter in COOP and worse by 0.15 meter in NCOOP mode in comparison to the CRLB.

The RMSE deviation results for the PF with parameters ($nP = 16$, $\sigma_{d_p}^2 = 8$, & $\sigma_{RSS}^2 = 8$) are tabulated in tables 5.5 and 5.6. There is higher Mean values for the PF except in Hybrid COOP where the FAs are WiFi-enabled and MOs are UWB-enabled. The STD ratio (PF/CRLB) for UWB COOP is almost the same as WiFi NCOOP. The STD for the PF is higher than the CRLB in all cases.
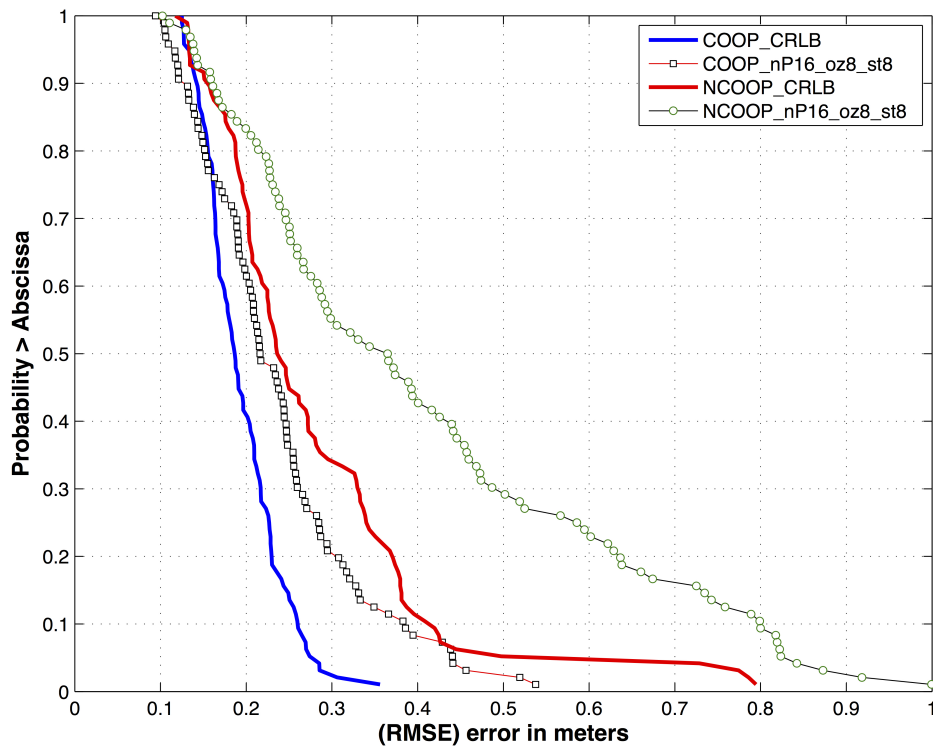
FIGURE 5.8: *Particle filter error versus CRLB operating in COOP and NCOOP mode using **Hybrid** signaling where FAs are UWB-enabled and MOs are WiFi-enabled.*

5.6   Summary

In this chapter, we implemented a Particle Filter for the non-linear, non-Gaussian channel models for RF localization in a Hybrid Cooperative configuration. We used UWB TOA-basedand WiFi RSS-based ranging techniques. We formulated the Bayesian approach to show the recursion step for Particle Filter implementation. We simulated and analyzed the quantitative performance of PF versus CRLB in Cooperative (COOP) and Non-Cooperative (NCOOP) both in Hybrid and non-Hybrid configurations. When the moving objects (MOs) and fixed anchors (FAs) are UWB-enabled, hence low error (RMSE) value, we showed that the PF performs poorly both in COOP and NCOOP compared to CRLB. However, in a case when moving objects and fixed anchors are all WiFi-enabled,

TABLE 5.5: RMSE deviation for PF with WiFi-enabled FAs

		Mean	STD
	WiFi-enabled MOs in Coop mode		
PF		5.0500	0.9775
CRLB		4.5540	0.8112
	WiFi-enabled MOs in NCoop mode		
PF		5.4630	1.1340
CRLB		5.0400	0.4436
	UWB-enabled MOs in Coop mode		
PF		2.4230	1.2320
CRLB		2.7010	1.1280
	UWB-enabled MOs in NCoop mode		
PF		5.8140	1.0890
CRLB		5.0670	0.4977

TABLE 5.6: RMSE deviation for PF with UWB-enabled FAs

		Mean	STD
	WiFi-enabled MOs in Coop mode		
PF		0.3631	0.1955
CRLB		0.2294	0.0778
	WiFi-enabled MOs in NCoop mode		
PF		0.4334	0.2079
CRLB		0.3104	0.1661
	UWB-enabled MOs in Coop mode		
PF		0.2361	0.0956
CRLB		0.1940	0.0459
	UWB-enabled MOs in NCoop mode		
PF		0.4083	0.2283
CRLB		0.2785	0.1350

hence high error (RMSE) value, the PF performs more closely and consistently compared to CRLB. In general, the particle filter performs much better in environment with high RMSE value in non-Hybrid configurations. We showed that in Hybrid WiFi/UWB and Cooperative configuration, the Particle Filter consistently performs well in either of low or high RMSE value environments.

6 Precise Tracking of Things

In this chapter, we focus on WiFi RF signaling simulation and analysis. We discuss our solution for overcoming the WiFi's sub meter error (accuracy) by introducing our novel Hybrid 3D Database for localization using Kernel Method Particle Filter to achieve sub centimeter precision. One important implementation issue in PF is the Resampling. Our implementation of the proposed PF is complemented by our 3D database where the stored Probability Mass Functions, PMFs of a Grid point is used for *Importance Sampling*. This is used in a similar fashion to Systematic Resampling as discussed in [109–111].

Due to complex nature of radio propagation and high degree of error in WiFi, a hybrid of Bluetooth and WiFi RF signaling along with fusion of LIDAR coordinate and IMU is proposed for creation of this high resolution signature database that includes PMF data per grid point. This database, cooperative (COOP) moving objects and Kernel Method Particle Filter is our solution to sub-centimeter localization and navigation. Employing Hybrid database and Cooperative localization has been gaining momentum. Accuracy of methods such as TOA and RSS are highly susceptible to non-linear, non-Gaussian channel models in indoor environments. The Particle Filter with a Kernel approach and Hybrid 3D database are chosen to perform with precision in an indoor environment. Unlike the previous chapter 5, the simulations are recreated exclusively for WiFi ranging using the theoretical, IEEE 802.11 channel model for RSS and the empirical

data for UWB ranging error is not applicable here as discussed in [44]. Furthermore, for the purpose of performance analysis, we leverage off our work in [61] to stay with eight fixed anchors (FAs) along with three moving objects (MOs). The new simulations are focused on WiFi ranging and line of sight assumption (LOS) which is more relevant for analysis to high resolution signature database. We analyze the effect of different parameters on PF performance versus CRLB, address limitations and discuss our novel solution for precise indoor localization. In our novel approach, we are not bounded by fixed anchor points and our reliance for precision is our high resolution signature databases hence, lower variance for distance measurement error. The high resolution signature databases are stored and accessed to and from the Cloud storage respectively.

The rest of the chapter is organized as follows: In section 6.1, we define channel model describing distance measurement error, power calculation based on 802.11 RSS model, variance of WiFi-link and finally describe *the Grid, the baseline for our high resolution signature database.* Section 6.2, we define our new approach to Kernel Method Particle Filter based on Bayesian method and empirical PMF. Section 6.3, we describe the Notations, Assumptions and simulation setup. Section 6.4, we analyze the effect of various parameter settings on Particle filter and compare the results to CRLB. Section 6.5, we summarize the conclusion of our research and findings. Appendix A, a brief CRLB formulation is outlined. Appendix B, The detailed derivation of Bayesian Recursion for Particle Filter.

6.1 Channel models and High Resolution Signature Database

In this section, a WiFi channel model is described by distance measurement error, WiFi-link variance is calculated according to RSS-based ranging technique [40], power calculation of Received Signal Strength (RSS) based on 802.11 RSS model.

Lastly, the high resolution signature database is described.

6.1.1 WiFi Channel Model

Considering M moving objects (MOs) and A fixed anchor points (FAs), the 2-dimensional coordinates for M MOs, L_M and A FAs, L_A are given by:

$$
\begin{aligned}
L_M &= [(x_1, y_1), ..., (x_M, y_M)]^T \\
L_A &= [(x_{f1}, y_{f1}), ..., (x_{fA}, y_{fA})]^T
\end{aligned}
\tag{6.1}
$$

where (x_i, y_i); $i = 1, ... , M$ denotes the x-y coordinate of M moving objects. and (x_{fj}, y_{fj}); $j = 1, ... , A$ denotes the x-y coordinate of A fixed anchors.

For pairs of MO-to-MO or MO-to-FA within the communication range, a measurement of Euclidean distance $d_{ij} = \sqrt{(x_i - x_j)^2 + (y_i - y_j)^2}$ can be obtained using RSS-WiFi ranging techniques. The ranging techniques are susceptible to noise variation of the channel models hence, the Distance Measurement Error (DME), ϵ_{ij} is defined as:

$$
\epsilon_{ij} = \hat{d}_{ij} - d_{ij}
\tag{6.2}
$$

where $\hat{d}_{ij}$ is the estimate of the distance between pairs. ϵ_{ij} will vary between the pairs according to link error discussed in subsection 6.1.2. This is how the location of moving object is determined with respect to fixed Anchor (FA) locations and compared to its true location.

We are only analyzing the ranging error variance resulting from distance estimate, $\hat{d}_{ij}$ using the non-linear, non-Gaussian channel model and Particle Filter estimator.

6.1.2   WiFi-link variance

The variance of Distance Measurement Error in (6.2) for WiFi-link is determined theoretically based on derivation outlined in [40]. The values of $\alpha,\ \sigma_\chi$ for LOS condition are listed in table 6.1.

$$\sigma^2_{\epsilon_{WiFi}} \geq (\frac{ln10}{10})^2 \cdot \frac{\sigma^2_\chi}{\alpha^2} \cdot d^2_{ij} \tag{6.3}$$

As evident from (6.3) the variance is directly impacted by the square of distance, d^2_{ij} hence, impacting Root Mean Square Error (RMSE) of localization accuracy. The RMSE can significantly be lowered due to confluence of Hybrid of WiFi, Bluetooth, LIDAR, IMU and smaller distances as a result of Grid density. That is how a high resolution signature database (HRSD) can enable us to achieve much lower RMSE and as result more precise localization and tracking.

6.1.3 Received Signal Strength calculation

The Received Signal Strength (RSS) for a WiFi-link between a pair is calculated based on the distance, d_{ij} according to:

$$RSS(d_{ij}) = RSS_{1m} - 10\alpha \cdot log(d_{ij}) + \chi \tag{6.4}$$

Where RSS_{1m} is the received signal strength at a reference distance of $1m$, α is the path loss gradient and χ is the lognormal shadow fading with zero mean and variance σ_χ^2. The values of α, σ_χ are chosen for Line of Sight (LOS) condition listed in table 6.1.

6.1.4 High Resolution Signature Database

A High Resolution Signature Database (HRSD) is pivotal to precise localization. We start with collection system known as the Mobile Indoor Geo-Location Survey Unit (MIGSU) to collect high resolution data to create signature databases. The MIGSU system is remotely controlled and collects Wi-Fi, Bluetooth, Magnetic and LIDAR data for the purpose of indoor Geo location and digital mapping. MIGSU is remotely controlled within a building or venue while it collects the signal data in real time, parses the data, and creates the signature databases. The 3D digital map is developed from LIDAR data during post processing. The MIGSU system uses specially designed hardware platform in a self-contained

TABLE 6.1: Path loss gradient and Shadow fading STD for Line of Sight condition

Condition	$RSS_{1m}(dBm)$	α	σ_χ
LOS	-42	2.0	8.0

mobile unit to collect the signals in real time. MIGSU utilizes a precision Inertial Measurement Unit (IMU) to precisely calculate its known position then uses the position data to tag the captured signals. The Wi-Fi collection component utilizes three dual band 802.11 a/b/g/n ($2.4/5.2\ GHz$) chip sets as the receivers. These receivers also collect Bluetooth 802.15 data. The three receivers antennas are spaced at precise lateral spacing of $25cm$ to provide uncorrelated position signal data. Experiments have shown that at $25cm$, which is the lowest common denominator for 2.4 and $5.2\ GHz$ wavelengths, the received signals are uncorrelated and independent. This means that at this spacing the RF signal is distinct. Each antenna and antenna cable are also measured using a network analyzer to create a calibration table for amplitude corrections to compensate for small differences in the receive chain.

A grid point is a position in space correlated to the venue in X,Y, Z coordinates for the building being mapped, *North(X), East(Y) and Down(Z), NED navigation.* Grid Spacing is the distance between grid points and defines the database density. Each grid point will consist of WiFi and Bluetooth RF signature as well as the fusion of LIDAR coordinate and IMU attributes.

LIDAR is a LASER Detection and Ranging technology and uses lasers to determine the range of an object by calculating the time of flight for the signal to hit an object and return plus its intensity. The magnetic fingerprint is created from the IMU and is binned and tagged by the database management with a position. The key difference with this data is that there is only a single emitter, earth's magnetic field. All magnetic collections are stored for a collection period creating an array of *X,Y,Z* axis magnetic measurements.

The Wi-Fi signature database is made up of individual grid points spaced at $25cm$ each. The collected data is pre-processed for faster cloud access and placed

in the signature. This data will consist of the Mean RSS, Standard Deviation RSS, Min RSS, and Max RSS values for each emitter. The Probability Mass Function (PMF) is also stored for each signature. The current required number of samples for the PMF is 50 samples per grid point per emitter. An *accurate timestamps* is crucial for correlating and fusion of LIDAR 3D coordinate and IMU attribute to ensure the accuracy of database. The effects of these *time varying fields, sample density on accuracy, stability of the database* will be submitted in a separate paper.

The outcome from this Novel approach in creation of high resolution database, is shorter spacing or distance hence, lower RMSE. Furthermore, the availability of Probability Mass Function (PMF) for use in Importance Sampling *of Kernel Method Particle Filter (KMPF).*

6.2 Particle Filter Formulation

The Particle Filter is chosen for this work due to nature of non-closed form, non-linear and non-Gaussian channel models for RF localization algorithm. The PF state is defined by uniformly Random X or Y movement of moving object (MO). The PF observation is modeled based on theoretical approach for WiFi-RSS ranging. The distance of the moving object is obtained with respect to fixed anchors (FA) and other moving objects when in cooperative mode. The published results in our previous work [84] was based on choice of Gaussian with a different variances for our *importance sampling.* It is important to note that the choice of more appropriate probability Mass function for *importance sampling* results in more realistic *Posterior* estimation. The PMF information and *RSS* values are provided by HRSD.

The main engine driving the Particle Filter implementation is the recursion for estimating *Posterior* and proper choice for *importance sampling*. The assumption and the derivation of Bayesian recursion for *Posterior* estimation is detailed out in Appendix B.

Our model for state are sample points shown on Fig. 6.1. The Observation model is defined in (6.4). However, this is just a Power measurement and is preprocessed along with fusion of LIDAR coordinates and IMU attributes as well as cross validation across different data points to ensure a robust build of HRSD as previously described in subsection 6.1.4.

Let us consider the *importance weight*, (6.5) derived in Appendix A:

$$Weight_p = \frac{\mathbb{P}(RSS_p/d_p)}{\mathbb{P}(RSS_p/RSS_{0:p-1})} \tag{6.5}$$

Given d_p, the numerator can be measured and the denominator is not dependent on the state, d_p. For the purpose of our simulation we will use a Gaussian *Prior* with variance σ^2_{RSS} and the mean is adjusted by the power calculated for d_p, RSS_p.

$$f_W(w_p) = \frac{1}{2\pi\sigma^2_{RSS}} exp\left\{-\frac{(RSS_{ref} - RSS_p)^2}{2\sigma^2_{RSS}}\right\} \tag{6.6}$$

RSS_{ref} is the power at the actual location. The state samples are also distributed in random using Gaussian with a different variance $\sigma^2_{d_p}$ prior to Observation (measurement). Simulations are performed using the pseudo steps in Algorithm 2.

In the case of Kernel Method Particle Filter (KMPF), the information provided by HRSD are further processed for the best candidate in PMFs. The best of three PMFs provided by HRSD is sorted out using *Kullback Leibler divergence* (KLD) method (6.7). The select, an empirical PMF will be used for *Importance Sampling*

instead of the theoretical Gaussian distribution that is used for simulations in Algorithm 2. Having a true sample representation for PMF will be pivotal for more precise localization and tracking of things, PToT.

$$D_{KL}(PMF_i||PMF_j) = \sum_{k=1}^{50} PMF_i(k) \times \log \frac{PMF_i(k)}{PMF_j(k)} \tag{6.7}$$

Next we evaluate our preliminary simulation results for parameter effects on performance of PF in section 6.4.

Algorithm 2 PF Algorithm flow

1: **if** (NCoop) **then**   ▷ MOs in NCoop mode
2:     RefPoints = 8;   ▷ 8 Fixed Anchors
3: **else**   ▷ 3 Coop MOs
4:     RefPoints = 11;
5: **end if**
6: **for** $S = 1 \rightarrow nSMP$ **do**   ▷ *Objects movement*
7:     **for** $R = 1 \rightarrow RefPoints$ **do**
8:         **for** $p = 1 \rightarrow nP$ **do**   ▷ *Particle iterations*
9:             *a) Measurement*
10:            *b) Weight update*
11:        **end for**
12:        *1) Normalize the Weight*
13:        *2) Randomly Sample the above CDF*
14:        *3) Pick maximum likelihood sample*
15:        *4) Selection of new State, hence lowest DME*
16:    **end for**
17: **end for**

6.3   Simulation Environment

In this section, we describe the notations, assumptions for Particle Filter implementation, describe CRLB for our analysis and the setup of our simulation environment.

6.3.1   Notations

The notations used are, $\mathbb{P}$ denoting probability, p denoting the index of a particle, nP denoting number of particles and $nSMP$ denoting number of samples and MO denoting a moving object. The PF State (or movement) and Observation (or measurement) are denoted by d_p and RSS_p respectively.

The legend in figures differentiates the COOP from NCOOP as well as PF versus CRLB. For example, *COOP_nP16_oz8_st2* in the legend of Fig. 6.3a, denotes a Particle Filter in cooperative mode with the parameters $nP = 16$, $\sigma^2_{RSS_p} = 8$ and $\sigma^2_{d_p} = 2$ and compared to CRLB also in cooperative mode, with the legend denotation as *COOP_CRLB*.

6.3.2   PF Assumptions

Given the random nature of MO movements and independent Observations, we assume that the current location of MO depends only on the previous location hence, a Markov Process for the MOs movement (PF State), and, the current PF observation, RSS_p depends only on the current PF state d_p, there is more details in Appendix B.

6.3.3   CRLB as a measure of performance

The Cramer-Rao Lower Bound (CRLB) is used as a measure of the lower bound on the variance of estimators for deterministic parameters [92, 112]. The CRLB defines that the bound on the variance of any unbiased estimator is at least as high as the inverse of the Fisher information [112]. From CRLB calculation we can easily find the lowest possible Root Mean Square Error (RMSE) among all

unbiased algorithms. The CRLB is routinely utilized in navigation application and science [113, 114]. CRLB is used to measure the max possible performance of localization algorithm and guidance on implementation feasibility of an algorithm [115]. In this chapter, the CRLB is used to measure the performance of our Particle Filter in different scenarios. To calculate the CRLB, we need to calculate the variance(s) of Distance Measurement Error(s) (DME) for all the links among the MOs and the MOs-to-FAs points. The CRLB provides a lower bound on the error covariance matrix for an unbiased estimate of L_M. For a given estimate of the MOs, $\hat{L}_M$ and Gaussian range measurement R. The CRLB calculation for this study is outlined in details in Appendix A. The $RMSE = \sqrt{trace(CRLB)}$ is used throughout this chapter for our performance analysis.

6.3.4 Simulation setup

In Fig. 6.1, there are eight FAs and three MOs, two moving clockwise and the third counter-clockwise. The X or Y movements are advanced randomly according to uniform distribution. The simulations are performed in WiFi-link mode and there has not been any consideration for NLOS, LOS is assumed throughout. The LOS assumption is due to the fact that in our future work we will be using the digital map that will include the LIDAR information which is based on having Line Of Sight, LOS. The collection of this digital map was discussed in subsection 6.1.4.

6.4 Simulation Analysis

In this section, we analyze the performance of Particle Filter with respect to CRLB in Cooperative (COOP) and Non-Cooperative mode. We first start by examining the effect of Particle Filters parameters such as Observation variance ($\sigma^2_{RSS_p}$), State variance ($\sigma^2_{d_p}$) and number of particles (nP) as it pertains to RMSE value. In subsection 6.4.1, we analyze Particle Filters accuracy (in terms of RMSE) under different parameter settings. After analyzing the results in subsection 6.4.1, we then select the best performing parameters for comparison to the lower bound of errors hence, CRLB in subsection 6.4.2.

6.4.1 Effect of Variances and number of Particles on PF

In this subsection, we are evaluating the effect of number of particles nP, different variance values for State and Observation in order to set the stage for the remaining simulation runs. In Fig. 6.2, we are evaluating the effect of doubling, 8 versus 16 particles ($nP = 8, 16$) where FAs and MOs are in WiFi-enable mode. In COOP mode, the results are very close however, in NCOOP mode the result for higher number of particles ($nP = 16$), is slightly better. For the remaining simulations we focus on using $nP = 16$. In Fig. 6.3(a) and 6.3(b), the nP is left at 16 and only the variances of State[1] (st) and Observation[2] (oz) are changed[3]. In Fig. 6.3(a), the Moving Objects (MOs) are in COOP mode where their location information are shared among each other. The RMSE value for the

---

[1] st, is used in legends for figures in place of d_p

[2] oz, is used in legends for figures in place of RSS_p

[3] oz8_st2, in figure legend, denotes that $\sigma^2_{RSS_p} = 8$ and $\sigma^2_{d_p} = 2$

$50th\ percentile$ mark, is the worst ($RMSE = 6.349$) when the state and observation variances[4] are set to 8. In Fig. 6.3(b), the Moving Objects (MOs) are in NCOOP mode where they do not share their location information. At the $50th$ $percentile$ mark, similar to COOP mode the RMSE is the worst ($RMSE = 7.293$) when the variances are set to 8. Conversely in a low variance environment when both State and Observation variances are set at 2, the RMSE is the lowest both in COOP ($RMSE = 6.07$) and NCOOP ($RMSE = 6.892$). In general, when in COOP mode, the RMSE is lower than NCOOP for all combination of variances. For example, at the $50th\ percentile$ mark, the RMSE ranges between $6.07 - 6.349$ in COOP mode and $6.892 - 7.293$ in NCOOP mode. There is about 1 meter improvement in RMSE value while in COOP mode. After this initial evaluation of parameter effect on PF, we continue using $nP = 16$. Next, we evaluate the performance of Particle filter versus CRLB considering the effect of $distance$ and variances ($\sigma_{d_p}^2$, σ_{RSS}^2) in subsection 6.4.2.

6.4.2 PF performance compared to CRLB

The simulation results discussed here are based on configuration values outlined in Table 6.2. In this subsection, we analyze the effect of Observation variance ($\sigma_{RSS_p}^2$) and State variance ($\sigma_{d_p}^2$) of Particle Filter and distance reduction in (6.3). Here, we compare the performance of Particle Filter *versus CRLB*. The results of the simulations for the effect of variance changes are captured in Fig. 6.4 and for the distance reduction in Fig. 6.5 respectively. The statistics (Mean and STD) of simulation runs for this subsection is tabulated in Table 6.3. Unlike the previous figures in subsection 6.4.1 where there were only Particle Filters with differing parameters, here the Particle Filter performance is *compared to CRLB*.

---

[4] $\sigma_{d_p}^2$ and $\sigma_{RSS_p}^2$
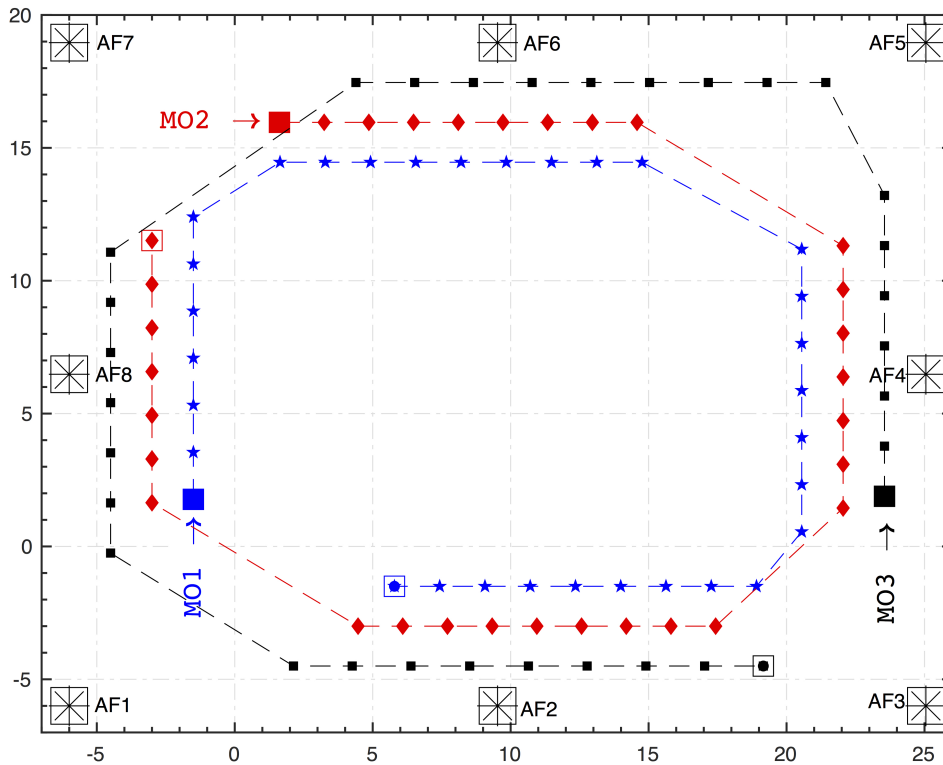
FIGURE 6.1: *Eight Fixed Anchors {AF1, AF2,.....,AF8} and three mov-
ing objects {MO1, MO2, MO3}. The objects MO1 and MO2 traverse
clockwise along the dotted lines and MO3 in the oposite direction, counter
clockwise.*

In our review of the results, we use the 50th percentile for our performance as-
sessment. The results are analyzed in the following order, Fig. 6.4, Fig. 6.5, and
Table 6.3.

In Fig. 6.4a and Fig. 6.4b, the results of PF simulations with two sets of variances
both in COOP and NCOOP mode are compared to CRLB. In Fig. 6.4a, shows
the result of simulation for high variances value of $\sigma_{d_p}^2$ and $\sigma_{RSS_p}^2$ where both are
set to 8 and Fig. 6.4b shows the result for low variances, where both are set to 2.

Despite the quadruple values of variances (8 versus 2) in two different scenarios,
the RMSE result in low variance scenario, is only better by 5%. This is a very
small improvement. It is evident that the variance does not have that drastic of
effect on Particle Filter performance (RMSE).
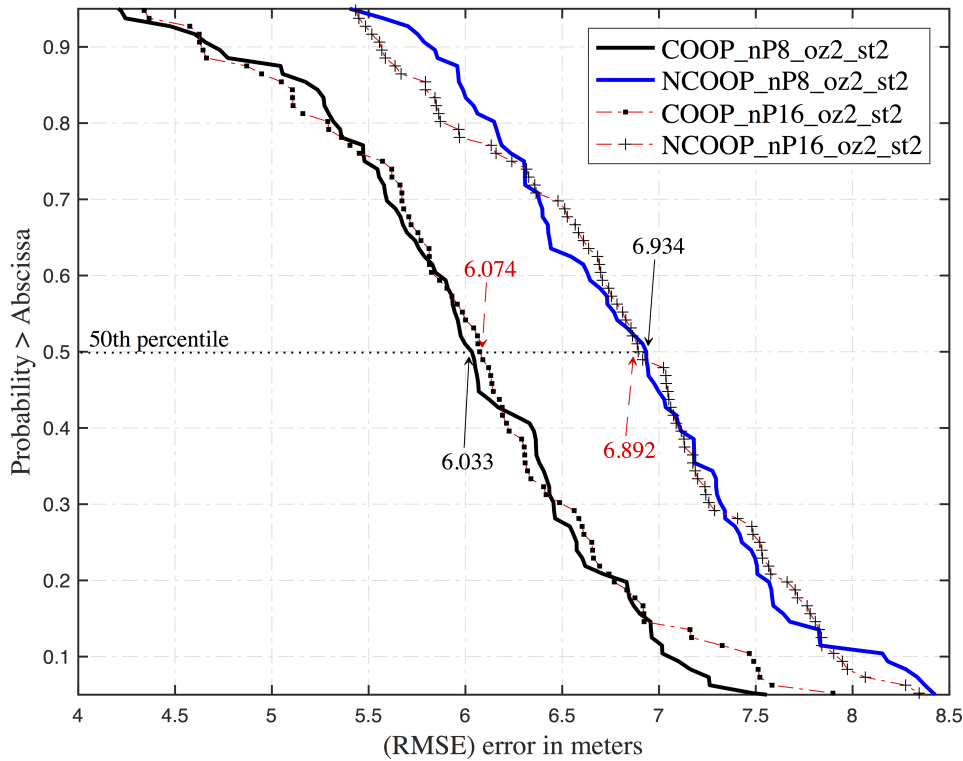
FIGURE 6.2: *Comparing the performance of **Particle filters** with different number of particles (8 versus 16) for the same set of State variance, $\sigma^2_{d_p}$ and Observation variance, $\sigma^2_{RSS_p}$ (both set at 2) in COOP and NCOOP modes.*

As for distance reduction, Fig. 6.5 shows the result of simulation where the distance is reduced by a factor of 2 and the variances are set to 2. Here is a great case for discussion, comparing this result with the one in Fig. 6.4b, the RMSE improvement is very noticeable. With half the distance, the RMSE is lowered by one-fourth. In COOP mode, the RMSE is lowered from 6.072 to 1.451 meter and from 6.838 to 1.675 meter in NCOOP mode. In our earlier introduction to grid, High Resolution Signature Database in subsection 6.1.4, the distances among grid points are only 25 centimeter apart. This dense spacing among the grid points would result in more stable RSS reading, less factor due to distance variation. We also can benefit from more accurate empirical PMF as opozed to a theoretical model (i.e. Gaussian) for our Particle Filter implementation.

TABLE 6.2: Simualtion environment for two sets of State (d_p) and Observation (RSS_p) Variances

Sim Parameters			PF Parameters		
$nSMP$	FAs	MOs	nP	$\sigma^2_{d_p}$	$\sigma^2_{RSS_p}$
32	8	3	16	2	2
32	8	3	16	8	8

In Table 6.3, the RMSE statistics, *Mean and STD* for the *PF performance* versus CRLB are tabulated for three different settings. *First*, the variances ($\sigma^2_{d_p}$, $\sigma^2_{RSS_p}$) are both set at 8. *Second*, the variances are set to 2. Lastly, in more optimal scenario, the variances are left at 2 and distance is reduced by a factor of $1/2$.

It is evident that overall there is an improving (lowering) RMSE from perspective of Mean and STD. Starting from high variance values of 8 to low values of 2. However, in case of distance reduction by a factor of $1/2$ ($d_p/2$), there is a significant improvement on statistics. *The low STD in the latter case ($d_p/2$), bodes well for our digital mapping approach, HRSD.*

6.5 Summary

In this chapter, we focus on WiFi localization and Line of Sight (LOS) simulation

TABLE 6.3: RMSE Mean and STD for three different set of parameters for Particle Filter simulation . State (d_p) and Observation (RSS_p) Variances for the first two modes and lastly State (d_p) or distance reduction.

Estimation	Parameters	COOP		NCOOP	
		Mean	STD	Mean	STD
PF	$\sigma^2_{d_p}, \sigma^2_{RSS_p} = 8$	6.287	1.2020	7.113	1.0160
CRLB		5.360	0.6943	6.239	0.6995
PF	$\sigma^2_{d_p}, \sigma^2_{RSS_p} = 2$	6.032	0.9558	6.822	0.9146
CRLB		5.385	0.9080	6.259	0.6289
PF	$\sigma^2_{d_p}, \sigma^2_{RSS_p} = 2$ with $d_p/2$	1.456	0.2313	1.680	0.2163
CRLB		1.340	0.1959	1.575	0.1737

in Cooperative and Non-Cooperative mode. A Particle Filter was chosen due to nature of Non-linear, non-Gaussian channel models for RF localization. The assumptions for our Particle Filter state (d_p) and observation (RSS_p) were stated upon which, the details of Bayesian Recursion were derived. We started with extensive simulation for the effect of different parameter settings on Particle Filter performance and pointed out limitation and introduced a new approach for more precise localization that comprises of a Hybrid 3D database (*High Resolution Signature Database*) and Kernel Method Particle Filter. In our simulation results we showed that the distance reduction has the most effect on lowering the Root Mean Square Error (RMSE) than low value of variances ($\sigma_{d_p}^2$, $\sigma_{RSS_p}^2$). We also showed the overall improvement of RMSE when the Moving Objects (MOs) collaborate (COOP mode). In order to achieve a more Precise Tracking of Things (PToT), we introduced two essential components, a High Resolution Signature Database (HRSD) and an *Empirical* choice for *Empirical Importance Sampling* of our Kernel Method Particle Filter. The results will be published in a separate paper.
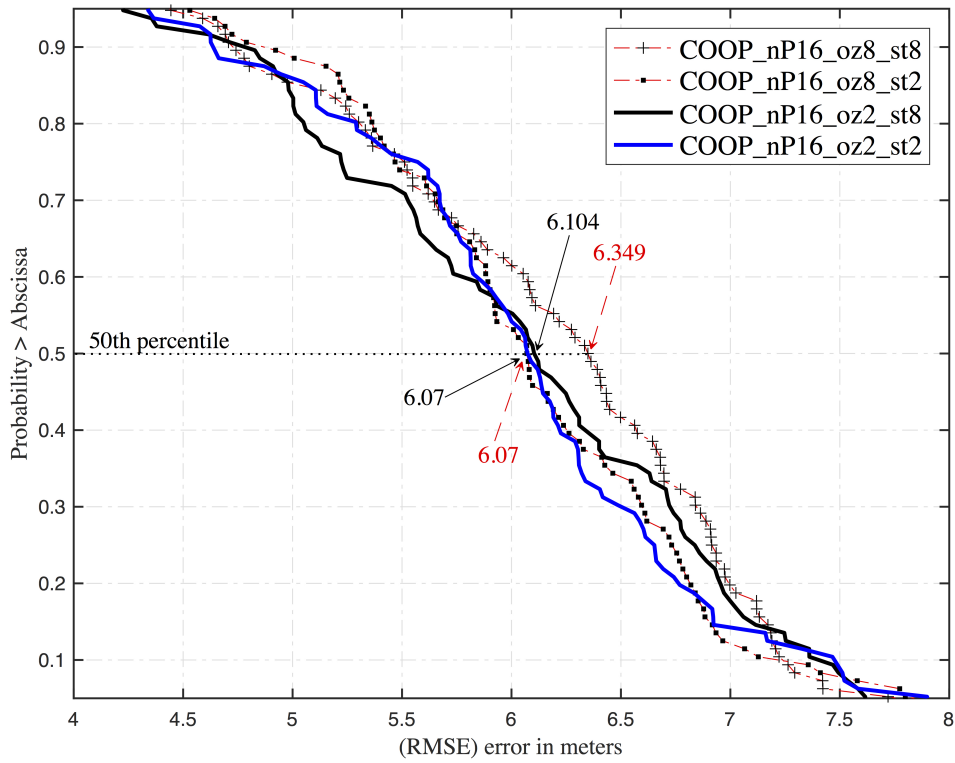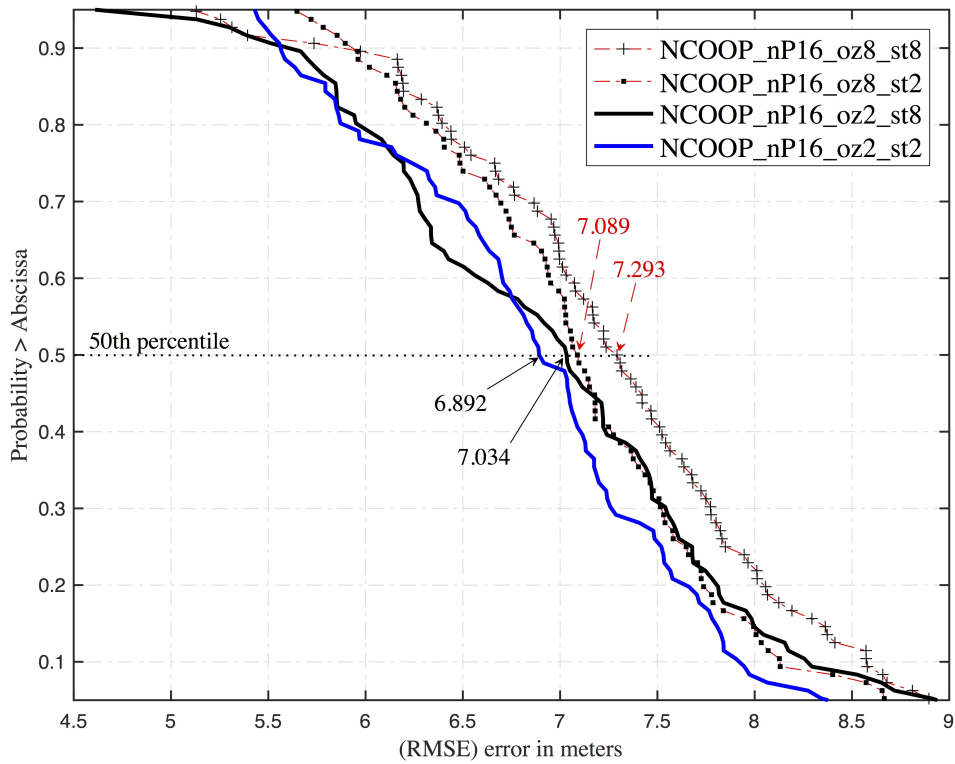
FIGURE 6.3: *Comparing the performance of **Particle filters** in **four** different combination of State variance, $\sigma^2_{d_p}$ and Observation variance, $\sigma^2_{RSS_p}$ in COOP and NCOOP modes:* **(a)** *PF in COOP mode* **(b)** *PF in NCOOP mode*
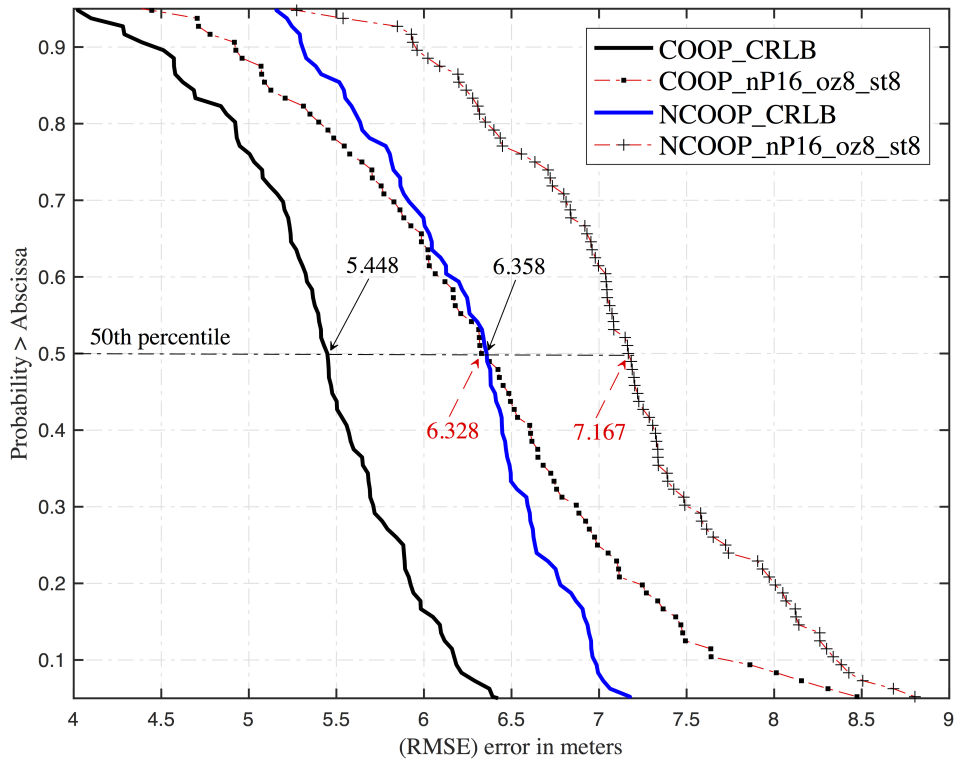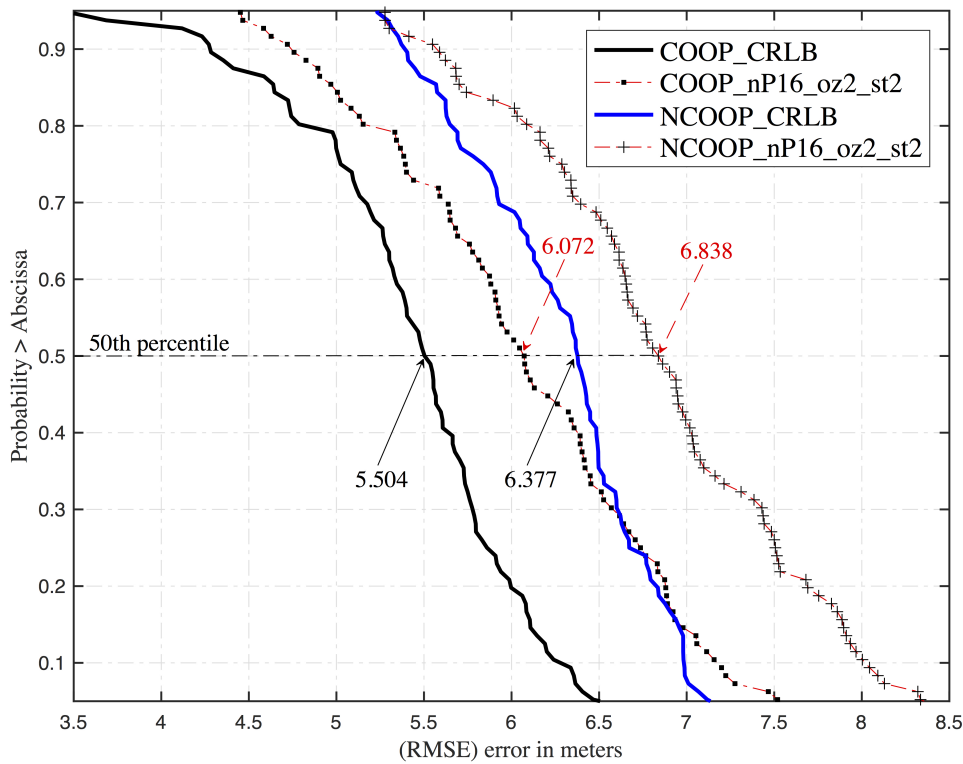
FIGURE 6.4: *Comparing the performance of **Particle Filter versus CRLB** both in COOP and NCOOP mode for **two** different sets of State and Observation Variance:* **(a)** $\sigma^2_{d_p}, \sigma^2_{RSS} = 8$ **(b)** $\sigma^2_{d_p}, \sigma^2_{RSS} = 2$
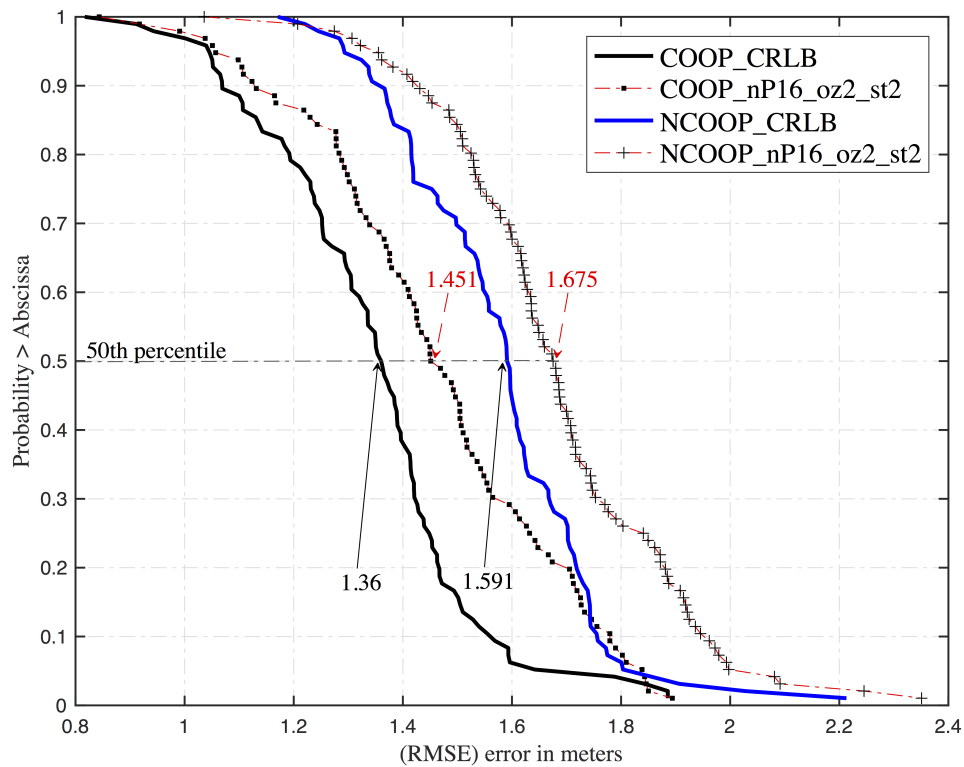
FIGURE 6.5: *The effect of **distance (d_p, the state) reduction by a factor of two** resulting an improvement on RMSE by a factor of four. Here, the state variance ($\sigma^2_{d_p}$) and observation variance ($\sigma^2_{d_p}$) are both set at 2, and simulations are run in COOP and NCOOP mode and the PF performance is compared to CRLB.*

7 Conclusion and Furture work

In this dissertation, we utilized two RF signaling medium, WiFi, and UWB. Although there are different methods for localization, we focused on two most popular, Wifi-RSS-, UWB-TOA-based methods. Due to the complexity of UWB theoretical model, we resorted to an empirical model. Due to nonlinear and non-Gaussian nature of our channel models, we opted for Particle Filter (PF) for our research. In our study, we explored many variants for optimal localization. From an environmental perspective, we examined the effect of, number of fixed anchors, cooperation among moving objects and, as for Particle Filter, we explored the efficiency regarding the number of particles, state and observation variances and resampling methods. And finally, we addressed ways to more accuracy by resorting to 3D finger- print database. Through our simulation, we always measured the performance of our methods and algorithm against CRLB. We showed that in three moving objects (MOs) and eight fixed anchors configuration, hybrid mode (WiFi & UWB) while MOs collaborate, resulted in 49 percent improvement over when they are not. We showed that in general, the particle filter performs much better in an environment with high RMSE value in non-Hybrid configurations. We demonstrated that in Hybrid (WiFi & UWB) and Cooperative configuration, the Particle Filter consistently performs well in either of low or high RMSE value environments.

In summary, the increase in the number of anchors and cooperation rendered

better localization. The Hybrid was superior to the WiFi-only method. As for Particle Filter, it behaved much better in the high RMSE environment than the low RMSE. More particle helps, and it is highly dependent on the size of the area. We also introduced the KMPF to achieve a more Precise Tracking of Things (PToT), we introduced two essential components, a High-Resolution Signature Database (HRSD) and an Empirical PMF feed for Importance Sampling of the Kernel Method Particle Filter (KMPF).

The precision is a never ending quest. Steps towards more precision rely on two step solution: High-resolution database and Empirically fed KMPF. There is more work in this area from the reliability perspective and accurate time-stamp! When it comes to location based services, there it goes the massive size of data that requires us to manage the size and the quality of the data. With the event of data mining, two areas warrant further research when it comes to wireless data. We need to extract proper features for more effective clustering of data. It should help us from the computational perspective and perhaps a better localization by eliminating the outlier signals.

On that note, it is worth looking into some understanding for dimensionality reduction [116–118] and feature extraction [119, 120]. For precise indoor localization, machine learning can play an influential role in adaptation and calibration [121–123]. We can also combine clustering techniques [124] and the intelligent source or transmitter selection [125] for a more optimal algorithm and dynamic localization.

A Derivation of CRLB

To calculate the CRLB, we need to calculate the variance(s) of Distance Measurement Error(s) (DME) for all the links among the MOs and the MOs-to-FAs points. The CRLB provides a lower bound on the error covariance matrix for an unbiased estimate of L_M. For a given estimate of the MOs, $\hat{L}_M$ and Gaussian range measurement R, the Fisher Information Matrix (FIM) can be represented by:

$$J(L_M) = E[\nabla_{L_M} ln f_R(r; L_M)][\nabla_{L_M} ln f_R(r; L_M)]^T \tag{A.1}$$

where $f_R(r; L_M)$ is the joint Gaussian PDF given by:

$$f_R(r; L_M) = \frac{1}{(2\pi)^K |\sum|^{\frac{1}{2}}} \times E \tag{A.2}$$

where

$$E = exp\left\{-\frac{1}{2}[r - \mu(L_M)]^T \sum{}^{-1}[r - \mu(L_M)]\right\} \tag{A.3}$$

and $\mu(L_M)$ is the vector of the actual distances between the nodes corresponding to available K measurements. FIM for the specific PDF in (A.2) can be written as:

$$J(L_M) = [G(L_M)]^T \sum{}^{-1} [G(L_M)] \tag{A.4}$$

$$G(L_M)^T = \begin{pmatrix} cos\phi_1 & cos\phi_2 & ... & cos\phi_k \\ sin\phi_1 & sin\phi_1 & ... & sin\phi_k \end{pmatrix} \tag{A.5}$$

where

$$\sum = diag(\lambda_1 \quad \lambda_2 \quad ... \quad \lambda_k) \tag{A.6}$$

ϕ_i representing the angle between the nodes from ith measurement and λ_i is the variance of range estimate from the ith measurement. The variance calculation are discussed in subsections 6.1.2 that are used to replace λ_i. The CRLB is given by:

$$CRLB = [J(L_M)]^{-1} \tag{A.7}$$

And, the Root-Mean-Square-Error, RMSE is given by:

$$RMSE = \sqrt{trace(CRLB)} \tag{A.8}$$

B Derivation of Bayesian Recursion

Let us recall the notations, $\mathbb{P}$ denoting probability, p denoting the index of a particle, the PF State (or movement) and Observation (or measurement) are defined as d_p and RSS_p respectively. Given the random nature of MO movements and independent Observations we assume that the current location of MO depends only on the previous location hence, a Markov Process for the MOs movement (PF State, d_p),

$$\mathbb{P}(d_p/d_{0:p-1}) = \mathbb{P}(d_p/d_{p-1}) \tag{B.1}$$

and, the current PF observation, RSS_p depends only on the current PF state d_p, therefore:

$$\mathbb{P}(RSS_p/d_{0:p}, RSS_{0:p-1}) = \mathbb{P}(RSS_p/d_p) \tag{B.2}$$

Leveraging off of the assumptions highlighted in (B.1) and (B.2), we start with Bayesian rule to arrive at the recursion for $Posterior$ of the PF State (d_p) based on our measurements, $\mathbb{P}(d_{0:p}/RSS_{0:p})$, applying Bayes rule:

$$\mathbb{P}(d_{0:p}/RSS_{0:p}) = \frac{\mathbb{P}(RSS_{0:p}/d_{0:p}) * \mathbb{P}(d_{0:p})}{\mathbb{P}(RSS_{0:p})} \tag{B.3}$$

Rewriting the numerator and denominator indices, $RSS_{0:p}$ to ($RSS_p, RSS_{0:p-1}$):

$$\mathbb{P}(d_{0:p}/RSS_{0:p}) = \frac{\mathbb{P}(RSS_p, RSS_{0:p-1}/d_{0:p}) * \mathbb{P}(d_{0:p})}{\mathbb{P}(RSS_p, RSS_{0:p-1})} \tag{B.4}$$

Applying the product rule to $\mathbb{P}(RSS_p, RSS_{0:p-1}/d_{0:p})$:

$$\mathbb{P}(d_{0:p}/RSS_{0:p}) =$$

(B.5)

$$\frac{\mathbb{P}(RSS_p/RSS_{0:p-1},d_{0:p})*\mathbb{P}(RSS_{0:p-1}/d_{0:p})*\mathbb{P}(d_{0:p})}{\mathbb{P}(RSS_p/RSS_{0:p-1})*\mathbb{P}(RSS_{0:p-1})}$$

Applying BAYES rule to: $\mathbb{P}(RSS_{0:p-1}/d_{0:p})$ in (B.5):

$$\mathbb{P}(d_{0:p}/RSS_{0:p}) =$$

(B.6)

$$\frac{\mathbb{P}(RSS_p/RSS_{0:p-1},d_{0:p})*\mathbb{P}(d_{0:p}/RSS_{0:p-1})*\mathbb{P}(RSS_{0:p-1})*\mathbb{P}(d_{0:p})}{\mathbb{P}(RSS_p/RSS_{0:p-1})*\mathbb{P}(RSS_{0:p-1})*\mathbb{P}(d_{0:p})}$$

Deleting the common term, $\quad \mathbb{P}(RSS_{0:p-1}) * \mathbb{P}(d_{0:p})$:

$$\mathbb{P}(d_{0:p}/RSS_{0:p}) = \frac{\mathbb{P}(RSS_p/RSS_{0:p-1},d_{0:p})*\mathbb{P}(d_{0:p}/RSS_{0:p-1})}{\mathbb{P}(RSS_p/RSS_{0:p-1})} \tag{B.7}$$

based on the independent observations(RSS) assumption:

$$\mathbb{P}(RSS_p/RSS_{0:p-1}, d_{0:p}) = \mathbb{P}(RSS_p/d_p) \tag{B.8}$$

therefore applying (B.8) into (B.7):

$$\mathbb{P}(d_{0:p}/RSS_{0:p}) = \frac{\mathbb{P}(RSS_p/d_p)*\mathbb{P}(d_p,d_{0:p-1}/RSS_{0:p-1})}{\mathbb{P}(RSS_p/RSS_{0:p-1})} \tag{B.9}$$

Applying Conditional Property to 2nd term in the numerator of (B.9):

$$\mathbb{P}(d_{0:p}/RSS_{0:p}) =$$

(B.10)

$$\frac{\mathbb{P}(RSS_p/d_p)*\mathbb{P}(d_p/d_{0:p-1},RSS_{0:p-1})*\mathbb{P}(d_{0:p-1}/RSS_{0:p-1})}{P(RSS_p/RSS_{0:p-1})}$$

based on the Markov Process assumption for the movement (PF state d_p):

$$\mathbb{P}(d_p/d_{0:p-1}, RSS_{0:p-1}) = \mathbb{P}(d_p/d_{p-1}) \tag{B.11}$$

Applying assumption in (B.11) to (B.10) :

$$\mathbb{P}(d_{0:p}/RSS_{0:p}) =$$

$$\frac{\mathbb{P}(RSS_p/d_p)}{\mathbb{P}(RSS_p/RSS_{0:p-1})} * \mathbb{P}(d_p/d_{p-1}) * \mathbb{P}(d_{0:p-1}/RSS_{0:p-1}) \tag{B.12}$$

Integrating over the past $p-1$ values of d:

$$\int \mathbb{P}(d_{0:p}/RSS_{0:p}) =$$

$$\frac{\mathbb{P}(RSS_p/d_p)}{\mathbb{P}(RSS_p/RSS_{0:p-1})} * \int \mathbb{P}(d_p/d_{p-1}) * \mathbb{P}(d_{0:p-1}/RSS_{0:p-1}) \tag{B.13}$$

After integrating over the $p-1$ of d we are only left with the current value, d_p hence:

$$\mathbb{P}(d_p/RSS_{0:p}) = \frac{\mathbb{P}(RSS_p/d_p)}{\mathbb{P}(RSS_p/RSS_{0:p-1})} * \mathbb{P}(d_p/RSS_{0:p-1}) \tag{B.14}$$

where $p = 1, 2, ..., nP$. nP denotes the total number of Particles.

Basically, we want to pick the most suitable next state d_p given the set of observations $RSS_{0:p}$. Obviously, we like to pick the most likely or highest marginal *Posterior*.

By observing (B.14), it appears that the *Prior* for the past $p-1$ observations are scaled to form the marginal *Posterior* on the left hand side. The Scale factor can be considered as *Importance Weight* where we can recursively update by

performing nP scaled version of $Prior$ to form a new $Posterior$ distribution.

$$Weight_p = \frac{\mathbb{P}(RSS_p/d_p)}{\mathbb{P}(RSS_p/RSS_{0:p-1})} \tag{B.15}$$

Given d_p, the numerator can be measured and the denominator does not depend on the state, d_p.

Bibliography

[1] A. Rai, K. K. Chintalapudi, V. N. Padmanabhan, and R. Sen, "Zee: zero-effort crowdsourcing for indoor localization," in Proceedings of the 18th annual international conference on Mobile

[2] M. M. Atia, A. Noureldin, and M. J. Korenberg, "Dynamic online-calibrated radio maps for indoor positioning in wireless local area networks," Mobile Computing, IEEE Transactions on, vol. 12, no. 9, pp. 1774-1787, 2013

[3] Spletzer, J., Das, A.K., Fierro, R., Taylor, C.J., Kumar, V., Ostrowski, J.P.: Cooperative localization and control for multi-robot manipulation. Intelligent Robots and Systems, 2001. Proceedings. 2001 IEEE/RSJ International Conference on Volume 2, 29 Oct.-3 Nov. 2001 Page(s):631 - 636 vol.2

[4] Rekleitis, I.M., Dudek, G., Milios, E.E.: Multi-robot cooperative localization: a study of trade-offs between efficiency and accuracy. Intelligent Robots and System, 2002. IEEE/RSJ International Conference on Volume 3, 30 Sept.-5 Oct. 2002 Page(s):2690 - 2695 vol.3

[5] S. Se, D. Lowe and J. Little: Mobile robot localization and mapping with uncertainty using scale-invariant visual landmarks. International Journal of Robotics Research vol. 21 no. 8, Page(s)735-758, 2002

[6] DiBernardo, Enrico, and Paolo Pirjanian. "Methods and apparatus for position estimation using reflected light sources." U.S. Patent 7,720,554, issued May 18, 2010.

[7] J.J. Leonard and H. F. Durrant-Whyte: Simultaneous map building and localization for an autonomous mobile robot. In Proceedings of IEEE/RSJ International Conference on Intelligent Robots and Systems (IROS'91), pp. 1442-1447, New York, USA, 1991.

[8] Durrant-Whyte, Hugh, and Tim Bailey. "Simultaneous localization and mapping: part I." IEEE robotics & automation magazine 13, no. 2 (2006): 99-110.

[9] Bailey, Tim, and Hugh Durrant-Whyte. "Simultaneous localization and mapping (SLAM): Part II." IEEE Robotics & Automation Magazine 13, no. 3 (2006): 108-117.

[10] K. Pahlavan, F., O., Akgul, M., Heidari, A., Hatami, J., M., Elwell, R., D., Tingley.: Indoor geolocation in the absence of direct path. IEEEWireless Communications, vol. 13, no. 6, pp. 50-58, 2006.

[11] K., Pahlavan, X., Li, and J.P., Makela.: Indoor geolocation science and technology. IEEE Communications Magazine, vol. 40, no. 2, pp. 112-118, 2002.

[12] Moghtadaiee, Vahideh, Andrew G. Dempster, and Samsung Lim. "Indoor localization using fm radio signals: A fingerprinting approach." In Indoor Positioning and Indoor Navigation (IPIN), 2011 International Conference on, pp. 1-7. IEEE, 2011.

[13] He, Jie, Yanwei Yu, and Qin Wang. "RSS assisted TOA-based indoor geolocation." International journal of wireless information networks 20, no. 2 (2013): 157-165.

[14] Tomic, Slavisa, Marko Beko, and Rui Dinis. "3-D Target Localization in Wireless Sensor Networks Using RSS and AoA Measurements." IEEE Transactions on Vehicular Technology 66, no. 4 (2017): 3197-3210.

[15] Sun, Xuqing, Jingyuan Duan, Yonggang Zou, and Ancun Shi. "Impact of multipath effects on theoretical accuracy of TOA-based indoor VLC positioning system." Photonics Research 3, no. 6 (2015): 296-299.

[16] Gholami, Mohammad Reza, Sinan Gezici, and Erik G. Strm. "TW-TOA based positioning in the presence of clock imperfections." Digital Signal Processing 59 (2016): 19-30.

[17] Zhao, Yubin, Xiaopeng Fan, Cheng-Zhong Xu, and Xiaofan Li. "ER-CRLB: An Extended Recursive CramrRao Lower Bound Fundamental Analysis Method for Indoor Localization Systems." IEEE Transactions on Vehicular Technology 66, no. 2 (2017): 1605-1618.

[18] Garcia, Nil, Henk Wymeersch, Erik G. Larsson, Alexander M. Haimovich, and Martial Coulon. "Direct localization for massive MIMO." IEEE Transactions on Signal Processing 65, no. 10 (2017): 2475-2487.

[19] Lazzari, Fabrizio, Alice Buffi, Paolo Nepa, and Sandro Lazzari. "Numerical Investigation of an UWB Localization Technique for Unmanned Aerial Vehicles in Outdoor Scenarios." IEEE Sensors Journal 17, no. 9 (2017): 2896-2903.

[20] K., Pahlavan.: WiFi and UWB RF Localization-Principles and Applications, Short Course, IEEE. PIMRC'06, Helsinki, Finland, Sep. 2006

[21] Shyamala, C., M. Geetha Priya, and K. A. Sumithra Devi. "WIRELESS SENSOR NETWORK FOR RESOURCES TRACKING AT BUILDING CONSTRUCTION SITES."

[22] Wang, Xuyu, Lingjun Gao, Shiwen Mao, and Santosh Pandey. "CSI-based fingerprinting for indoor localization: A deep learning approach." IEEE Transactions on Vehicular Technology 66, no. 1 (2017): 763-776.

[23] Chen, Zhenghua, Han Zou, Hao Jiang, Qingchang Zhu, Yeng Chai Soh, and Lihua Xie. "Fusion of WiFi, smartphone sensors and landmarks using the Kalman filter for indoor localization." Sensors 15, no. 1 (2015): 715-732.

[24] Kaltiokallio, Ossi, Huseyin Yigitler, and Riku Jantti. "A three-state received signal strength model for device-free localization." IEEE Transactions on Vehicular Technology (2017).

[25] Zhuang, Yuan, Jun Yang, You Li, Longning Qi, and Naser El-Sheimy. "Smartphone-based indoor localization with bluetooth low energy beacons." Sensors 16, no. 5 (2016): 596.

[26] Frattasi, Simone, and Francescantonio Della Rosa. Mobile positioning and tracking: from conventional to cooperative techniques. John Wiley & Sons, 2017.

[27] Nicoli, Monica, Sinan Gezici, Zafer Sahinoglu, and Henk Wymeersch. "Localization in mobile wireless and sensor networks." EURASIP Journal on Wireless Communications and Networking 2011, no. 1 (2011): 197.

[28] Pahlavan, K., F. Akgul, Y. Ye, T. Morgan, F. Alizadeh-Shabdiz, M. Heidari, and C. Steger. "Taking positioning indoors wi-fi localization and gnss." Inside GNSS 5, no. 3 (2010): 40-47.

[29] Rekimoto J, Miyaki T and Ishizawa T. Lifetag: Wifi-based continuous location logging for life pattern analysis. In Proceedings of the 3rd international conference on Locationand context-awareness. pp. 35-49

[30] Cunche M. I know your mac address: targeted tracking of individual using wi-fi. Journal of Computer Virology and Hacking Techniques 2014; 10(4): 219-227

[31] Pahlavan, Kaveh, Prashant Krishnamurthy, and Yishuang Geng. "Localization Challenges for the Emergence of the Smart World." Access, IEEE, 3, no. 1 (2015): 3058-3067.

[32] D. Lymberopoulos, J. Liu, X. Yang, R. R. Choudhury, V. Handziski, and S. Sen, "A realistic evaluation and comparison of indoor location technologies: experiences and lessons learned," in Proceedings of the 14th International Conference on Information Processing in Sensor Networks, pp. 178-189, ACM, 2015

[33] J., Silverstrim, R., Passmore, K., Pahlavan, B., Sadler.: Wireless sensor networks with geolocation. Defense Tech Briefs, Vol. 3, No. 3, June 2009, pp14-15

[34] Gonzlez, Javier, Jose-Luis Blanco, Cipriano Galindo, A. Ortiz-de-Galisteo, Juan-Antonio Fernndez-Madrigal, Francisco Angel Moreno, and Jorge L. Martnez. "Mobile robot localization based on ultra-wide-band ranging: A particle filter approach." Robotics and autonomous systems 57, no. 5 (2009): 496-507.

[35] Wang, Yuxi, Kaishun Wu, and Lionel M. Ni. "Wifall: Device-free fall detection by wireless networks." IEEE Transactions on Mobile Computing 16, no. 2 (2017): 581-594.

[36] Chen, Dan, Zhixin Liu, Lizhe Wang, Minggang Dou, Jingying Chen, and Hui Li. "Natural disaster monitoring with wireless sensor networks: a case study of data-intensive applications upon low-cost scalable systems." Mobile Networks and Applications 18, no. 5 (2013): 651-663.

[37] A., Hatami, K., Pahlavan.: Performance Comparison of RSS and TOA Indoor Geolocation Based on UWB Measurement of Channel Characteristics. 17th Annual IEEE International Symposium on Personal Indoor and Mobile Radio Communications (PIMRC'06), Helsinki, Finland, 11-14 Sept. 2006

[38] Zhao, Xiaojie, Zhuoling Xiao, Andrew Markham, Niki Trigoni, and Yong Ren. "Does btle measure up against wifi? a comparison of indoor location performance." In European Wireless 2014; 20th European Wireless Conference; Proceedings of, pp. 1-6. VDE, 2014.

[39] Luo, Xiaowei, William J. OBrien, and Christine L. Julien. "Comparative evaluation of Received Signal-Strength Index (RSSI) based indoor localization techniques for construction jobsites." Advanced Engineering Informatics 25, no. 2 (2011): 355-363.

[40] Qi, Yihong, and Hisashi Kobayashi. "On relation among time delay and signal strength based geolocation methods." In Global Telecommunications Conference, 2003. GLOBECOM'03. IEEE, vol. 7, pp. 4079-4083. IEEE, 2003

[41] Khan, Umair I., Kaveh Pahlavan, and Sergey Makarov. "Comparison of TOA and RSS based techniques for RF localization inside human tissue." In Engineering in Medicine and Biology Society, EMBC, 2011 Annual International Conference of the IEEE, pp. 5602-5607. IEEE, 2011.

[42] Gholami, Mohammad Reza, Reza Monir Vaghefi, and Erik G. Strm. "RSS-based sensor localization in the presence of unknown channel parameters." IEEE Transactions on Signal Processing 61, no. 15 (2013): 3752-3759.

[43] Veletić, Mladen, and Milan unjevari. "On the Cramer-Rao lower bound for RSS-based positioning in wireless cellular networks." AEU-International Journal of Electronics and Communications 68, no. 8 (2014): 730-736.

[44] Alsindi, N.A.: Cooperative Localization Bounds for Indoor Ultra-Wideband Wireless Sensor Networks. Hindawi Publishing Corporation EURASIP Journal on Advances in Signal Processing Volume 2008, Article ID 852509, 13 pages

[45] Savvides, A., Garber, W.L., Moses, R.L., Srivastava, M.B.: An analysis of error inducing parameters in multihop sensor node localization. Mobile Computing, IEEE Transactions on Volume 4, Issue 6, Nov.-Dec. 2005 Page(s):567 - 577

[46] Wang, Xiangli, Wei Yi, Mingchi Xie, Bowen Zhai, and Lingjiang Kong. "Time management for target tracking based on the predicted Bayesian Cramer-Rao lower bound in phase array radar system." In Information Fusion (Fusion), 2017 20th International Conference on, pp. 1-5. IEEE, 2017.

[47] Konchenko, Inna, and Felix Yanovsky. "Geometrical arrangement of multilateration surveillance system components by means of Cramer-Rao lower bound analysis." In Proc. of SPIE Vol, vol. 7502, pp. 75020Y-1. 2009.

[48] Hamschin, Brandon, and Michael Grabbe. "An approximate Cramer-Rao lower bound for multiple LFMCW signals." IEEE Transactions on Aerospace and Electronic Systems (2017).

[49] S., Gezici, Z., Tian, G., B., Giannakis, H., Kobayashi, A., F., Molisch, H., V., Poor, Z., Sahinoglu.: Localization via ultra-wideband radios. IEEE Signal Processing Magazine (Special Issue on Signal Processing for Positioning and Navigation with Applications to Communications), vol. 22, issue 4, pp. 70-84, July 2005

[50] Sanjeev Arulampalam, M., Simon Maskell, Neil Gordon, and Tim Clapp. "A tutorial on particle filters for online nonlinear/non-Gaussian Bayesian tracking." Signal Processing, IEEE Transactions on 50, no. 2 (2002): 174-188.

[51] Doucet, Arnaud, and Adam M. Johansen. "A tutorial on particle filtering and smoothing: Fifteen years later." Handbook of nonlinear filtering 12, no. 656-704 (2009): 3.

[52] Maskell, Simon, and Neil Gordon. "A tutorial on particle filters for on-line nonlinear/non-Gaussian Bayesian tracking." Target tracking: algorithms and applications (Ref. No. 2001/174), IEE 2 (2001): 21-215.

[53] Ristic, Branko, Sanjeev Arulampalam, and Neil Gordon. "Beyond the Kalman filter." IEEE Aerospace and Electronic Systems Magazine 19, no. 7 (2004): 37-38.

[54] Wang, Bo, Li Yu, Zhihong Deng, and Mengyin Fu. "A Particle Filter-Based Matching Algorithm With Gravity Sample Vector for Underwater Gravity Aided Navigation." IEEE/ASME Transactions on Mechatronics 21, no. 3 (2016): 1399-1408.

[55] J.M Pak, C. K. Ahn, Y. S. Shmaliy, and M. T. Lim, "Improving reliability of particle filter-based localization in wireless sensor networks via hybrid particle/fir filtering," IEEE Transactions on Industrial Informatics, vol. 11, no. 5, pp. 1089-1098, 2015

[56] Orchard, Marcos E., Pablo Hevia-Koch, Bin Zhang, and Liang Tang. "Risk measures for particle-filtering-based state-of-charge prognosis in lithium-ion batteries." IEEE Transactions on Industrial Electronics 60, no. 11 (2013): 5260-5269.

[57] Zevedei, D., M. Jurian, and A. Scutariu. "Application of particle filter algorithms in an accurate and reliable localization and tracking of WSN's mobile devices." In Design and Technology in Electronic Packaging (SIITME), 2012 IEEE 18th International Symposium for, pp. 329-332. IEEE, 2012.

[58] Patterson, Donald J., Lin Liao, Dieter Fox, and Henry Kautz. "Inferring high-level behavior from low-level sensors." In UbiComp, pp. 73-89. 2003.

[59] Sheng, Xiaohong, Y-H. Hu, and Parameswaran Ramanathan. "Distributed particle filter with GMM approximation for multiple targets localization and tracking in wireless sensor network." In Information Processing in Sensor Networks, 2005. IPSN 2005. Fourth International Symposium on, pp. 181-188. IEEE, 2005.

[60] Wang, Hui, Henning Lenz, Andrei Szabo, Joachim Bamberger, and Uwe D. Hanebeck. "WLAN-based pedestrian tracking using particle filters and low-cost MEMS sensors." In Positioning, Navigation and Communication, 2007. WPNC'07. 4th Workshop on, pp. 1-7. IEEE, 2007.

[61] Bargshady, Nader, Nayef A. Alsindi, Kaveh Pahlavan, Yunxing Ye, and Ferit Ozan Akgul. "Bounds on performance of hybrid WiFi-UWB cooperative RF localization for robotic applications." In Personal, Indoor and Mobile Radio Communications Wo:wrkshops (PIMRC Workshops), 2010 IEEE 21st International Symposium on, pp. 277-282. IEEE, 2010.

[62] Golden S and Bateman S. Sensor measurements for wifi location with emphasis on time-of-arrival ranging. IEEE Trans Mobile Comput 2007; 6(10): 1185-1198

[63] Geng, Yishuang, and Kaveh Pahlavan. "Design, Implementation and Fundamental Limits of Image and RF Based Wireless Capsule Endoscopy Hybrid Localization." Mobile Computing, IEEE Transactions on, PP, no. 99 (2015): 1-15.

[64] Zheng, Zengwei, Yuanyi Chen, Tao He, Lin Sun, and Dan Chen. "Feature Learning for Fingerprint-Based Positioning in Indoor Environment." International Journal of Distributed Sensor Networks 2015 (2015).

[65] Yang Z, Wu C and Liu Y. Locating in fingerprint space: Wireless indoor localization with little human intervention. In MobiCom. pp. 269-280

[66] F. Zhao, H. Luo, X. Zhao, Z. Pang, and H. Park, "Hyfi: Hybrid floor identification based on wireless fingerprinting and barometric pressure," IEEE Transactions on Industrial Informatics, 2009

[67] S. Kumar, R. M. Hegde, and N. Trigoni, "Gaussian process regression for fingerprinting based localization," Ad Hoc Networks, 2016

[68] Kaemarungsi, Kamol, and Prashant Krishnamurthy. "Properties of indoor received signal strength for WLAN location fingerprinting." In Mobile and Ubiquitous Systems: Networking and Services, 2004. MOBIQUITOUS 2004. The First Annual International Conference on, pp. 14-23. IEEE, 2004

[69] S.-S.Jan, S.-J.Yeh, and Y.-W.Liu, "Received signal strength database interpolation by kriging for a wi-fi indoor positioning system," Sensors, vol. 15, no. 9, pp. 21377-21393, 2015

[70] N. Bargshady, N. A. Alsindi, K. Pahlavan: Performance of TOA- and RSS-Based Indoor Geolocation for Cooperative Robotic Applications. LNCS, vol. 5801, Page(s): 255 - 266, 2009.

[71] Yang, Zhice, Zeyu Wang, Jiansong Zhang, Chenyu Huang, and Qian Zhang. "Wearables can afford: Light-weight indoor positioning with visible light." In Proceedings of the 13th Annual International Conference on Mobile Systems, Applications, and Services, pp. 317-330. ACM, 2015.

[72] Li, Liqun, Pan Hu, Chunyi Peng, Guobin Shen, and Feng Zhao. "Epsilon: A Visible Light Based Positioning System." In NSDI, pp. 331-343. 2014.

[73] Hu, Pan, Liqun Li, Chunyi Peng, Guobin Shen, and Feng Zhao. "Pharos: Enable physical analytics through visible light based indoor localization." In Proceedings of the Twelfth ACM Workshop on Hot Topics in Networks, p. 5. ACM, 2013.

[74] Randall, Julian, Oliver Amft, Jrgen Bohn, and Martin Burri. "LuxTrace: indoor positioning using building illumination." Personal and ubiquitous computing 11, no. 6 (2007): 417-428.

[75] Kuo, Ye-Sheng, Pat Pannuto, Ko-Jen Hsiao, and Prabal Dutta. "Luxapose: Indoor positioning with mobile phones and visible light." In Proceedings of the 20th annual international conference on Mobile computing and networking, pp. 447-458. ACM, 2014.

[76] Zhang, Chi, Josh Tabor, Jialiang Zhang, and Xinyu Zhang. "Extending mobile interaction through near-field visible light sensing." In Proceedings of the 21st Annual International Conference on Mobile Computing and Networking, pp. 345-357. ACM, 2015.

[77] Xu, Qiang, Rong Zheng, and Steve Hranilovic. "IDyLL: Indoor localization using inertial and light sensors on smartphones." In Proceedings of the 2015 ACM International Joint Conference on Pervasive and Ubiquitous Computing, pp. 307-318. ACM, 2015.

[78] Xie, Bo, Guang Tan, and Tian He. "Spinlight: A high accuracy and robust light positioning system for indoor applications." In Proceedings of the 13th ACM Conference on Embedded Networked Sensor Systems, pp. 211-223. ACM, 2015.

[79] Ravi, Nishkam, and Liviu Iftode. Fiatlux: Fingerprinting rooms using light intensity. na, 2007.

[80] Azizyan, Martin, Ionut Constandache, and Romit Roy Choudhury. "SurroundSense: mobile phone localization via ambience fingerprinting." In Proceedings of the 15th annual international conference on Mobile computing and networking, pp. 261-272. ACM, 2009.

[81] Rajagopal, Niranjini, Patrick Lazik, and Anthony Rowe. "Visual light landmarks for mobile devices." In Proceedings of the 13th international symposium on Information processing in sensor networks, pp. 249-260. IEEE Press, 2014.

[82] Bargshady, Nader, Pahlavan, Kaveh, and Krishnamurthy, Prashant. "Fundamentals of RF Localization," eeee-17-0014, Wiley Encyclopedia of Electrical and Electronics Engineering, 2017.

[83] Bargshady, Nader, Gabe Garza, and Kaveh Pahlavan. "Precise Tracking of Things via Hybrid 3-D Fingerprint Database and Kernel Method Particle Filter." IEEE Sensors Journal 16, no. 24 (2016): 8963-8971.

[84] Bargshady, Nader, Kaveh Pahlavan, and Nayef A. Alsindi. "Hybrid WiFi/UWB, cooperative localization using particle filter." In Computing, Networking and Communications (ICNC), 2015 International Conference on, pp. 1055-1060. IEEE, 2015.

[85] Pahlavan, Kaveh, and Allen H. Levesque. Wireless information networks. Vol. 93. John Wiley and Sons, 2005.

[86] Pahlavan, Kaveh, and Prashant Krishnamurthy. Principles of wireless access and localization. John Wiley & Sons, 2013.

[87] M. Hassan-Ali and K. Pahlavan, "A new statistical model for site-specific indoor radio propagation prediction based on geometric optics and geometric probability," IEEE JSAC Wireless, Vol. 1, No. 1, Jan. 2002.

[88] A. Hatami and K. Pahlavan, "In-building Intruder Detection for WLAN Access" The IEEE Aerospace and Electronic Systems Society conference, PLANS, Monterey, CA, April 2004.

[89] Bardia Alavi, Distance Measurement Error Modeling for Time-of-Arrival Based Indoor Geolocation, Ph.D. dissertation, Worcester Polytechnic Institute, May 2006.

[90] Alomainy, A. Hao, Y. Yuan, Y. Liu, "Modelling and Characterisation of Radio Propagation from Wireless Implants at Different Frequencies" Wireless Technology, 2006. The 9th European Conference on, pp. 119-122, 10-12 Sept. 2006.

[91] Alavi, B., Pahlavan, K.: Modeling of the TOA-based distance measurement error using UWB indoor radio measurements. Communications Letters, IEEE Volume 10, Issue 4, Apr 2006 Page(s):275 - 277

[92] H. L. V. Trees, Detection, Estimation, and Modulation Theory. New York: Wiley, 1968.

[93] Phillips C, Sicker D and Grunwald D. A survey of wireless path loss prediction and coverage mapping methods. Communications Surveys & Tutorials, IEEE 2013; 15(1): 255-27

[94] Kulas, L. "Simple 2-D Direction-of-Arrival Estimation Using ESPAR Antenna." IEEE Antennas and Wireless Propagation Letters (2017).

[95] Pratap Misra and Per Enge, Global Positioning System: Signals, Measurements, and Performance, Revised Second Edition, Ganga-Jamuna Press, 2010.

[96] E.D. Kaplan, Understanding GPS: Principles and Applications, Artech House Publishers, 1996.

[97] Chen, Y. and Kobayashi, H. (2002). Signal Strength Based Indoor Geolocation. Proceedings of the IEEE International Conference on Communications. pp 436-439. 28 April - 2 May 2002. New York.

[98] Liu H, Darabi H, Banerjee P et al. Survey of wireless indoor positioning techniques and systems. IEEE Trans Syst, Man, Cybern C, Appl Rev 2007; 37(6): 1067-1080

[99] The First International Workshop on Opportunistic RF Localization for Next Generation Wireless Devices, WPI, Worcester, MA, June 16-17 http://www.cwins.wpi.edu/workshop08/index.html

[100] Z. Chen, Q. Zhu, and Y. C. Soh, "Smartphone inertial sensor-based indoor localization and tracking with ibeacon corrections," IEEE Transactions on Industrial Informatics, vol. 12, no. 4, pp. 1540-1549, 2016

[101] A. Mahtab Hossain, Y. Jin, W.-S. Soh, and H. N. Van, "Ssd: A robust rf location fingerprint addressing mobile devices" heterogeneity," Mobile Computing, IEEE Transactions on, vol. 12, no. 1, pp. 65-77, 2013

[102] Nader Moayeri , Jalal Mapar, Stefanie Tompkins and Kaveh Pahlavan (Editors), Special Issue on Localization and Tracking for Emerging Wireless Systems, IEEE Wireless Communications, April 2011.

[103] P. Bahl and V. N. Padmanabhan. "RADAR: An In-Building RF-based User Location and Tracking System," Proc. IEEE INFOCOM'00, pp. 775-784, March 2000.

[104] Q. H. Spencer, B. D. Jeffs, M. A. Jensen, and A. L. Swindlehurst, "Modeling the Statistical Time and Angle of Arrival characteristics of an Indoor Multipath Channel", IEEE JSAC, vol. 18, No. 3, pp. 347-360, March 2000.

[105] R. Tingley and K. Pahlavan, "Time-space measurement of indoor radio propagation," IEEE Trans. Instrumentation and Measurements, Vol. 50, No. 1, February 2001, pp. 22-31.

[106] A. Mallat, J. Louveaux, and L. Vandendrope. "UWB based positioning in multipath channels, CRBs for AOA and for hybrid TOA-AOA based methods," in Proceedings of the IEEE International Conference on Communications (ICC), Glasgow, Scotland, June 2007.

[107] Y. Qi, Wireless geolocation in a none-line-of-sight envrionment. PhD Thesis. Princeton University. 2003.

[108] N. A. Alsindi, K. Pahlavan, B Alavi and Xinrong Li: A Novel Cooperative Localization Algorithm for Indoor Sensor Networks, PIMRC 2006, Nov. 14, Pages:1-6, 2006

[109] Douc, Randal, and Olivier Capp. "Comparison of resampling schemes for particle filtering." In Image and Signal Processing and Analysis, 2005. ISPA 2005. Proceedings of the 4th International Symposium on, pp. 64-69. IEEE, 2005.

[110] Bolic, Miodrag, Petar M. Djuric, and Sangjin Hong. "Resampling algorithms and architectures for distributed particle filters." IEEE Transactions on Signal Processing 53, no. 7 (2005): 2442-2450.

[111] Pitt, Michael K., and Neil Shephard. "Filtering via simulation: Auxiliary particle filters." Journal of the American statistical association 94, no. 446 (1999): 590-599.

[112] H.V. Poor, An introduction to signal detection and estimation, Springer Science and Business Media, 1994

[113] N. Patwari, J.N. Ash, S. and et, al., Locating the Nodes: Cooperative Localization in Wireless Sensor Networks, IEEE Signal Processing Magazine, Vol.22, No.4, pp.54-69, Jul. 2005

[114] F. Gustafsson and F. Gunnarsson, Mobile Positioning Using Wireless Networks, Possibilities and Fundamental Limitations Based on Available Wireless Network Measurements, IEEE Signal Processing Magazine, Vol.22, No.4, pp.41-53, Jul. 2005

[115] N. Patwari, A.O. Hero, M. Perkins and et, al., Relative Location Estimation in Wireless Sensor Networks, IEEE Transactions on Signal Processing, Vol.51, No.8, pp.2137-2148, Aug. 2003

[116] Baek, Kyungim, Bruce A. Draper, J. Ross Beveridge, and Kai She. "PCA vs. ICA: A Comparison on the FERET Data Set." In JCIS, pp. 824-827. 2002.

[117] Zheng, Chun-Hou, De-Shuang Huang, Lei Zhang, and Xiang-Zhen Kong. "Tumor clustering using nonnegative matrix factorization with gene selection. " Information Technology in Biomedicine, IEEE Transactions on 13, no. 4 (2009): 599-607.

[118] Dy, Jennifer G., and Carla E. Brodley. "Feature selection for unsupervised learning." The Journal of Machine Learning Research 5 (2004): 845-889.

[119] Asif, M. Salman, Adam Charles, Justin Romberg, and Christopher Rozell. "Estimation and dynamic updating of time-varying signals with sparse variations." In Acoustics, Speech and Signal Processing (ICASSP), 2011 IEEE International Conference on, pp. 3908-3911. IEEE, 2011.

[120] Charles, Adam, M. Salman Asif, Justin Romberg, and Christopher Rozell. "Sparsity penalties in dynamical system estimation." In Information Sciences and Systems (CISS), 2011 45th Annual Conference on, pp. 1-6. IEEE, 2011.

[121] H. Zou, X. Lu, H. Jiang, and L. Xie, "A fast and precise indoor localization algorithm based on an online sequential extreme learning machine," Sensors, vol. 15, no. 1, pp. 1804-1824, 2015

[122] H. Zou, B. Huang, X. Lu, H. Jiang, and L. Xie, "A robust indoor positioning system based on the procrustes analysis and weighted extreme learning machine," Wireless Communications, IEEE Transactions on, vol. 15, no. 2, pp. 1252-1266, 2016

[123] C. K. Williams and C. E. Rasmussen, "Gaussian processes for machine learning," the MIT Press, 2006

[124] M. Youssef, A. Agrawala, and U. Shankar, "WLAN Location Determination via Clustering and Probability Distributions, Proc. First IEEE Intl Conf. Pervasive Computing and Comm. (PerCom 03), pp. 143-150, Mar. 2003.

[125] Y. Chen, Q. Yang, J. Yin, and X. Chai, "Power-Efficient Access- Point Selection for Indoor Location Estimation, IEEE Trans. Knowledge and Data Eng., vol. 18, no. 7, pp. 877-888, July 2006.